DEVELOPING FLOOD MITIGATION MEASURES FOR BALEDWAYNE CITY, SOMALIA, BY USING THE HEC-RAS MODEL

A Thesis Submitted to
the Graduate School
İzmir Institute of Technology
in Partial Fulfilment of the Requirements for the Degree of

MASTER OF SCIENCE

in Civil Engineering

by
Abdullahi Abdulwahid IBRAHIM

June 2022
İZMİR

ACKNOWLEDGEMENTS

ABSTRACT

DEVELOPING FLOOD MITIGATION MEASURES FOR BALEDWYNE CITY, SOMALIA, BY USING THE HEC-RAS MODEL

This study covers the investigation of the flood mitigation measures required to protect the city of Baledwayne, which is located in the Hiran region of Somalia and has been subject to frequent floods recently.

In the HEC-HMS model, the precipitation data measured in 2019 and DEM at the Baledwayne and Bulo-Burti stations of the Hiran region were used as input. The observed discharge in the Shabelle river in 2019 of both stations was imported into the model to compare the simulated rainfall-runoff hydrographs. The rainfall-runoff hydrographs of 2019 were simulated with the HEC-HMS model using these parameters, SCS Curve Number for analyzing runoff volume, Snyder Unit Hydrograph for estimating direct runoffs, and Constant Monthly for calculating the baseflow and Muskingum for channel routing. The outflow hydrographs at both stations were successfully simulated.

With the 1D&2D HEC-RAS model, flood maps were generated using various alternatives to protect the study area from floods of Q500 flow rate with a return interval of 500 years. The Deyr 2019 flood event was used for the calibration of the model. The model determined the flood extent and depth of this flood event by changing the roughness coefficient at specific intervals. Various flood mitigation measures have been investigated after calibration. It has been found that the best protection can be achieved by the combination of these four flood mitigation measures: (1) rehabilitation of the Warabole diversion channel, (2) construction of detention ponds at the upstream of the floodplain, (3) levees along both sides of the river and (4) improvement of the river.

Keywords: *Baledwayne ·Shabelle River ·Hydrological and Hydraulic modelling ·HEC-RAS ·HEC-HMS ·ArcGIS*

ÖZET

HEC-RAS MODELİ KULLANILARAK SOMALİ'DEKİ BALEDWAYNE ŞEHRİ İÇİN SEL ÖNLEME YÖNTEMLERİNİN GELİŞTİRİLMESİ

Bu çalışma, Somali'nin Hiran bölgesinde bulunan ve son zamanlarda sıkça taşkınlara maruz kalan Baledwayne şehrinin taşkınlardan korunması için gereken önlemlerin araştırılmasını kapsamaktadır. HEC-HMS modelinde Hiran bölgesinin DEM ve Baledwayne ve Bulo-Burti istasyonlarında 2019'da ölçülen yağış verileri girdi olarak kullanılmıştır. Shabelle nehrinde 2019'da ölçülen debi, yağış-akış simülasyonu için, modele yüklenmiştir. HEC-HMS modeli ile 2019 taşkın hidrografı simüle edilmiştir. SCS Ağri Numarası (SCS Curve Number) ile akış hacmi, Snyder Birim Hidrograf ile direk akış, Constant Monthly ile taban akımı, ve Muskingum yöntemi taşkın öteleme hesaplanmıştır. Her iki istasyondaki debi hidrograflarının başarıyla simülasyonu gerçekleştirilmiştir.

1D&2D HEC-RAS modeli ile, dönüş aralığı 500 yıl olan Q_{500} debi için, çalışma alanını taşkınlardan koruyabilecek çeşitli alternatifler üzerine taşkın haritaları çıkartılmıştır. Modelin kalibrasyonu için Deyr2019 taşkın olayı kullanılmıştır. Bu taşkın olayının kapladığı alan, pürüzlülük katsayısının belli aralıklarda değiştirilmesiyle, model ile üretilmeye çalışılmış ve başarılmıştır. Kalibrasyondan sonra çeşitli taşkın koruma yöntemleri araştırılmıştır. En iyi korumanın dört farklı yöntemin birlikte kullanılmasıyla olabileceği gösterilmiştir: (1) Warabole derivasyon kanalı, (2) taşkın alanı yukarısında sel kapanları, (3) nenrin her iki yakasında nehir boyunca seddeler, ve (4) nehir restorasyonu.

Anahtar Kelimeler: *Baledwayne ·Shabelle Nehri ·Hidrolojik ve Hidrolik modelleme ·HEC-RAS ·HEC-HMS ·ArcGIS*

TABLE OF CONTENTS

LIST OF FIGURES

LIST OF TABLES

LIST OF ABBREVIATIONS

ADPC	Asian Disaster Preparedness Centre
BCM	Billion Cubic Mater
CRED	Centre for Research on the Epidemiology of Disasters
DEM	Digital Elevation Model
DTM	Digital Terrain Map
ECHO	European Commission Humanitarian aid Office
FAO	Food and Agriculture Organization
FSAU	Food Security Analysis Unit
GDP	Gross Domestic Product
GIS	Geography Information System
HEC-HMS	Hydrologic Engineering Center's Hydraulic Modeling System
HEC-RAS	Hydrologic Engineering Center River Analysis System
HEC-SSP	Hydrologic Engineering Center's Statistical Software Package
IFRC	International Federation of Red Cross and Red Crescent Societies
OCHA	Office for the Coordination of Humanitarian Affairs
SWALIM	Somalia Water and Land Information Management
UNCT	United Nations Country Team
UNDP	United Nations Development Programme
UNESCAP	United Nations Economic and Social Commission for Asia and the Pacific
USACE	U.S. Army Corps of Engineers
UTM	Universal Transverse Mercator
WGS	World Geodetic System
WHO	World Health Organization

CHAPTER 1

INTRODUCTION

1.1   Background of the Study

Floods are the most frequent natural catastrophe and happen when an overflow of water usually submerges dry land. Floods result from many factors, such as heavy precipitation, rapid snowmelt, storm surge or tsunami in coastal zones, dam break or dike overflow, increased urbanization, change in land use, insufficient infrastructures and impacts of climate change. Floods can cause loss of life, widespread destruction of agricultural lands, economic loss, and damage to private and public property such as buildings, roads, and health centres.

Between 1998 and 2017, floods affected more than 2 billion individuals worldwide. The vulnerability to floods is high in countries with low income and GDP. Also, a lack of warning systems and awareness of flooding hazards increase the impact of the flood (WHO, n.d.).

Types of floods vary based on sources, causes, flood depth, flow velocity, and impacts of the floods. Coastal overflows, river floods, flash floods, and urban overflows are the common types of flooding. River overflows occur when the river level exceeds its maximum bank level (Merz et al., 2021). River floods are among the most dangerous and costliest type of floods. River floods affect 58 million people and cause more than 145 billion USD economic loss worldwide. It is expected to increase the impact of river floods due to many factors, such as rapid population growth in flood-prone areas and the effects of climate change (Dottori et al., 2018)**.**

Every year Somalia experiences two significant types of inundations, river and flash overflows, which usually occur during rainy seasons. River Floods happen along Juba and Shabelle Rivers, while flash floods occur in low-lying areas of the country. In 2006, heavy rains caused massive floods; these floods impacted at least 300,000 people and damaged 57 houses. Riverine and flash floods in 2012 induced at least 25 deaths, loss of 5,000 livestock animals, and displacement of 20,000 people from their homes. In 2013,

50,000 people were displaced from their houses, and almost seven individuals were killed. In 2018, 215,000 individuals flew from their houses, and floods impacted more than 630,000 people. On 19 May 2020, riverine and flash flooding in Somalia caused 24 deaths, affected about 919,000 individuals, and displaced 412,000 from their homes. Baledwayne city was the most affected area along the Shabelle River; the river overflowed its banks and flooded about 75% of Baledwayne city. According to the city flood task force, almost 240,000 individuals were displaced from the city and surrounding villages between 12 and 18 May 2020. In the Jowhar district, riverine flooding has affected around 98,000 individuals in 37 locations, which brings the total affected in Hirshabelle state to 338,000 people (OCHA, 2020)

1.2   Statement of the Problem

Floods are among the most frequent and disastrous natural hazards globally, causing massive losses to human life, economics and societal properties (FAO-SWALIM, 2016). Flooding is a common disaster in Somalia that affects thousands of people. The climatic changes and anthropogenic factors increased the effects and damages of floods throughout the whole country. Riverine flooding occurs mainly along Shabelle and Juba River basins, and flash floods common in low-lying and built-up areas are the two types of floods in Somalia. These floods commonly occur during the rainfall seasons in the country, Gu (from April to June) and Deyr (from October to December). During those seasons, the flow rate of the rivers is a maximum, and during the same period, the basin catchment of the river, located in the Ethiopian Highlands, receives extreme precipitations.

Baledwayne city is among the areas with the highest risk of riverine and flash flooding in districts along the Shabelle River. The city experienced consecutive extreme flood events such as in 2006/2007, 2009/2010, 2011/2012, 2013, 2018/2019 and 2020. Between October and the beginning of November 2019, the city experienced one of the worst flood events ever. Shebelle River flooded the city and submerged more than 85% of the city, as indicated in Figure 1.1. This massive flood affected many people in and around the city economically and socially. Almost 11 people were carried away by the floods. Besides that, more than 45,500 households (273,00 people) were displaced,

51,473 hectares were flooded, including 36241 hectares of farmland were damaged (OCHA, 2019).

Figure 1.1. Flooding in Baledwayne City October 2019

Due to the topographical and landscape configuration, the flooded water quickly spread to the Baledwayne city, causing massive impacts. Furthermore, illegal settlements of floodplains and lack of flood mitigation measures increased the vulnerability and damages of floods throughout the city. Before the civil war, mitigation measures, regulations, and guidelines existed to avoid and manage floods. These included developing dikes, diversion channels, and reservoirs for flood protection and irrigation. These structures are mostly not functioning now; if immediate actions were not taken, the vulnerability and effects of floods would increase in the future. So, this study analyzes the extent and occurrence of the flood in the Baledwayne city and then develops different flood mitigation measures to propose the most appropriate mitigation measure. Such research does not exist in the study area, and most academics present comprehensive flood reports in the country, particularly in Baledwayne city, but there is one research related to flood extent and impacts on the study area.

1.3   Research Questions

- ➤ How do we determine the flood frequency estimation using different distributions?
- ➤ Using hydrological and hydraulic models, what is the magnitude and map of the Deyr 2019 flood in Baledwayne?
- ➤ After applying different flood mitigation measures, what is the most appropriate flood mitigation measure for Baledwayne city?

1.4   Objective of the Study

1.4.1 General Objective

The primary objective of this study is to investigate a set of alternatives as remedial measures for flood control purposes to protect the Baledwayne city from Shabelle River flooding.

1.4.2 Specific Objective

The specific objectives of the study are:
- ➤ To assess flood frequency analysis of different distributions fits for the flood events.
- ➤ To investigate the magnitude and map of the Deyr 2019 flood in Baledwayne city using hydrological and hydraulic models.
- ➤ To analyze and compare different flood mitigation measures to determine the most appropriate flood mitigation measure for Baledwayne city.

1.5   Scope of the Study

This study does not evaluate all floods that occur in Somalia because such a study requires an enormous financial and time burden and comprehensive data to conduct, but this study focuses on the flooding of the Shebelle River at Baledwayne city, which is the highest risk zone of flooding. The river divides the city into two parts; last decade, the city experienced consecutive and extreme floods due to climate changes. This study concentrates on hydro-meteorological floods and investigates and compares different flood mitigation measures to protect the city from flooding.

1.6   Significance of the Study

Flooding is the most catastrophic natural hazard globally, and they cause loss of life, destruction of public and private properties, and economic and health crisis. Flooding is a common disaster in Somalia that affects thousands of people and their belongings. Baledwayne city experiences extreme flood events every year that damage the city and its neighbouring villages. It became essential to have effective flood mitigation measures to protect the city from flooding. Effective flood mitigation measure is integral for reducing and eliminating the impact of any flood disasters.

This study would contribute to understanding the role of effective flood mitigation measures in protecting the study area from flooding. Also, this study would add significant results to Somalia's national flood mitigation plan to protect the study area from riverine and flash floods. The results of this study would also be helpful to scholars and would be a crucial guide for further related studies on the region and the country. Furthermore, it would contribute to efforts to reduce the impact of floods on humans and their properties by developing mitigation measures.

1.7   Limitation of the Study

The limitations of this study are divided into limitations related to the data and the model.

- ➤ There is only one rain gauge station and hydrometric systems in the city with some missing data.
- ➤ The 10 m DTM layer of the data, which is an essential layer for the geometry layer, was limited to a thin strip along the Shabelle River.
- ➤ Sediment, future climate change, land use & land cover are not considered.

1.8   Structure of the Thesis

Including the Introduction chapter, this thesis is constituted of SIX chapters. The remaining FIVE chapters are:

- ✓ **CHAPTER 2: Literature review**
  The literature review delivers an exhaustive overview of floods and their effects; following this is the history of floods in Somalia, their causes and their damages. Finally,

a brief description of the flood mitigation measures and hydrological and hydraulic models.

✓ **CHAPTER 3: Description of the Study Area and Data**

This chapter explains the background, climate, geology, land use & land cover and soil properties of the study area. It also gives an overview of the Shabelle river basin in the study area. Furthermore, this chapter discusses collecting all necessary data and their usage during this research. Finally, this chapter performs a homogeneity test of data using Rainbow software.

✓ **CHAPTER 4: Methodology and Results**

This chapter discusses the overview of flood frequency distribution analysis and then performs the GOF test of the data using EasyFit software. It also performs flood frequency analysis using the HEC-SSP model to generate the design value of peak discharge.

This chapter again conducts the hydrological modelling of the study area using the HEC-HMS model to simulate the rainfall-runoff hydrograph of the study area.

Finally, it performs the hydraulic modelling of the study area using the HEC-RAS model to generate the inundation map of the Deyr 2019 flood event in the study area.

✓ **CHAPTER 5: Flood Mitigation Measures**

This chapter initially generates the inundation map of a 500-year flood and then discusses the existing different mitigation measures in the study area. After that, this chapter analysis and generates the inundation map of several remedial alternatives to flood mitigation measures.

Finally, this chapter compares and discusses the results of those mitigation measures to select the most appropriate measures to protect the study area against the peak discharge of a 500-year flood.

✓ **CHAPTER 6: Summary, Conclusions and Recommendations**

This chapter summarizes and concentrates on the main conclusions of the thesis and outlines potential outcomes and suggestions for future work.

CHAPTER 2

LITERATURE REVIEW

2.1   Overview of Floods

Natural Disasters every year causes losses of human lives, health problems, destruction of public and private infrastructures, economic loss and environmental crises. The deteriorating issue of climate change leads to an increase in natural disasters in terms of frequency, scope, complexity, and destructive capacity (Schipper & Pelling, 2006). The number of people impacted by natural catastrophes rose from 16,000 people in 1975 to 2.4 million in 2011 (UNDP, 2012).

Flooding can be categorized as the most dangerous type of natural disaster and the ultimate cause of casualties from natural phenomena across the globe. Regarding the data compiled by Munich Reinsurance Company (Munich Re), floods are responsible for roughly half of all deaths and a third of the global economic losses of natural disasters (Munich, 2000). Floods can be described as when usually dry land is submerged by water. Every year more than 90 countries and nearly 196 million people are subjected to flood disasters. Between 1980 and 2000, floods caused 170,000 deaths worldwide (UNDP, 2004).

Due to extreme hydrometeorological events, increasing population growth and improper urbanization, and inadequate disaster reaction, flood damages and casualties have swiftly risen globally in recent decades (Wu et al., 2012). Changing precipitation regimes due to climate change leads to extreme flooding and drought events. Recent analyses indicate that the frequency and intensity of significant flood events are predicted to rise worldwide. In 2012, floods led to an enormous economic loss estimated to be over $19 billion globally. Based on climate practices and future strategies, floods will impact around 450 million individuals and 430,000 square kilometres of cultivated land by 2050 (Haltas et al., 2021)**.**

Many factors are responsible for floodings, such as extreme rainfall, rapid snowmelt, severe winds over water, landslides, tsunamis, increased urbanization,

accidents, and failure of hydraulic structures such as dams and levees (Nfor et al., 2019; Zaifoglu et al., 2019).

Types and categorizations of floods contrast based on origins, causes, flood depth, flow velocity, and impacts of the floods. The main types of floods include coastal floods, storm surges and tsunamis, river floods, groundwater rise, flash floods, urban floods, dam break floods, and overtopping levees or embankments (Kron, 2005). Flooding is among the most frequent and disastrous natural hazards. Floods have severe effects on the population and the environment. Their effects include loss of life, livestock, health problems, destruction of buildings, agricultural and cropland, social and economic damages, and environmental problems (Haltas et al., 2021). In 1954, heavy rainfall in the Yangtze River Basin caused an extreme flood event that damaged most of the Hubei Province, China. Official agencies registered more than 30,000 death tolls. Also, this massive flood caused the breakdown of diseases and other cascading events, which increased the casualties. They reported that 200,000 death and more than 18 million people were strongly affected by this flood event (Hamidifar & Nones, 2021).

Floods hit Mozambique in 2000, caused 700 deaths, destroyed more than 150,000 homes, and affected numerous people also; it led to a fall in the GDP growth from 10 to 2 in the country (DFID, 2004). In 2010 flooding in Benin caused a considerable impact; floods roughly destroyed 55,000 houses, 500 schools, and 90 health centres, leading to at least 150,000 people being homeless; and 81,000 heads of livestock were lost. Furthermore, floods destroyed around 133,047 hectares of crops and inundated 12,000 tons of stored food (Guha-sapir et al., 2015).

Due to economic, lack of policy and regulations, responsiveness, and awareness of natural disasters, Somalia has experienced recurring floods and droughts. Somalia is one of the most vulnerable to natural disasters such as droughts and floods (UNDP, 2004). In 2011, the country was hit by extreme drought, leading to around 6.7 million people needing urgent humanitarian assistance. In 2018 riverine and flash floods hit Somalia's central and southern regions. The riverine floods hit 16 districts and have affected 500,120 individuals, of whom 214,596 were displaced. At the same time, the flash flooding hit 13 districts and affected about 272,436 persons, of whom 15,004 were displaced. The total number of affected people was 6.2 million, which worsened the situation since the country

was already suffering from drought spanning over four successive rainy seasons, leaving 5.4 million individuals in need of humanitarian aid (OCHA, 2018). Last decades, Somalia faced significant political insecurity risks and capacity regulations; these delayed regulations, policies, responses, and awareness of risk disasters. Moreover, the country is one of the most vulnerable to natural disasters globally. The intensity and frequency of climatological events facing Somalia will increase in the forthcoming years (MOP, 2020; Patrick, 2011).

In Somalia, floods from Shabelle and Juba rivers are common natural disasters, occurring almost every year. The leading cause of these floods is heavy precipitation that falls upstream of the catchments located in the Ethiopian highlands. Because of climate change, the catchments experience raised intensity and frequency of rainfall than in Somalia. Moreover, in the dry season, farmers illegally open the embankments and dikes of the rivers to irrigate their agricultural land, which leads to artificial flooding. In Deyr 2019, Somalia experienced extreme flooding, which caused a massive impact. About 50 million USD additionally is needed for an immediate flood response as reported by the UN Floods repose. Besides that, the Somalia Humanitarian and United Nations Central Emergency Response released around 20 million USD for life-saving humanitarian aid. Furthermore, for emergency funding to respond to the floods, the prime minister of Somalia initiated to release of 500,000 USD (OCHA, 2020).

2.2   Causes of Floods

Floods generally result from natural causes related to hydrological and meteorological extreme events, such as extreme flow and precipitation. Regardless, they can also happen due to artificial activities, such as unexpected growth and development in floodplains, leading to property and land flooding. Also, these artificial activities include a dam breach or overtopping of levees or an embankment that fails to defend planned developments. Due to multiple factors such as rapid population growth, people usually move from rural regions to cities or within cities, and they frequently settle in zones highly exposed to flooding in many parts of the globe. The absence of flood risk awareness, preparedness measures, and flood protection infrastructures can make people highly vulnerable to floods. Developments and land-use changes in urban areas decrease soil permeability, which increases surface rainfall-runoff, and this, in turn, increases the

risk of flooding and surplus drainage systems that were previously not prepared to manage increased flows in many cases (Jha et al., 2012).

Somalia experiences various flood events: river flooding occurs mainly along Shabelle and Juba River basins, and flash floods are common in low-lying and built-up areas. These floods are caused mainly by climatic and anthropogenic processes. The riverine flooding is primarily caused by drainage from the upstream catchment of Rivers Juba and Shabelle basins located in the Ethiopian Mountains. These highlands experience more rainfall than usual and more consecutive precipitation than what occurs in Somalia. Moreover, during the dry season, the farms illegally create artificial openings on the levee or dikes and embankments of the rivers to create an outlet for irrigation purposes. These human activities increase flood extend, reaching areas far from the river and weakening the dikes and protection systems during flooding seasons. Before the civil war, there were mitigation measures, regulations, and guidelines to avoid and manage floods. These included developing dikes, diversion channels, and reservoirs for flood protection and irrigation. These structures are in deterioration and mostly are not functioning now (Gadain, H. M. and Jama, 2009).

2.2.1 Natural Causes

The natural cause of floods includes precipitation (downpour, rainfall, hail & snowmelt), landslides (seismic activity, slope instability, erosion), storm surges (lower pressure in the ocean causing rising tidal levels), increased groundwater levels (thus faster runoff in chalk catchments), glacier melts or falls due to volcanic activity. Climate changes that affect the intensity of rainfall lead to increased rainfall and rising groundwater levels. Rainfalls can saturate the pedological and geological layers of soil leading to problems with infiltration, thus creating conditions for the concentration of surface water in the river valleys and riverbeds (Street & Niksic, 2020).

2.2.2 Manmade Causes

These causes are; dam failures (overtopping, catastrophic, piping) and failures of the embankment (river & coastal flood protection embankments), floodplain encroachment (loss of storage, construction on floodplains), modification of land use (crop change, deforestation, compaction of soil), poor drainage capacity and siltation,

insufficient integration between the river and subsurface drainage or sewer schemes, insufficient maintenance (metropolitan watercourses, blockage of culverts and sewer schemes), lack of proper planning and management of the whole catchment area (local & national) (Jha et al., 2012).

2.3   Types of Floods

Flooding is a body of water that increases to flood ground that is not usually inundated and usually results from heavy precipitation and other factors. There are three main classes and several unique types of floods. These primary types are riverine flood, flash flood, and storm surge, where the unique types of floods include dam-break and levee overtopping floods, backwater (e.g., driven by a landslide that intercepts a watercourse), tsunami, waterlogging, groundwater increase, debris flow events, and others (Kron, 2005).

A flood can be defined and categorized according to the flood's source, cause, and impact. Based on those aspects, floods can commonly be divided into river (fluvial) floods, pluvial (overland), groundwater rise, coastal, or the failure of artificial water schemes such as dam breaks. According to the speed and velocity of the flood, they can be categorized into urban floods, flash floods, semi-permanent floods, and gradually rising floods (Jha et al., 2012).

River (or fluvial) floods and flash floods are the main two floods in Somalia. The river floods regularly occur along the Shabelle and Juba Rivers in Somalia's Southern and Central regions. Flash floods commonly occur along the intermittent streams in the country's northern regions. Both these floods cause massive casualties and significant economic damage (FAO-SWALIM, 2016).

All the types of floods mentioned above can severely impact metropolitan areas; therefore, they can be listed as urban overflows. It is vital to comprehend the cause and velocity of each type to comprehend their potential impacts on urban zones and how to mitigate their effects. Table 2.1 summarises the class and causes of floods.

Table 2.1. Kinds and causes of floods (Source: Jha et al., 2012; Sumi et al., 2022).

Types of Floods	Naturally Caused	Artificial induced	Speed and velocity of the flood	Duration of the flood
Urban Floods	River (or fluvial) flood Flash Flood Pluvial (Overland) flood Coastal flood Groundwater	Saturation of drainage and sewage capability. Decrease of soil permeability due to raised concretization Lack of management and incorrect drainage system.	It changes depending on the cause.	From a few hours to days
Pluvial (Overland) floods	Convective thunderstorms, excessive rain, breakage of an ice jam, glacial lake burst, earthquakes consequential in landslides	Changes in land use in the urbanizations. Increase in surface rainfall runoff.	Varies	Changes depending upon initial conditions
Coastal Tsunami (or seismic sea waves, storm surge)	Earthquakes Submarine volcanic eruptions. Subsidence, Coastal erosion	Development of coastal zones Collapse of coastal natural flora (e.g., mangrove)	It varies but is usually relatively rapid.	Usually takes a brief time; however, it sometimes takes a long time to decrease.
Groundwater	Increased water table level merged with heavy precipitation. Implanted effects	Growth in low-lying places and interference with natural aquifers	Usually, slow	Lengthier duration
Flash flood	It can be generated by the river, pluvial or coastal systems; convective thunderstorms; Glacial Lake Outburst Floods.	The disastrous failure of water retaining systems Insufficient drainage infrastructure.	Fast	Usually, short often, only a few hours
River (or fluvial) flood	Extreme precipitation, Snow melting, blockage of the flow	Breaking or failure of dikes or dams next to the river	It changes depending on the cause.	Changes depending upon initial conditions
Semi-permanent flooding	Land subsidence, sea level rise	Drainage overload, failure or collapse of a coastal structure, improper urban development, Inadequate groundwater management	Usually, slow	Long time or permanent

2.4   Effects of Floods

Floods are described as one of the most destructive natural catastrophes worldwide, which cause enormous damage to buildings, health, the environment,

economics and human losses. There is a significant increase in the human and economic impacts caused by floods around the globe (ADPC & UNDP, 2005). Regarding to the Centre for Research on the Epidemiology of Disasters (CRED), disasters of flood events account for 43% of all global natural disasters. Between 1994 and 2013, floods affected 2.5 billion people and caused the deaths of 160, 000 thousand of people (CRED, 2015).

According to ECHO (2019), several parts of central Vietnam experienced heavy rain, which caused extreme flooding, at least three casualties and five people were injured in the Nghe An territory. Also, floods destroyed 5,250 houses, 2,819 hectares of crops and 1,668 hectares of marine farms. Furthermore, schools in Huong Son and Huong Khe districts of Ha Tinh province were closed due to thunderstorms over southern Vietnam on 22 October (ECHO, 2019). In 2019, severe floods hit the Mid-western United States; the extent of these floods reached a total area of 492,797.4 square kilometres. The floods-affected many states such as Nebraska, Wisconsin, Iowa, Kansas, Missouri, Minnesota, Illinois and South Dakota. Also, they caused massive economic damage, which is estimated at 4 billion USD, of which Iowa city contributed 1.6 billion USD (FloodList, 2019).

In December 2021, heavy rainfall and storms caused massive floods hit the cities of Itamaraju and Porto Seguro in the Bahia province in Brazil. The Superintendence for Protection and Civil Defence of the State of Bahia (Sudec) reported that at least 12 individuals passed away, 267 people were wounded, and about 15,199 were displaced from their homes. It is registered that the floods impacted 220,297 individuals. Both the Gabo Bravo and Jucuruçu rivers flooded into isolated provinces of Bahia and Minas Gerais state. The floods led to damaging houses and infrastructures such as roads and bridges. The Brazilian Government declared an emergency condition for around 50 affected cities in Bahia and Minas Gerais provinces. According to the Brazilian Red Cross, floods affected and displaced over 7,000 individuals and 3,000 people, respectively, the Jucuruçu city. Furthermore, the electricity of Medeiros Neto city left, and around 1,000 people were isolated (IFRC, 2022).

According to WHO (2013), 50 of the 53 nations in the World Health Organization European Province experienced flood events during the past decades, including the United Kingdom, the Russian Federation and Romania. The increase in climate change

causes extreme meteorological events such as heavy and intensive precipitation, resulting in more frequent and extreme floods such as flash inundation; extensive, longer-lasting fluvial and pluvial (River) floods; snowmelt and coastal floods. If immediate measures are not taken, the river flooding will affect 250,000-400,000 extra individuals per year in European regions by the 2080s; this is more than the double number of people affected by floods from 1961 to 1990 (Menne et al., 2013). From 14-16 May 2014, extreme rainfall caused massive floods in the parts of Serbia, eastern Croatia and northern Bosnia, leading to more than 79 people deaths and the displacement of 19,730 people from their homes. Furthermore, the flooding water destroyed around 0.5 million square kilometres of cultivated land (Street & Niksic, 2020).

The Asian province encounters more frequent flood catastrophes of high magnitude than the rest of the world; this led to rise in the total number of people affected and economic losses by the floods disasters in the region. Between 1970 and 2014, it is reported that 11,985 natural disasters events worldwide, of which 5,139 or (42.9%) occurred in the Asia and Pacific regions. Floods and storms were the most recurring in the province, counting for 64% of such events registered from 1970 to 2014. News on flooding in the region significantly increased, from 11 events between 1970-1979 to 72 events per year from 2000 to 2009. Between 1970 and 2014, 1779 flood events in the region caused 199,733 deaths, 370 billion USD economic losses, and over 3.35 billion people were affected by the floods (U.N ESCAP, 2015).

In Africa, due to many factors such as poverty, lack of management systems and weak flood mitigation measures, many people settle in flood-prone areas; this increases the number of people overexposed to flooding (Mensah & Ahadzie, 2020). In November 2019, Djibouti experienced extreme precipitation, which caused flash floods. It is registered nine losses, including seven children and more than 30,000-40,000 households or (150,000-250,000 people) were impacted by the floods in Djibouti city. Also, the floods damaged dwellings, schools, and other infrastructures and caused a loss of access to electricity in some areas. In the Tadjourah region, flash floods badly damaged roads, including the newly launched Tadjourah-Balho road. Also, the road that connects the region to Djibouti suffered extreme damage, and the bridge in the Arta area (PK53) is at risk of collapsing. These worsened the situation in the region since about 300 households affected by the floods needed urgent humanitarian aid (Govt. Djibouti & UNCT Djibouti,

2019). In April 2020, heavy rainfalls triggered flash floods in many parts of Ethiopia, such as the Somali, Afar, and SNNP regions. About 219,000 people were affected, and 107,000 people were displaced. Also, the flash floods destroyed more than 299 houses and 234 hectares of farming land. On the other hand, the riverine flood occurred in Jinka, and SNNP damaged social infrastructures and impacted livestock (National Disaster Risk Management & Commission (NDRMC), 2020).

According to flood-induced mortality across the globe 1975–2016 study, Somalia was mentioned in the second group of countries with the most significant death toll. The group included Vietnam, Brazil, Colombia, Iran, Afghanistan, Nepal, Philippines, and North Korea; Napel was the highest with a toll death of 5617 people, whereas Colombia is the least with a toll death of 2337 people (Hu et al., 2018). In Somalia, river flooding occurs mainly along River Juba and Shabelle basins during seasonal precipitation, while flash floods are typical in low lying and built-up areas. Due to many factors, floods in Somalia have become regular events; for example, floods happened in 1991/92, 1994/95, 1997/98, 2002/03, 2006/07, and 2009/10. The riverine floods in central and southern Somalia cause significant damage and losses. Between 1997 and 1998, massive flooding impacted over 900,000 individuals and above 440,000 individuals in 2006/2007 (FAO-SWALIM, 2016). In April 2020, heavy rainfalls led to riverine and flash floods, causing the death of 24 people and affecting approximately 919 0001 people, of whom 411 905 were displaced. Also, Juba and Shabelle Rivers overflowed more than 100,000 square kilometres of farming lands. The floods caused massive damage and losses to Baledwayne city in the Hiraan region; most of the city was submerged by floods for more than two weeks leading to the displacement of many people from their homes to save places. The 2020 flood events caused massive casualties and health crises in the country; this was mainly due to COVID-19 pandemic restrictions to mitigate the impact of the pandemic have exacerbated humanitarian needs and slowed the initial and quick responses of humanitarian agencies to the people affected by floods (FAO, 2020).

2.5   History of Floods in Somalia

Both Shabelle and Juba rivers are the main streams in Somalia, and they are considered crucial water sources and offer water for crop production, domestic use and livestock. Floods typically occur during the rainfall seasons in the country, Gu (from April

to June) and Deyr (from October to December). During those seasons, the flows of the rivers reach their maximum level, and during the same period, heavy precipitations receive in the catchment area of both rivers located in the Ethiopian Highlands. The flooding caused by the two rivers has become regular during rainy seasons, which induces disastrous effects and humanitarian crises. A significant increase in flooding along the two rivers has been observed in the last decades, especially after the El Nino 1997/98 rainfall season (Gadain, H. M. and Jama, 2009).

2.5.1 Past Floods

The first flood event recorded on the Shabelle and Juba Rivers in Somalia was in 1961, and this comes at least eight years after the hydrometric systems were installed on both rivers. Those floods were considered occasions when both rivers exceeded their banks. Between 1961and 2008, numerous floods were recorded in Somalia, though there is missing data between 1991 to 2002. Some of the notable floods are floods that happened in 1961, 1968, 1981, 1997/98, 2000, 2002, 2005, and 2006. Between 1961 and 2008, there were six extreme flooding occasions along the Shabelle and Juba Rivers. The Deyr seasons of 1961, 1977, 1997, and 2006 and Gu seasons of 1981 and 2005 were the most severe flood events. Weighty and widespread precipitation happened during the Deyr 1961, which induced extreme floods in the Juba and Shabelle floodplains. Flooding mainly is caused by overbank spills of the rivers in low-lying areas. These floods affected many people in the country, and they displaced thousands of people from their houses and destroyed infrastructures such as roads. At the same time, these floods were seen in numerous parts of Eastern Africa (Gadain, H. M. and Jama, 2009).

2.5.2 Recent Floods

The floods along Shabelle and Juba rivers in 1997/1998 and 2006 were among the significant flood events in recent years. 100-300 % above the average exceptional heavy rainfall over the catchment basins of the two rivers in the Ethiopian Highlands caused extreme riverine floods in 1997/1998 in Somalia. The floods induced a massive effect on the environment and the people. Nearly the whole Shabelle and Juba valley areas were flooded and destroyed most agricultural lands, irrigation and flood control infrastructure.

During the flooding, the defence dikes of the Juba and Shabelle Rivers were overtopped and suffered breaches at several places, which led both rivers to overflow into all the settlements along the river basins. Moreover, the inundated water surrounded some towns for an extended period and caused land degradation and extensive soil erosion. For instance, the Shabelle flooded and submerged many towns along the river for a long time. The flooding affected around 1 million people and displaced hundreds of thousands of individuals from their homes. Overall the 1997/1998 floods along the Juba and Shabelle Rivers caused approximately 2,000 deaths and displaced nearly two million individuals. Also, they led to the destruction of almost all the enormous irrigation systems and damaged all main flood relief channels, roads and other significant infrastructures.

In earlier November of 2006, the level of the Shabelle River at Baledweyne reached the mark of the flood level associated with river discharges of the 50-year return period. The river inundated the town's primary bridge, and most of the Baledwayne city was underwater for many days. While the Juba River, it was assessed that the flood stage at Luuq district reached the 20-year return period flood stage. During the first weeks of November 2006, floods displaced more than 350,000 people living along the rivers (Gadain, H. M. and Jama, 2009).

The Flash floods and riverine floods in Somalia during Deyr 2019 was the most severe flood event in recent years. These floods affected nearly 1.5 million people, and the flooded area reached more than 201,205 ha, including 154147 ha of agricultural lands. According to UNCR, almost a million individuals were moved between July and November 2019 across Somalia; floods caused 71%, conflict/insecurity (15%) and (13%) were drought-related (FSNAU, 2019).

Baledwayne city experienced both flash floods and riverine floods during the Deyr season in 2019. Flooding water submerged more than 85 % of the city for long periods and displaced over 45,500 households (273,00 people) from their homes. Furthermore, the flooding destroyed 35,000 croplands (FAO-SWALIM, 2019). Table 2.2 summarises the causes and effects of recent floods in Somalia.

Table 2.2. Causes and effects of recent floods in Somalia (Source: FAO-SWALIM, 2019; Gure, 2018).

Date	Causes	Effects of flood	Most affected areas
April 2010	River flooding	100 households were damaged, 3000 people displaced	Baledwayne city
September 2012	Extreme rainfall caused both flash and river flooding	25 people died, over 20,000 people were displaced, and 5000 livestock drowned	Baledwayne city and other parts of Southern Somalia
May 2013	Flash and river flooding	7 children died, 50,000 people were displaced, and 64,000 hectares of farmland were damaged.	Baledwayne, Jowhar and Baidio.
Deyr season 2013	River flooding	111,678 hectares of agricultural land were damaged.	Jowhar, Balcad.
October 2014	Extreme rainfall caused both flash and river flooding.	Ten houses were damaged, and over 2,500 people were displaced.	Kooshin and XawoTako villages in Baledwayne City
Gu season 2015	Flash floods and river flooding	32,200 people were displaced, and 6,800 hectares of farmland damaged	Lower, middle Shabelle regions and Galkayo town
Gu season 2016	River flooding	134,632 hectares were flooded, including 84,890 hectares of farmland damaged	Baledwayne, Jowhar, Luuq
November 2017	Extreme rainfall caused both flash and river flooding.	More than 70,000 were displaced	Hiran and Bay regions.
Gu season 2019	River flooding	214,800 people were displaced, and 206,757 hectares of farmland damaged	Baledwayne, Jowhar, Jamaame.
Deyr season 2019	River flooding	45,500 households (273,00 people) were displaced, 51,473 hectares were flooded, including 36241 hectares of farmland damaged	Baledwayne, Jowhar, Balcad.
Gu season 2020	River flooding	28,244 hectares were flooded, including 15,628 hectares of farmland damaged	Kooshin and XawoTako villages in Baledwayne City.
Deyr season 2020	River flooding	120,388 hectares were flooded, including 104,166 hectares of farmland damaged	Baledwayne, Jowhar, Balcad.

2.6 Flood Mitigation Measures

Flooding can be defined as one of the most frequent natural tragedies. Every year floods cause loss of life and billions of dollars in damage and endanger vulnerable societies worldwide. It is unattainable to eliminate the impact of flooding, though the damage and effects of the flooding can be reduced by utilizing practical methods of flood mitigation measures. Flood hazard reduction means reducing the magnitude of flood or vulnerability of the affected area. Flood Mitigation measures are separated into structural and non-structural mitigation measures. Structural mitigations are usually expensive;

nevertheless, they can be more achievable for long-term planning and defence (Alabbad et al., 2022).

Structural mitigation plans are traditionally known practices of flood mitigation, and they have been used in corporations with general flood managing approaches in most flood plain areas. Structural mitigation includes the construction of flood levees or embankments, dams, floodwalls, channel improvements, diversion schemes, reservoirs, river training works, and others. Non-structural mitigation standards such as flood-resistant materials have been generally used to reduce flood impacts. They are cost-effective, efficient, recovery time reduction, and minimize economic losses.

Non-Structural mitigation approaches improve dependability and the chance of success during flooding. Non-Structural mitigation measures include floodplain regulations, growth, flood forecasting and alert with an evacuation plan, floodproofing, public health measures, flood fighting, flood insurance, provision of relief, and recovery.

Furthermore, the effects of floods can be reduced by altering the characteristics of the elements impacting rainfall-runoff of the catchment so that runoff is delayed. These approaches include modifying the land use, afforestation and deforestation, controlling flow from urban areas, and others. These measures may be integrated and named watershed management. While this approach may be appropriate for managing rainfall-runoff from small catchments, its usefulness for extensive catchments appears to be petty because, in large catchments, the effects of watershed control methods are negligible in the downstream areas (Sivakumar, 2015). Integrating structural and non-structural flood mitigation measures can encourage residents to resist extreme floods (Heidari, 2009).

Selecting the most appropriate mitigation requires a comprehensive study of potential risk and damages and resembling the costs and benefits of various mitigation classes. Flood damage conclusion is an essential element for hazard control, but also it is an important parameter in evaluating mitigation plans regarding the kind and extent of measures. Regardless, in the design phase, quantification of flood effects reduction is unavoidable for different alternatives, for example, structural mitigations or size of protection measures. The damage analysis determines the best protection alternative and the optimum scope of the protection structure (Alabbad et al., 2022).

2.7 HEC HMS Model

HEC-HMS stands for Hydrologic Engineering Center's– Hydrologic Modeling System. The model simulates the entire hydrologic processes, such as rainfall-runoff processes of dendritic watershed designs. HEC-HMS model can be applicable in a broad scope of geographic areas to crack the broadest possible problems, including natural watershed or small urban rainfall runoffs, ample river basins, and flood hydrology. The model uses different hydrological analysis methods such as traditional hydrologic analysis methods (e.g., event infiltration, hydrologic routing and unit hydrographs) and procedures essential for continuous simulation (e.g., evapotranspiration, soil moisture and snowmelt analysis). Also, the model has advanced capabilities to provide for gridded rainfall-runoff simulation by using linear quasi-distributed rainfall-runoff transform (ModClark). The additional analysis tools providing the HEC-HMS model include sediment transport and erosion, model optimization, forecasting streamflow, assessing model uncertainty, depth-area reduction, and water quality. The hydrographs created by the model can be utilized directly or in conjunction with different programs for other analyses such as urban drainage, prospective urbanization effect, water availability, flow forecasting, reservoir and spillway designs, reduction of flood damage, regulation of floodplain, and systems operation (USACE, 2022a).

2.8 HEC RAS Model

HEC-RAS is a shortened from Hydrologic Engineering Center's – River Analysis System. The model was developed as a component of the Hydrologic Engineering Center's "Next Generation" (NexGen) hydrologic engineering software. The NexGen scheme encompasses several parts of hydrologic engineering, including river hydraulics (HEC-RAS), rainfall-runoff analysis (HEC-HMS); reservoir system simulation (HEC-ResSim); flood damage analysis (HEC-FDA and HEC-FIA); and real-time river forecasting for reservoir processes (CWMS). HEC-RAS is an incorporated software method designed for interactive usage in a multi-tasking environment. The procedure comprises a graphical user interface (GUI), different analysis features, data storage and management abilities, graphics, mapping and reporting structures. Likewise, the HEC-RAS model performs the following four river analysis features: 1D steady flow and water

surface profile analyses, 1D & 2D unsteady flow simulation, 1D water quality computation and partially or fully unsteady flow transportable boundary sediment transport analyses (1D and 2D). The essential element is that all those four components use a common geometric data model and standard geometric and hydraulic calculation routines. Additionally, to the four river computation elements, the model has various hydraulic design components that can be mustered after analyzing water surface profiles. HEC-RAS also has a mapping procedure (HEC-RAS Mapper) and a comprehensive spatial data integration (USACE, 2022c).

CHAPTER 3

DESCRIPTION OF THE STUDY AREA AND DATA

3.1   Description of the Study Area

Baledwayne is the Hiran region's capital city and is located in the central part of Somalia. The city lies at 4°44′09″ N and 045°12′13″ E, about 210 miles 345 km north of the capital city of Mogadishu, as shown in Figure 3.1. The city is a productive industrial zone and is a busy retail hub supplying agricultural products and livestock to regional and international markets via Berbera and Bossaso seaports. Baledwayne also has a large livestock market which brings together livestock vendors from all over the country. The total area of Baledwayne city is estimated at 50 km^2 with a 55,410 population (World Population Review, 2020). Shabelle River is the primary source of the city's irrigation and livestock water demands. Also, in some areas in the city, the Shabelle River is an essential source of domestic water use.

Shabelle River divides Baledwayne city into eastern and western provinces. Shabelle River rises on the eastern Ethiopian highlands' eastern flanks, the most elevated point being 4,230 m. The total area of the catchment of Shabelle River at its junction with Juba River is almost 297,000 km^2; two-thirds (188,700 km^2) of the total area lies in Ethiopia, and the rest (108,300 km^2) is in Somalia. Shabelle River and its branches in the eastern Ethiopian highlands are extremely incised and steep slopes. The total length of the Shabelle River's main course from the source to the Somalia border is around 1,290 km, and it traverses a distance of 1,236 km within Somalia before it meets the Juba River (Basnyat, 2009).

The total area of the central gauging station of the Shabelle River basin at Baledwayne city is 207,488 km^2. The maximum and minimum annual discharge of the river basin at Baledwayne city is 473.6 m^3/s and 138.5 m^3/s, respectively. The maximum annual rainfall recorded at Baledwayne station was measured as 745.5 mm in 2015. Finally, the long-term mean annual flow rate of the Shabelle River basin at the Baledwayne runoff station is 44.8 m^3/s, with an Annual Runoff volume of 2.4 billion cubic meters (BCM) (FAOSWALIM, n.d.).
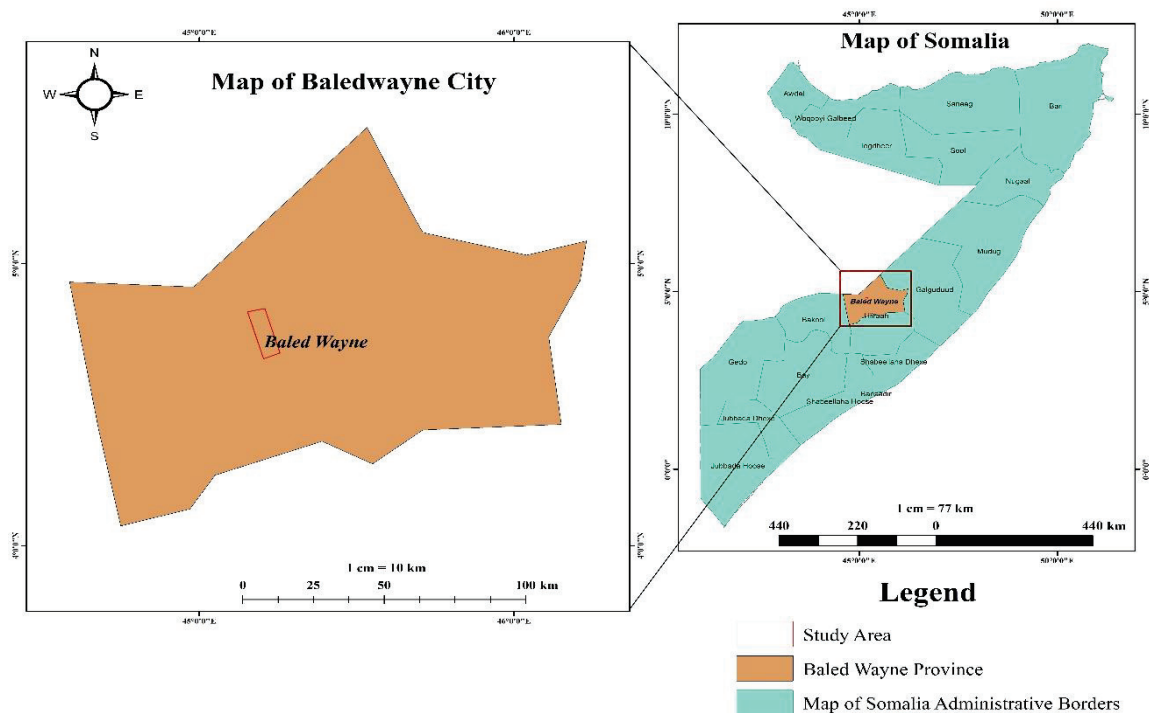
Figure 3.1. Map of the Study Area

3.2 Climate

Somalia commonly has an arid to semi-arid climate; rainfall is a major part of the climate and has significant spatial and temporal variability. The climate of Somalia is defined by the north and south motion of the Inter-Tropical Convergence Zone (ITCZ). Most locations of Somalia result in two rainy seasons - the Gu rainy season is the period when the zone passes northwards, whereas the Deyr rainy season is the period as the zone moves south. The Gu rainy season dominates over the Deyr season in abundance and reliability of precipitation, and it is regarded as the primary precipitating season of the country (P.W, 2007).

The climate conditions for the Shabelle River basins, including the study area, can be defined as primarily arid and semi-arid. The climate of Baledwayne City is influenced by the north and southeasterly airflows of the Intertropical Convergence Zone (ITCZ). The north and southeasterly air masses encounter the Intertropical Front (ITF) and lift air upwards to form precipitation. The ITCZ shifts northwards in the first six months of the year, returning southwards during the year's second half. The main rains occur after the beginning of April and May; therefore, the first overflow season in Somalia occurs during

23

April and June. Many regions of the country experience the Gu rainy season during that time. The return motion of the ITF (approximately south-westwards) initially influences the northern province of the Shabelle River catchment during October, and then it overpasses the southern regions of the Juba River catchment in December. Deyr season, the second overflow season, appears between September and November. The term between January and March is typically dry seasons, and the discharge of the Shabelle River is deficient and dries in some areas (Sebhat, 2015).

Baledwayne City lies 183 m above sea level and Baledwayne has a desert climate. The dry season (Jilaal) is between January and March, whereas April to June (Gu) and September to November (Deyr) are rainy seasons for the city. The mean annual rainfall of Baledwayne city is approximately 330 mm, while the average temperate of the city is roughly 28.6ºC. The highest Potential Evapotranspiration (PET) along the Shabelle River basin occurs in the Hiran region, which exceeds > 2100 mm per year.

3.3   Temperature

The climate of Somalia generally is hot, varying from dry to tropical semi-arid conditions. In the winter months, the maximum mean daily temperature in Somalia is 29ºC, while 38ºC during the summer months. The weather of Somalia can be divided generally into two dry seasons and two wet seasons.

The first dry season is described as the dominance of the northeast monsoon, while the second dry season is characterized as the dominance of the southwest monsoon. The first wet season in the country occurs in the spring change of the monsoon system, while the second wet season occurs during the autumn change of the monsoon system. The monsoon seasons in Somalia are usually windy but dry. The Northeast Monsoon stars from December through March, producing some rainfall in the highlands. This season is locally called *Jilaal*. During the Jilaal season, the maximum temperature varies from 27ºC in the highlands to 43ºC in the center of the southern. During this period, the ITCZ is in the southern hemisphere, and the whole country is under the effect of the dry north-easterlies.

The spring transition, locally named *GU* season, starts from April to June. During this season, conditions are at their most destructive, with low clouds, rains and

thunderstorms detected mainly in the south. The temperature of this season varies from 27°C in the south to 38°C in the northern, especially in coastal areas. During that period, most of the country obtains precipitation. The ITCZ is over Somalia, and the southeast trades are warm enough to get moisture from the Indian Ocean. If precipitations are weighty, overflowing can occur in the low-lying places along the annual and seasonal rivers.

The southwest monsoon, which starts from July to September, gets a return to a few showers of rain over the southern parts of the country with sustained, powerful winds, blowing dust, and sand. This season locally is called ***Hagaa*** season. The temperature of this season ranges from 27°C in the south to over 38°C along the Gulf of Aden. During this period, the ITCZ is in the northern portions of Somalia, and the coastal zones receive what is known as coastal rains.

The fall transition term, locally named the ***Deyr*** season, starts from October to November and forms the second and shorter precipitating season. The Arabian ridge amplifies and expands approximately southwest from Arabia towards the equator during this period; this forms a weak zone of diverging winds. Those winds on the ridge's eastern side may merge with the weakening southeast monsoons over the central portions of Somalia, carrying slightly intense precipitation over these places. If precipitations are weighty, flooding can happen in the low-lying places along the annual and seasonal rivers. The northern part of the country is under dry air from the Arabian Peninsula and thus obtains less precipitation (Mutua, Francis M. – Balint, 2009).

3.4   Shabelle River Basin

Shabelle and Juba Rivers basins are transboundary river basins in the Horn of Africa, drained from Ethiopia and then through Kenya and Somalia. These two rivers can describe almost all of Somalia's surface water resources, whereas Somalia's runoff contribution to these rivers usually is minimal or almost negligible. Both Shabelle and Juba Rivers are critical freshwater sources in southern Somalia, and people are strongly dependent on these rivers. Water resources in both rivers are used for agricultural, livestock, and domestic water demands. The people who live along the Shabelle and Juba River basins produce almost all the crops and vegetables consumed across the country.

Also, they contribute two-thirds of livestock in the country. In addition, some of the crops and livestock are exported, which brings in much income for the country.

Shabelle River basin is more prominent in size and is longer than the Juba River, as shown in Figure 3.2. However, the Juba River has higher annual runoff and flow than the Shabelle River due to geological and climatic conditions in the catchment. The two rivers recharge groundwater aquifers in the southern areas, and together these two water sources feed the extended agricultural and livestock, pastoralist activities, ecosystems and local inhabitants.

Shabelle River rises on the eastern Ethiopian highlands' eastern sides, and the highest point is 4,230 m. The total catchment area of the river at its junction with the Juba River is about 297,000 km^2, two-thirds of the catchment area (188,700 km^2) of which lies in Ethiopia, and the rest area (108,300 km^2) is in Somalia. Shabelle River basis elevation ranges from roughly 20 m above sea level in the south of Somalia to over 3000 m on the Eastern Ethiopian highlands (Basnyat, 2009).

The Shabelle River enters from Somalia at Baledwayne city and is extended over six regions and 22 districts. The primary regions and districts extended by the Shabelle basin in Somalia are the Hiran region (Baledwayne, Bulo-Burti, Jalalaqsi), Middle Shabelle region (Shabelle Cadale, Balcad, Jowhar), Lower Shabelle region (Afgooye, Qoryooley, Marka, Kurtuwaarey, Sablaale, Baraawe, Wanla Wayne). Table 3.1 summarizes the characteristics of the Shabelle river basin at Baledwayne City (Basnyat, 2009).

Table 3.1. Shabelle River catchment characteristics in Baledwayne City

Basin Location	Catchment Area (km^2)	Elevation (m)	Annual Maximum (m^3/s)	Annual Minimum (m^3/s)	High-Risk Levels (m)	Bank Full (m)
Baledwayne	207,488	182	473.6	138.5	7.30	8.30
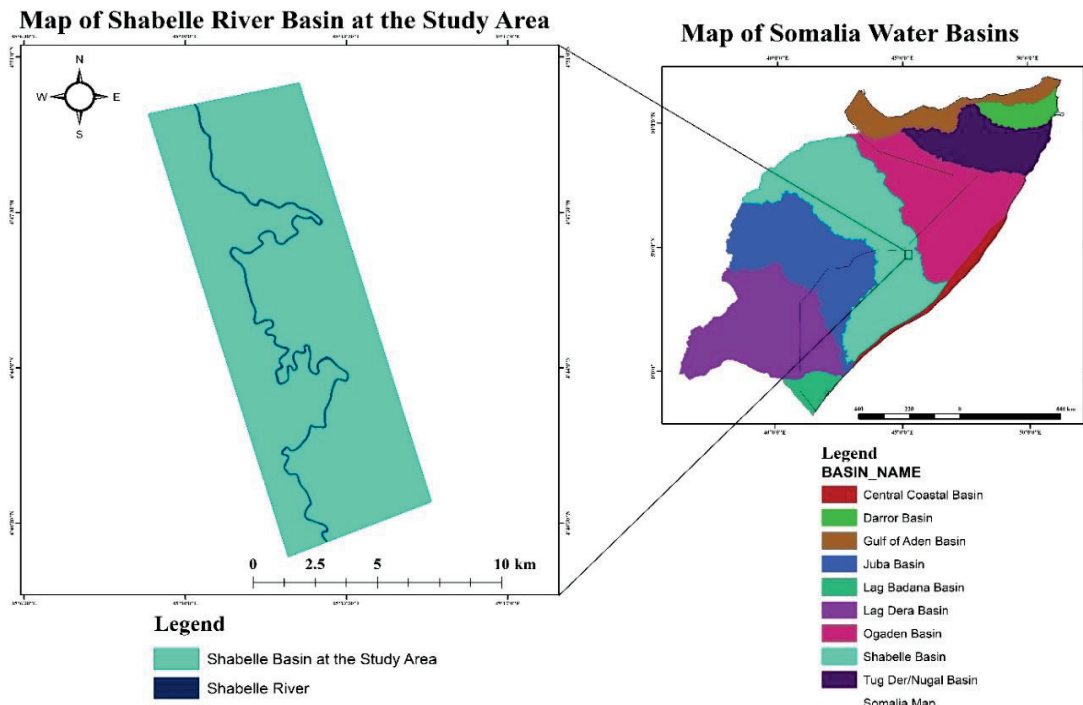
Figure 3.2. Map of Shabelle River basin at the Study Area

3.5   Geology

The geology of the study area is formed from the outcropping of complex metamorphic basements, such as granite and migmatite. Besides that, sedimentary rocks such as sandstone, limestone, and gypsiferous limestones were found. Also, Fluvial deposits, mainly consisting of sandy clay, gravel, and sand, were seen along the Shabelle River basin in the study area (Sebhat, M. Y., & Wenninger, 2014).

3.6   Land Cover Land Use

The land cover of the study area has the following characteristics, as shown in Figure 3.3:

1- The natural water body covered in the study area is the Shabelle River valley, which transverse the undulating morphology of the area.

2- Natural trees, grass, scrub and shrub and vegetation, have covered some areas of the study area.

27

3- Agricultural lands and crop fields (both rainfed and irrigated agriculture crops) cover most of the study area.

4- Urban and residential areas, Bare grounder are some of the other cover types of the study areas.

The land use of the study area includes farming, grazing and wood gathering for cooking and building. Camels, cattle, goats and sheep graze in the rangelands of Shabelle River catchments. Grasslands, bushlands and natural vegetations are examples of land cover associated with this land use. The farmers in the study area combine animal husbandry with crop production. They manage to keep lactation animals such as cattle and camels, with a few goats and sheep near their homes. At the same time, non-lactating animals have been herded further away from their houses. On the other hand, rainfed and irrigation farmers raise a fair quantity of livestock, mainly cattle, goats and small ruminants. The farmers in the study area utilize their animals for many purposes, such as milk and meat production, livestock trading, agricultural traction and animal manure which they use as a fertilizer to increase soil productivity. They feed their animals from the corn and maize stover, crops or food leftovers. Farms use the Shabelle River as a primary source of watering their animals and irrigating their agricultural land. There are a few boreholes and hand-dug wells in the study area; thus, farmers mainly use groundwater as drinking water.

The landform of the study area can be categorized into four groups as shown in Figure 3.4, alluvial plain, frequently inundated floodplain, episodically inundated floodplain and low gradient footslope. Table 3.2 summarises the types of Landcover at Baledwayne City (Karra et al., 2021).

Table 3.2. Types of Landcover at Baledwayne City

Type of Land Cover	Area (km^2)	Percentage (%)
Agricultural lands (Rainfed and irrigated agriculture crops)	63.72	54.4
Trees (e.g., dense vegetation and wood, wooded vegetation)	3.72	3.18
Scrub and Shrub (e.g., sparse shrubs and savannas grass)	30	25.61
Urban and Residential Areas	16.63	14.2
Bare Ground (e.g., exposed rock or soil and dunes)	0.26	0.22
Waterbody (Shabelle River valley)	2.75	2.35
Grassland (e.g., open savanna and pastures)	0.05	0.04

Land Cover Land Use of the Study Area

Land Cover Land Use of Hiran Region
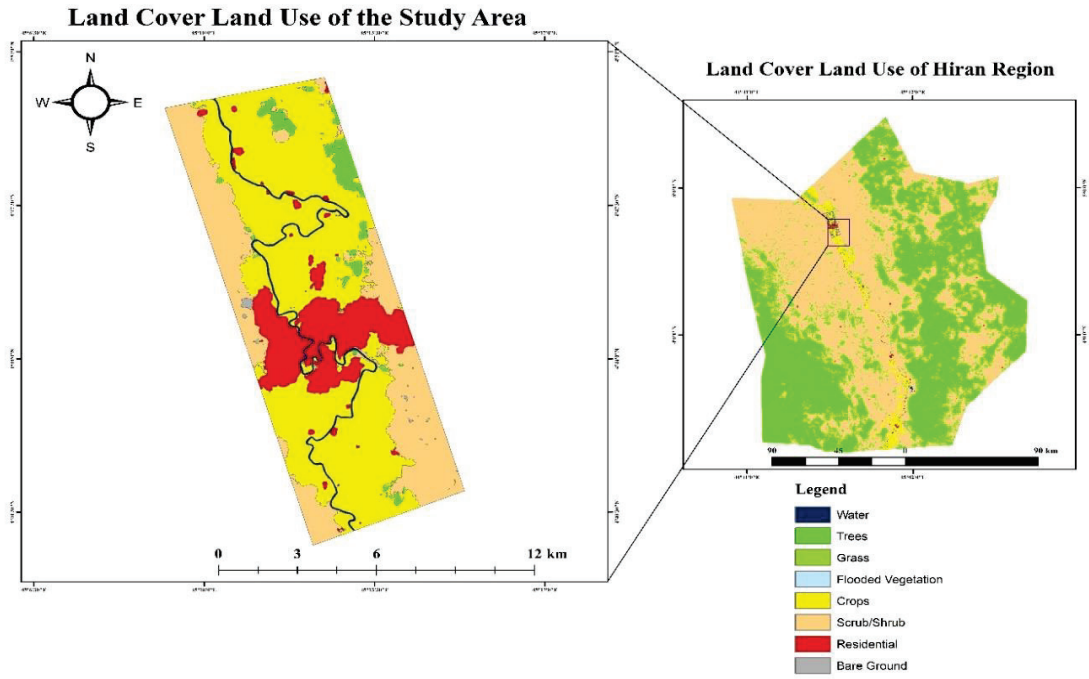
Figure 3.3. Map of Land Cover Land Use at the Study Area

Map of Study Area Landforms

Map of Hiran Region Landforms
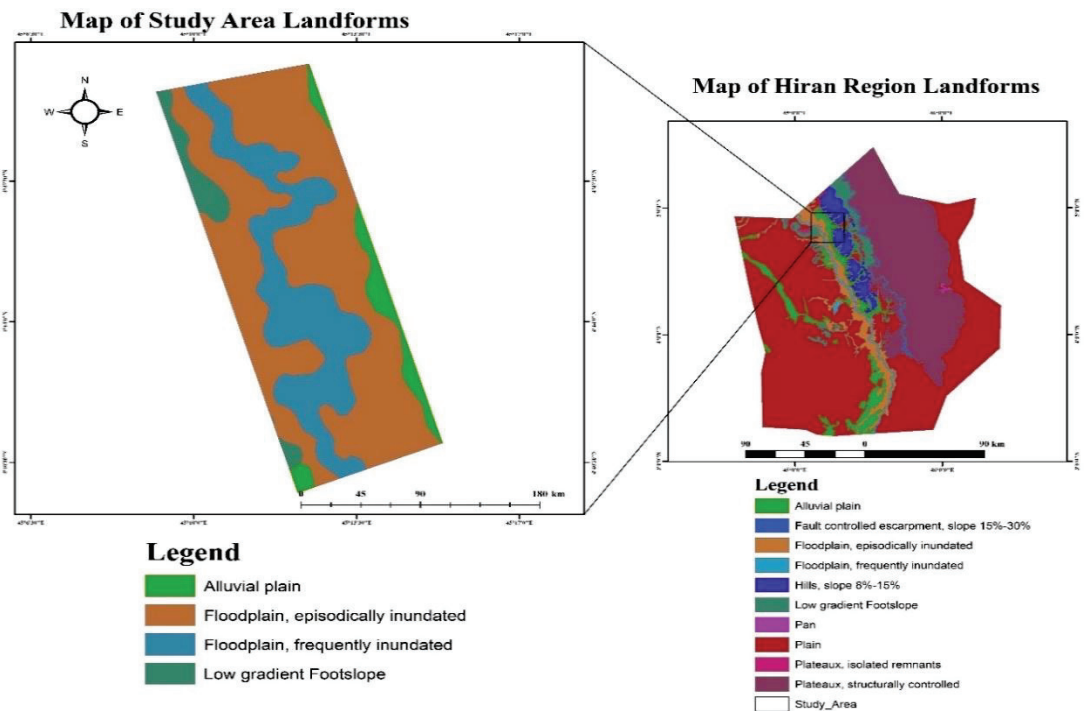
Figure 3.4. Map of Landforms at the Study

3.7   Soil Properties

The climate of the Baledwayne city is described as a semi-arid climate and has little effect on the soil formation process of the area. This effect lightly led the study area to share common characteristics of soil such as heavy texture (clay), poor drainage and low permeability in some areas. Fluvisols type is the primary soil type in the study area, as shown in Figure 3.5. Fluvisols are generally immature soils in alluvial, lacustrine, deltaic, or marine sediments, and they can be found worldwide (ISRIC - World Soil Information, 2020). This type of soil generally starts 25 cm depth from the soil surface and reaches not less than 50 cm depth from the soil surface. Fluvisols soil of the study area is found commonly on the Shabelle River floodplains. This type of soil is suitable for cultivating dryland crops and grazing in the dry season. Different fluvisols soil are found in the study area such as Calcic Fluvisol, Haplic Fluvisol. The other soil types found in the area include Calcisols, Vertisols, Regosols, and Leptosols. Table 3.3 summarizes the soil type and landscape found in the study area (FAOSWALIM, 2019).

Table 3.3. Soil type and landscape at Baledwayne City

Soil Type	Landscape	Area (km^2)	Percentage (%)
Calcic Fluvisol (Siltic) / Calcic Mazic Vertisol (Calcaric)	Alluvial Plain	39.21	34
Haplic Fluvisol (Calcaric, Clayic)	Floodplain (Meandering River plain)	57.08	49.4
Haplic Calcisol (Siltic, Chromic)	Piedmont (Alluvial fan)	0.94	0.8
Hyperskletic Laptosol (Aridic)/ Haplic Regosol (Skeletic)	Hilland	7.85	6.8
Haplic Calcisol (Siltic, Chromic)	Piedmont (Alluvial fan)	1.4	1.2
Calcic Mazic Vertisol (Pellic)	Alluvial Plain	5.45	4.7
Lithic Leptosol (Aridic) Epileptic Calcisol (Aridic, Siltic)	Lateral valley (River plain)	0.43	0.4
Haplic Regosol (Skeletic, Calcaric)	Hilland	3.09	2.7
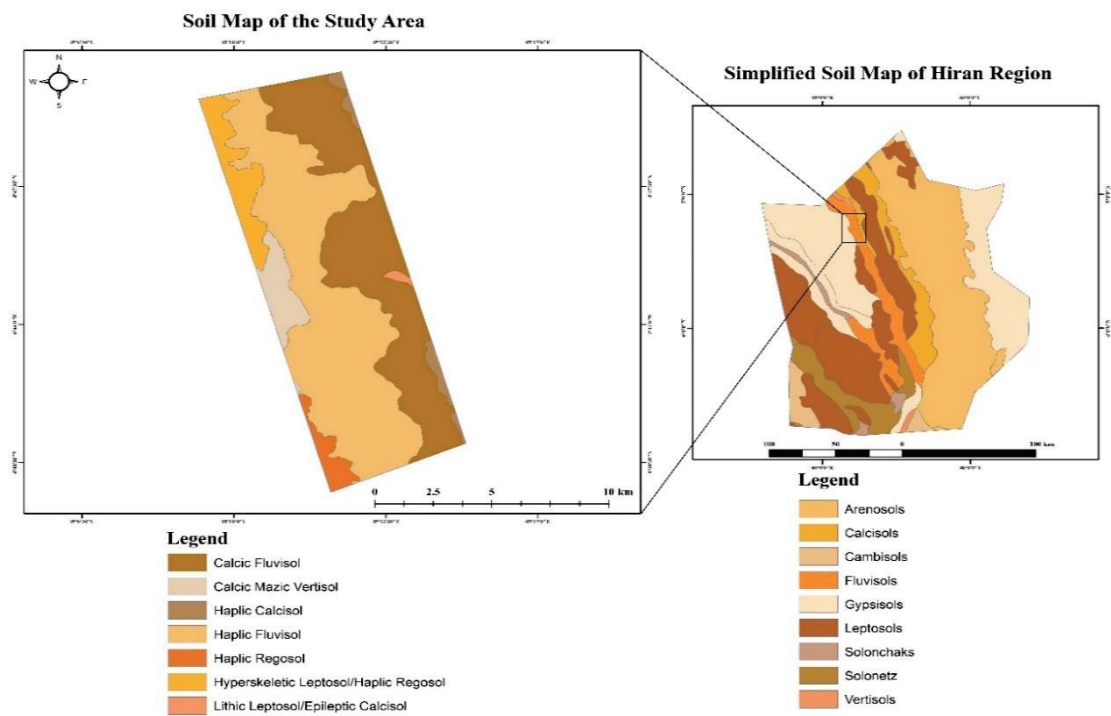
Figure 3.5. Soil Map of the Study Area

3.8 Used Data

This study applied different datasets. The selection and usage of data were governed by the hydrological and hydraulic models used in this study. The raw data used in this study include topography data (DEM and DTM), as shown in Figure 3.6. Also, Geology data, soil properties, land use & land cover data, and hydrometeorological data (precipitation, observed flow rate and water level) were used in this study. Besides that, this study used unprocessed satellite imagery from Google Earth Pro and GIS format data from SWALIM.
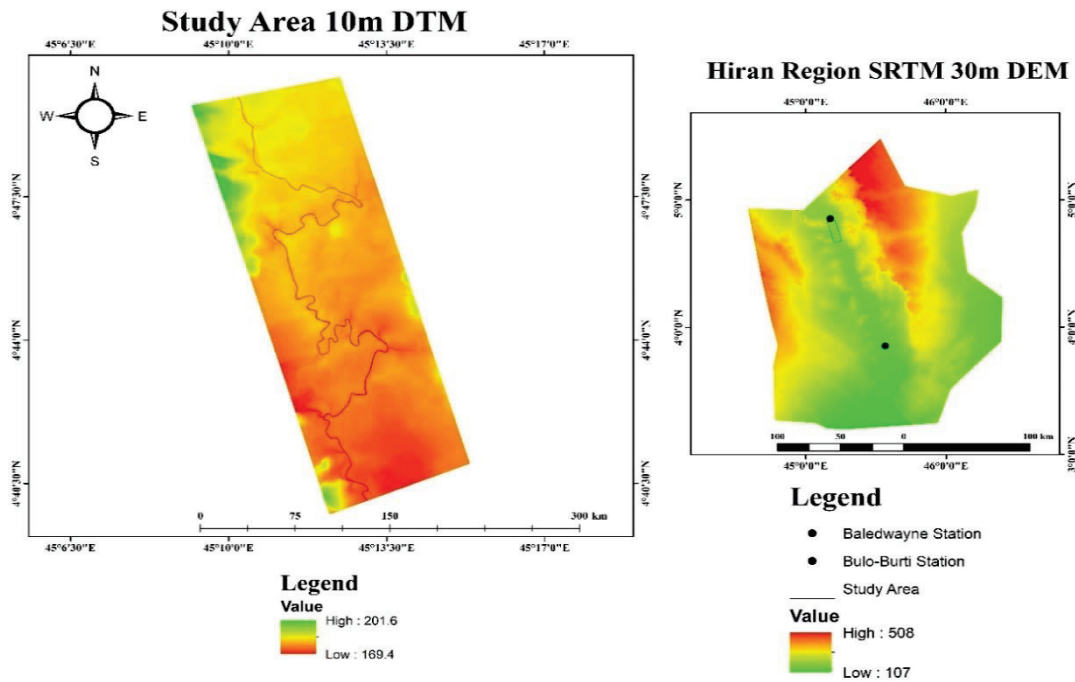
Figure 3.6. The DEM and DTM of the Study Area

3.8.1 Topographic Data

The Digital Elevation Model (DEM) data was obtained from the Regional Centre for Mapping of Resources for Development (RCMRD), with a resolution of 30 m, as shown in Figure 3.6. The DEM terrain is used for delineating the watershed and generating the stream network and sub-catchments in the Hydrological Model. The Digital Terrain Model (DTM) is obtained from SWLIM with a pixel size of 10 m, as shown in Figure 3.6. The DTM terrain was used in Hydraulic Model to extract the geometry 1D and 2D data, including the centerline and banks of the river, elevation and slope of the 2D areas.

3.8.2 Stream Flow Rate and Water Level

This study used a daily series of flow rates and the water level of the Shebelle River at Baledwayne city and Bulo-Burti town stations. The data was obtained from

SWALIM and is available in SI unit format. Due to the civil wars in the country, all the hydrometeorological monitoring networks collapsed. In 2006, the Ministry of Agriculture of Somalia, with the support of technical expertise from the SWALIM, put efforts to re-establish the monitoring network and recover all available data. Only they succeeded in recovering data from 1963 to 1990 and from 2002 to the present day. The Data available for the Shabelle River were obtained from two gauging stations located at the main river, namely, Baledwayne and Bulo-Burti. The 2019 daily discharge of Baledwayne and Bulo-Burti stations, as shown in Figure 3.7, were used in the hydrological model. The maximum discharge of Baledwayne and Bulo-Burti stations is 470.1 m^3/s and 419.42 m^3/s, whereas the minimum at the two stations is 1.98 m^3/s and 1.55 m^3/s, respectively.
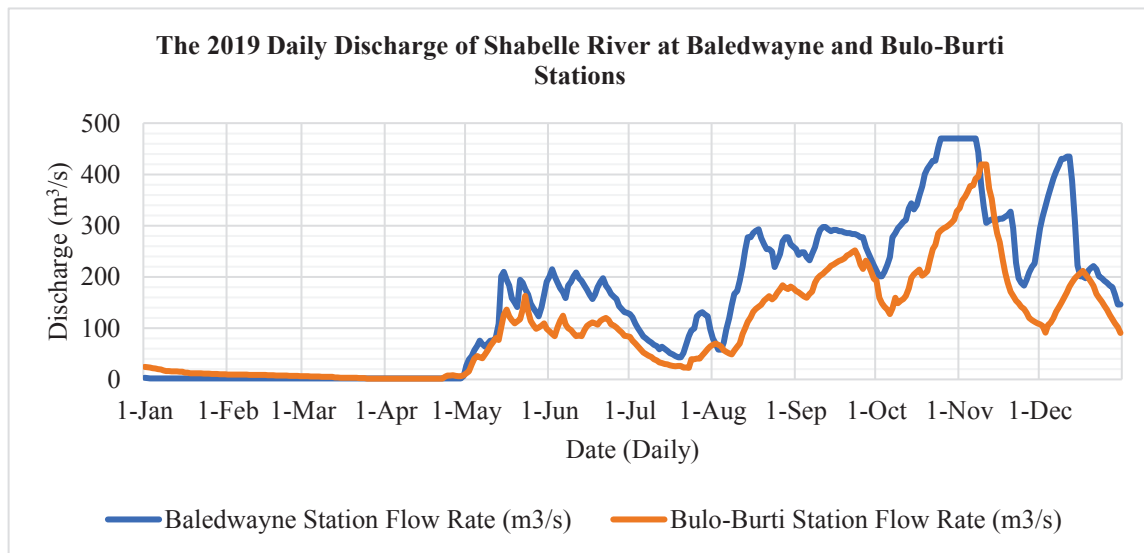
Figure 3.7. The 2019 Daily Discharge of Shabelle River at two stations

3.8.3 Precipitation Data

Daily series of rainfall data at Baledwayne and Bulo-Burti were used in the hydrological model. The data was obtained from SWALIM, and it is available in SI unit format. The 2019 daily rainfall of Baledwayne and Bulo-Burti stations was used in the hydrological model. The annual rainfall of Baledwayne and Bulo-Burti stations is 468.5 mm and 406.5 mm, respectively. Figure 3.8 shows annual rainfall data observed at meteorological gauge stations in Baledwayne and Bulo-Burti. Besides the streamflow,

water level and precipitation data, there are other data used in the study. Table 3.4 summarizes the type, source, and description of used data in this study.
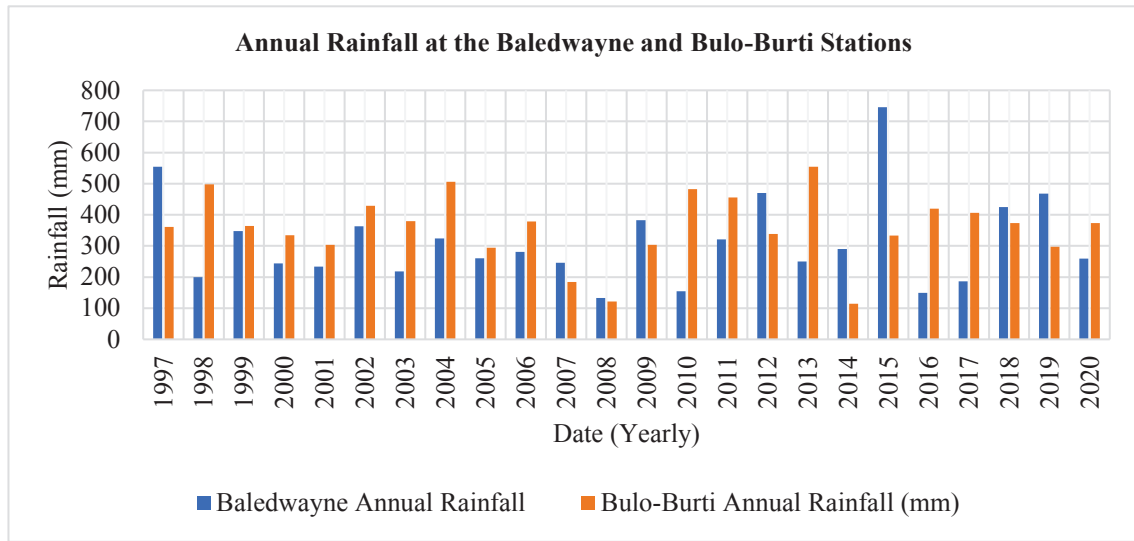
Figure 3.8. Annual Rainfall of Baledwayne and Bulo-Burti stations

Table 3.4. Summary of used data in this research

Data Type	Source	Usage
Hiran region SRTM DEM 30 meters	RCMRD	It is used in the HEC-HMS model for hydrological analysis to delineate the watershed in the study area.
Daily rainfall series 2019 at Baledwayne and Bulo-Burti stations	SWALIM	It is used in the HEC-HMS model for hydrological analysis to simulate rainfall-runoff hydrograph.
Daily Discharge series 2019 at Baledwayne and Bulo-Burti stations	SWALIM	It is used in the HEC-HMS model for hydrological analysis to calibrate the model results.
Soil type and properties at Baledwayne and Bulo-Burti stations	SWALIM	It is used in the HEC-HMS model for hydrological analysis to extract the infiltration parameters.
Observed annual discharge at Baledwayne station from 2002 to 2020	SWALIM	It is used in the HEC-SSP model for flood frequency analysis to generate different flood return periods.
Baledwayne DTM 10 meters	SWALIM	It is used in the HEC-RAS model for hydraulic analysis to extract all geometry parameters in the study area.
The 2020 Land cover land use of 10m resolution.	ESRI	It is used in the HEC-RAS model for hydraulic analysis to extract Manning's Roughness Coefficients in the study area.
Observed Deyr 2019 River Level at Baledwayne station	SWALIM	It is used to calibrate the Model output River Level at the study area.
Observed Deyr 2019 Flood Map	SWALIM	It is used to compare the output inundation map in the study area.

3.9   Homogeneity Test of the Data

The quality of historical hydrometeorological data was screened and checked using Rainbow software. The software tests the homogeneity of the data and analyses the hydrometeorological frequency analysis of historical data sets. The software uses to cumulative deviations method (Buishand, 1982)to test the homogeneity of data, and it is based on modified partial addition or cumulative deviations from the mean:

$$S_k = \sum_{i=1}^{k}(x_i - \bar{x}) \tag{1}$$

$$k = 1,2,3 \dots., n \tag{2}$$

Where X_i is the recorded from the series X_1, X_2, …, X_n and $\bar{X}$ the mean, S_k has values from 0 to n. The plot of S_k is also known as the residual mass curve, which can easily detect any changes in the mean. For a record X_i above average, the $S_k = i$ increases, while for a record below average $S_k = i$ decreases. The homogeneity of the data is rejected with respectively 90, 95 and 99% probability when the deviation crosses one of the horizontal lines (Raes, D., Willems, P., & Gbaguidi, 2006). The flow rate data set of the Shabelle River station at Baledwayne city, which ranges from 2002 to 2020, was used in the Rainbow software. As shown in Figures 3.9, the rejection of the probability shows that the data set is good and homogenous.
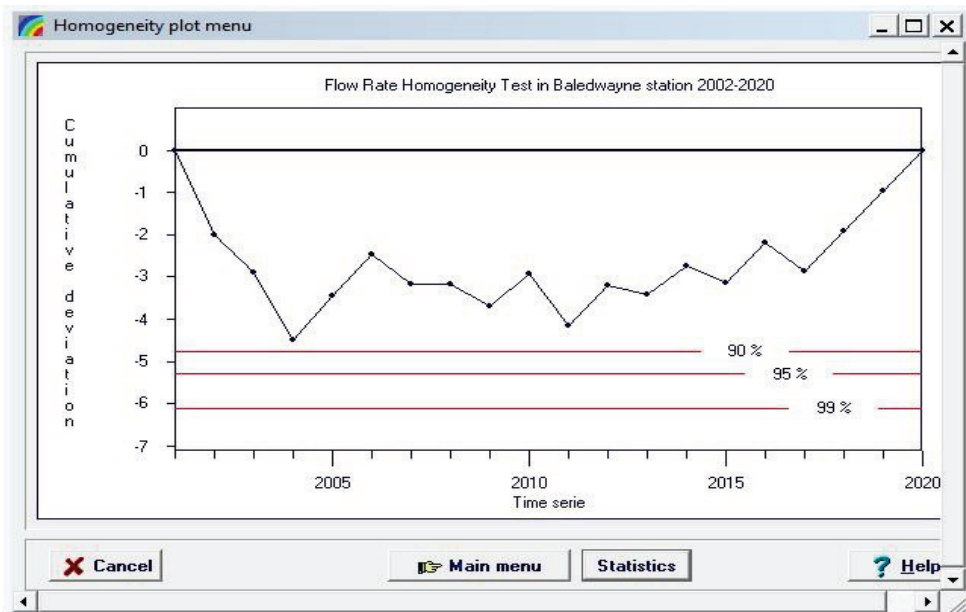
Figures 3.9. Homogeneity Test of flow rate for the Shabelle River
at Baledwayne Station

CHAPTER 4

METHODOLOGY AND RESULTS

4.1 General Methodology

The general methodology of this study is summarized in Figure 4.1.
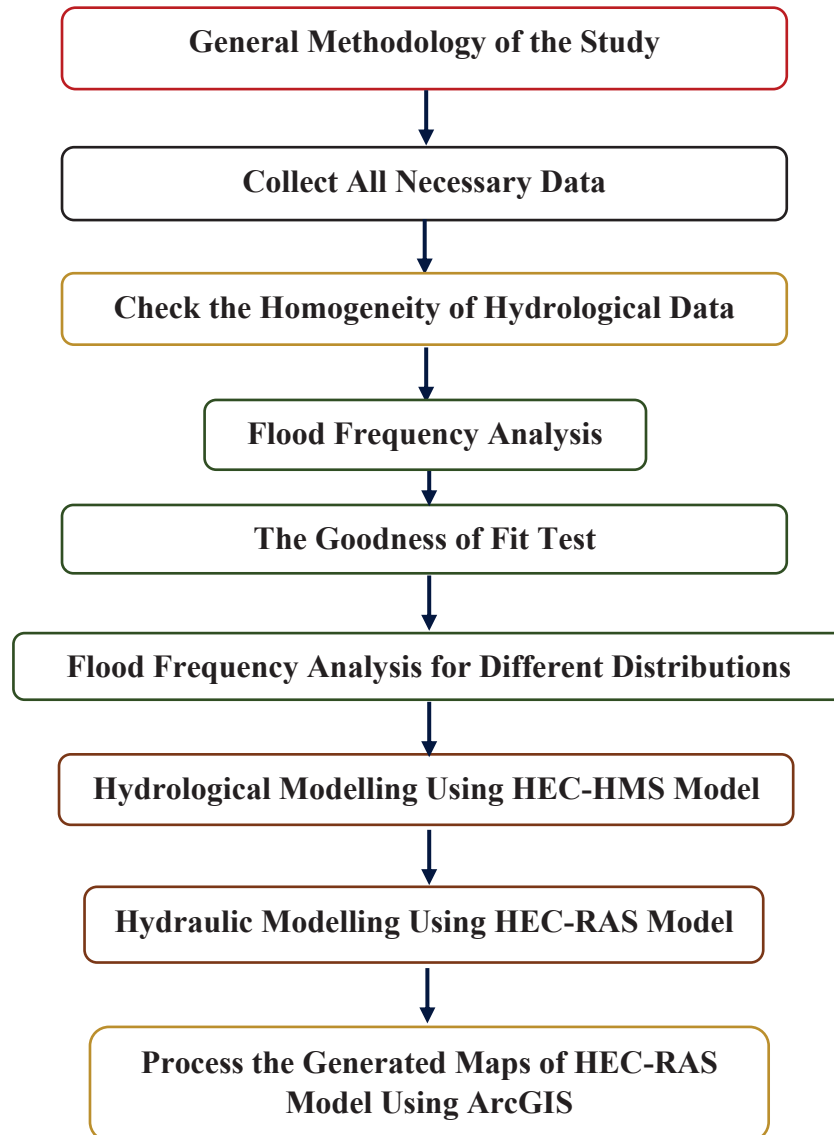
Figure 4.1. General Methodology of this Study

4.2 Flood Frequency Analysis

Flood frequency study predicts the flow corresponding to a specific return period along a river channel. Gumbel was introduced in the 1950s using statistical frequency curves to overflows by utilising yearly peak discharge data and has been known for several years. The flood frequency estimation utilises the calculation of statistical parameters such as standard deviation, mean and skewness to generate frequency distribution diagrams. Different frequency distribution methods include Lognormal, Normal, Gumbel, Exponential, and Log Pearson Type 3. Behind selecting the probability distribution best fits the maximum yearly discharge data, flood frequency curves can be plotted to evaluate the design discharge values compared to typical return periods, which is vital for future hydrologic planning and designing purposes (Rumsby, 1991).

Flood frequency analysis estimates maximum design flow values with a specified return period, which is essential for designing hydraulic structures, for example, dams, culverts, bridges, levees, channels, drainage systems and other structures. It is necessary to use flood frequency analysis to estimate the most suitable layout specification for the hydraulic designs to discourage under-designing or over-designing. Besides that, flood frequency analyses are valuable for flood zoning activities and insurance. Eventually, accurate flood frequency analysis enables engineers to design safe structures and protect against financial losses due to the maintenance of structures (Calver et al., 2009).

4.2.1 Normal Distribution

This distribution derives from the middle limit formula and describes a series of arbitrary variables X_i which is separately distributed with mean μ and variance $σ^2$, the distribution of the aggregate of n such arbitrary variables, $Y = \sum_{i=1}^{n} X_i$, leans to the normal distribution with average $nμ$ and variance $nσ^2$ while n gets big. The critical idea is that what the ever value of probability distribution function of X is. So, for instance, the probability distribution of the mean sample $\bar{x} = \frac{1}{n}\sum_{i=3}^{n} x_i$, can be compared to normal with mean n and variance $\left(\frac{1}{n}\right)^2 nσ^2$ in no case what the distribution of X is. The hydrological parameters, for example the yearly rainfall, computed as the totality of the impacts of several independent happenings, tend to pursue the normal distribution. The

major constraints of this distribution for representing hydrologic variable quantity are that it ranges more than a infinite range **[-∞, ∞]**, although the majority of the hydrologic variable quantity are nonnegative, as well as it is symmetric around the mean. In contrast, hydrologic data have a tendency to be skewed (Chow et al., 1988).

The normal distribution is one of the methods utilised in frequency calculation for fitting empirical distribution to the observed hydrological data, for example, maximum annual discharge. The following equation calculates the predicted discharge values with a specified return period using the normal distribution method.

$$Q_p = \mu + K_T \delta \qquad (4.1)$$

Q_p in m^3/s is the predicted discharge values of a specific return period, μ is the mean of the arithmetic mean of the sample, K_T is the frequency factor and δ is the standard deviation of the sample.

$$\mu = \bar{x} = \frac{x_1 + x_2 + x_3 + \cdots\cdots x_n}{n} = \frac{1}{n}\sum_{i=1}^{n} x_n \qquad (4.2)$$

$$\delta = \delta_x = \sqrt{\frac{\sum(x_i - \mu)^2}{n}} \qquad (4.3)$$

$$K_T = w - \frac{2.515517 + 0.802853w + 0.010328w^2}{1 + 1.432788w + 0.189269w^2 + 0.001308w^3} \qquad (4.4)$$

$$w = \left[ln\left(\frac{1}{p^2}\right) \right]^{1/2} \qquad (4.5)$$

n is the number of terms, where P is the probability factor of the required return period (T) in percentage; P=1/T (%).   Where   (0<P≤0.5)

4.2.2 Lognormal Distribution

If the arbitrary variable quantity $Y = log(X)$ exists normally distributed, and the X is expressed as lognormal distributed. Chow (1954) concluded that this distribution applicable to hydrologic variable quantity originated as the products of other variable quantity   since   if $X = X_1 + X_2 + X_3 + \cdots\cdots\cdots + X_n,$ then $Y = log(X)$ =

39

$\sum_{i=1}^{n} log\,(x_i) = \sum_{i=1}^{n}(y_i)$ which leans to the normal distribution for a significant value of n provided that the X_i are independent and identically distributed. The lognormal distribution has been discovered to explain the distribution of hydraulic conductivity in a porous medium, such as the distribution of raindrop sizes in a storm and other hydrologic variables. (Freeze, 1975). The lognormal distribution has benefits over the normal distribution due to its bound (X > 0). The log transformation reduces the positive skewness generally observed in hydrologic data for the reason that taking the logarithms tends to reduce significant digits proportionately over small numbers. The limitation of this distribution is that it needs the logarithms value of the data series to be symmetric just about their mean.

The Lognormal distribution has the same formula and procedure as the Normal distribution, except it needs applying the logarithms value of the variable quantity to their mean ($\bar{y}$) and standard deviation (δ_y) of the data (Chow et al., 1988).

$$Q_p = Y_T = \bar{y} + k_T \delta_y \qquad (4.6)$$

$$Y = log(X) \qquad (4.7)$$

4.2.3 Extreme Value Distribution

In this distribution, extreme values of the data set are selected. For instance, the yearly maximum flow rate at a provided location is the most significant historical recorded flow rate value for the period of a year. The yearly maximum flow rate values for every year of historically recorded data make up a collection of excessive values that can be statistically calculated. Extreme value distribution (EV) has three types: Type I, II, and III. In 1928, Fisher and Tippett converged on one of three structures of extreme value distributions after the quantity of chosen extreme values were big. The three types of Extreme Value distributions EV were further developed for the Extreme Value distribution Type I (EVI) distribution by Gumbel (1941), for the Type II (EVII) distribution by Frechet (1927), and the Extreme Value distribution Type III (EVIII) by Weibull (1939). In 1955 Jenkinson showed exceptional cases of individual distribution and called General Extreme Value (GEV) distribution. Extreme value distributions, especially the EVI, also known as the Gumbel distribution, have mainly been utilised in

hydrologic as well as meteorological analyses. For example, the projection of flood peak discharges and maximum precipitations for a specific period. EV Distribution forms the standardized procedure of flood frequency estimation in Great Britain (Natural Environment Research Council, 1975). The following equation was driven by Chow (1953) for the extreme value type I distribution (Chow et al., 1988).

$$Q_p = \mu + K_T \delta \qquad (4.8)$$

$$K_T = -\frac{\sqrt{6}}{\pi}\left\{0.67 + ln\left[ln\left(\frac{T}{T-1}\right)\right]\right\} \qquad (4.9)$$

Q_p in m^3/s is the expected discharge values along with a specific return period, μ is the mean of the arithmetic mean, K_T is the frequency factor, and δ is the standard deviation of the data.

4.2.4 Log-Pearson Type III Distribution

If log X follows a Pearson Type III distribution, then X is described to follow a log-Pearson Type III distribution. Log-Pearson Type III distribution is the standard distribution method for frequency estimation of maximum yearly floods in the USA (Benson, 1968). This distribution was developed to fit a curve to data, and it has yielded promising results in many applications in hydrologic and meteorological studies. So, it is widely used and recommended, especially for inundation peak data.

The first step in this distribution is to calculate the logarithms value of the hydrologic data set, $Y = log(X)$. The corresponding mean $\bar{y}$, standard deviation δ_y and coefficient of skewness C_s are then analyzed from the logarithms values of the data (Chow et al., 1994). The frequency factor K_T depends on value of the return period T and the coefficient of skewness C_s. While $C_s = 0$, the frequency factor equals the standard normal variable quantity K_T in norm distribution method when $C_s \neq 0$ Kite (1977) expressed the values of K_T as:

$$K_T = z + (z^2 - 1)k + \frac{1}{3}(z^3 - 6z)k^2 - (z^2 - 1)k^3 + zk^4 + \frac{1}{3}k^5 \qquad (4.10)$$

$$k = \frac{C_s}{6} \tag{4.11}$$

Where the coefficient of skewness C_s can be found as:

$$C_s = \frac{n \sum_{i=1}^{n}(y_i - \bar{y})}{(n-1)(n-2)\delta_{\bar{y}}^3} \tag{4.12}$$

So, the expected discharge values with a specific return period Q_p in m³/s can be calculated as:

$$q_p = Y_T = \bar{y} + k_T \delta_y \tag{4.13}$$

$$Q_p = 10^{Y_T} \tag{4.14}$$

4.2.5 The Goodness of Fit Test (GOF)

GOF test is used to check whether a particular distribution fits a given data set. Applying statistical parameters, the excellence of fit for the observed data set is ranked. The GOF of a probability distribution can be checked by comparing the theoretical and the cumulative frequency function or sample values of the relative frequency. The most widely used methods for GOF tests are Kolmogorov–Smirnov (KS), Chi-squared and Anderson–Darling (AD) tests (Samantaray & Sahoo, 2020).

4.2.5.1   Kolmogorov–Smirnov (KS) Test

This test is based on the empirical cumulative distribution function (ECDF) and is utilized to decide if a sample comes from a hypothesized continued distribution. The empirical CDF is given by

$$F_n(x) = \frac{1}{n} \cdot [Number\ of\ Observations \leq x] \tag{4.15}$$

The Kolmogorov–Smirnov test statistic (K) can be calculated from the prevalent perpendicular difference in hypothetical and experiential CDF:

$$K = \frac{max}{1 \leq i \leq n} \left[F(x_i) - \frac{i-1}{n}, \frac{i}{n} - F(x_i) \right] \tag{4.16}$$

42

The hypothesis about the distributional form is denied at the selected larger values (α) if the test statistic, K, is larger than the critical value received from table 4.1.

Table 4.1. Critical values of different GOF tests for number size (n)of 19.

The goodness of Fit Test	Alpha (α)				
	0.20	0.10	0.05	0.05	0.01
Kolmogorov–Smirnov	0.237	0.271	0.301	0.337	0.361
Anderson–Darling	1.375	1.929	2.502	3.289	3.907

4.2.5.2   Chi-Squared Test

This GOF test decides if a sample comes from a population with a typical distribution. This test is used to bin data, so the value of the test statistic relies on how the data set is binned. The Chi-Squared statistic test is given as:

$$X^2 = \sum_{i=1}^{k} \frac{(O_i - E_i)^2}{E_i} \qquad (4.17)$$

Where O_i is the observed frequency, i is the observation number, and E_i is the expected frequency and is given by:

$$E_i = F_{(x_2)} - F_{(x_1)} \qquad (4.18)$$

F is the cumulative distribution of the probability distribution being tested, and x_1, x_2 are the limits of bin i where the following formula can be used for the number of bins (K):

$$K = 1 + log_2 n \qquad (4.19)$$

Where n is the sample size.

4.2.5.3   Anderson–Darling Test

This test is generally used to evaluate the fitness of an observed cumulative distribution function CDF in order to predicted cumulative distribution function CDF. This GOF method provides additional value to the tails compared to the Kolmogorov-Smirnov test method. The following formula is given the Anderson-Darling Test.

$$A^2 = -n - \frac{1}{n}\sum_{i=1}^{n}(2i - I) \cdot \left[\ln F(X_i) + \ln\left(1 - F(X_{n-i+1})\right)\right] \qquad (4.20)$$

The hypothesis about the distributional form is rejected at the selected significance level (α) if the test statistic, A^2, is more than the critical value received from a table 4.1.

4.2.6 Parameter Estimation Methods

There are many methods used to estimate parameters in flood frequency analysis. However, the most widely used methods include maximum likelihood estimation (MLE) and the method of moment (MOM).

The MLE is the most theoretically accurate method of fitting probability distributions, and it generates most efficient parameter estimation for evaluating the population parameters with the minimum average error. However, there is no analytical solution for all the parameters in terms of sample statistics for some probability distributions, so the log-likelihood function have to be numerically increased, and this may be problematic.

The MOM is more accessible to apply than the maximum likelihood method and more appropriate for practical hydrologic investigations, such as flood frequency analysis that begins with estimating the statistical parameters needed for a suggested probability distribution through the method of moments from the provided data (Chow et al., 1988).

4.2.6.1 Maximum Likelihood Estimation Method (MLE)

This method was established by R. A. Fisher (1922). This method states that the best parameter number of a probability distribution function (PDF) must be that number that maximizes the likelihood or the common probability of amount from the observed data. However, many probability density functions (PDF) are exponential functions, so it is from time to time more suitable to perform with the log-likelihood function as given in this equation:

$$ln\,L = \sum_{i=1}^{n} ln\,[f(x_i)] \qquad\qquad (4.21)$$

$f(x_i)$ is the exponential probability density function for a given value of x_i.

4.2.6.2 Method of Moment Method (MOM)

The Method of Moment (MOM) was established by Karl Pearson (1902). In this estimation of the parameters method, the probability distribution function (PDF) is obtained by comparing the moments of the model with the moments of the probability distribution function (PDF). Pearson considered first that reasonable evaluations of the parameters of a probability distribution are those for which moments of the probability density function about the center are equal to the equivalent moments of the observed data (Chow et al., 1988). The first moment of observation has the corresponding the centroid of the probability density function and is given by

$$\mu = \int_{-\infty}^{\infty} x f(x)\, dx \qquad (4.22)$$

Similarly, the second and third moments of the probability distribution can be set equal to their sample values to estimate the parameters values of the probability distribution function. Pearson initially considered only moments about the origin, but afterwards, it became standard to estimate the second and third parameters of the distribution (Vivekanandan, 2015). The following formula estimates the variance as the second central moment (σ) and the coefficient of skewness as the standardized third central moment (γ).

$$\sigma^2 = E[(x - \mu)^2] \qquad (4.23)$$

$$\gamma = \frac{E[(x-\mu)^3]}{\sigma^3} \qquad (4.24)$$

4.2.7 Used Date for Flood Frequency Analysis

Observed maximum annual discharge of Shabelle River at Baledwayne station was used for flood frequency analysis. The data set utilized in this analysis ranges from 2002 to 2020, as shown in Figure 4.2. The maximum annual discharge value is 477.16 m³/s, and it was observed in 2005, whereas the minimum annual discharge value is 197.34 m³/s, and it was observed in 2002. The goodness of fit test was conducted utilizing the EasyFit software to determine the best-fit distribution method for flood frequency

analysis. To calculate maximum flood discharges with specific return periods of different distributions, the HEC-SSP model was used.
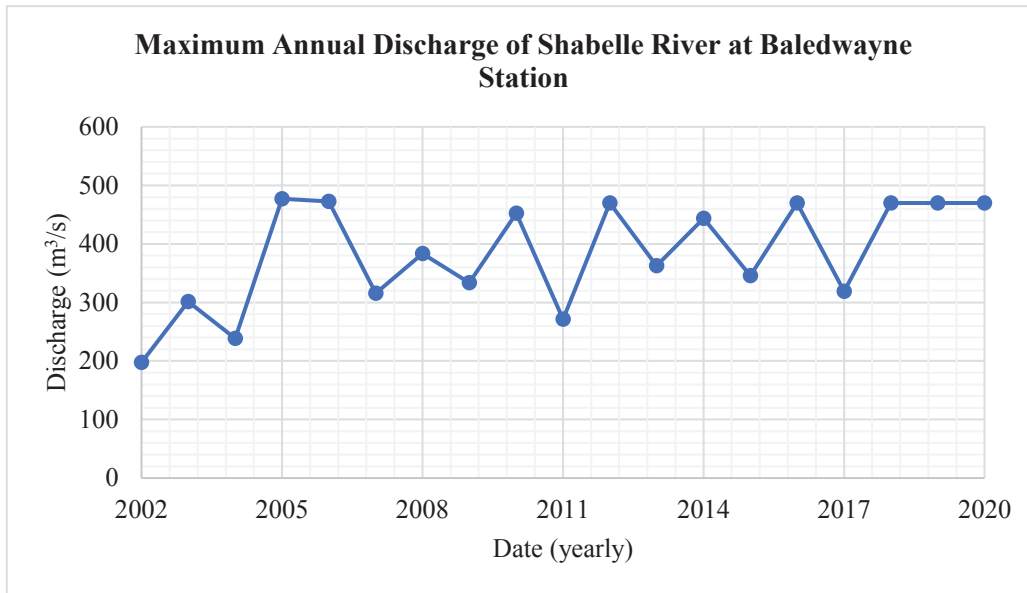
Figure 4.2. Maximum Annual Discharge of Shabelle River at Baledwayne Station.

4.3   EasyFit Software

EasyFit software is a fitting distribution application that facilitates probability data analysis and best model preference. It allows to efficiently and quickly decides the probability distribution that fits best to the data set. This model supports over 40 continuous and discrete distributions. EasyFit calculates the GOF statistics for each fitted distribution using Kolmogorov-Smirnov (KS), Anderson-Darling and Chi-Squared tests. Then, it ranks all the distributions and displays them in the form of a hypertext report. The software utilizes one of the following parameter estimation methods for every supported distribution: method of moments (MOM), maximum likelihood estimates (MLE), method of L-moments and least-squares estimates (LSE).

The annual maximum observed discharge of Shabelle River at Baledwayne station is input data in this software. The data ranges from 2002 to 2020 (see Appendix A). Different flood distribution methods were used to select the probability distribution that best fits the data set. These distributions include the General Extreme Value, Log-Pearson 3, Normal, Log-Normal, and Gumbel-Max distributions. The GOF of each distribution was tested and ranked according to their best-fit distribution of the data set.

The Kolmogorov-Smirnov, Anderson-Darling and Chi-Squared tests were used for the GOF test of the annual maximum observed discharge data. According to the KS test, it was observed that the General Extreme Value (GEV) is the best fitting distribution, and it ranked first place with a KS value of 0.18928. In contrast, the other distributions that fit the input data are the Log-Pearson Type III, the Normal, the Lognormal and the Gumbel Max. According to the Anderson Darling test, it is found that Log-Pearson Types III is the most appropriate distribution for all of the above distributions, whereas the GEV is ranked second. According to the Chi-square test, it is observed that the Lognormal is the most fitting distribution, and it ranked first place. Table 4.2 summarizes the best-fitting distributions according to the goodness of fit tests. Also, it shows the rank of each distribution using the GOF tests mentioned above.

Table 4.2. Goodness of Fit-Summary

No	Distribution	Kolmogorov Smirnov		Anderson Darling		Chi-Squared	
		Statistics	Rank	Statistics	Rank	Statistics	Rank
1	GEV	0.18982	1	0.8949	2	0.84358	5
2	Gumbel Max	0.26221	5	1.5234	5	0.04585	2
3	Log-Pearson 3	0.20127	2	0.85764	1	0.43793	4
4	Lognormal	0.23004	4	1.0107	4	0.0441	1
5	Normal	0.22243	3	0.96367	3	0.38642	3

According to the GOF tests, it was observed that the computed data sets fit into five commonly used probability distributions. However, according to KS and Anderson Darling tests, GEV and Log-Pearson Type III are the probability distributions that best fit the data set. The detailed results of the Goodness of Fit tests of the five distributions and parameter estimation values are shown in Appendix B.

In this study, the distribution method used for flood frequency estimation is the Log-Pearson Type III which is widely used and recommended, particularly for the flood peak data. Furthermore, this distribution has yielded good results in many applications in hydrologic analyses (Chow et al, 1988).

4.4 HEC-SSP Software

The Hydrologic Engineering Center's Statistical Software Package (HEC-SSP) is the software that allows users to conduct statistical analyses of hydrological data, such as the flood frequency analysis. This analysis is contingent on Bulletin 17B, released in 1982 by the Interagency Advisory Committee on Water Data, and Bulletin 17C, which the Subcommittee of Hydrology published in 2018. The Bulletin-17-B procedures recommend a method for calculating flood risk analysis contingent on the maximum annual flood peak each year. This analysis produces calculations of the probability that the yearly peak flood in every year will be greater than or less than any specified discharge. In contrast, Bulletin-17-C is the advanced guideline of Bulletin-17-B.

The HEC-SSP software also performs other Hydrological analyses, such as duration analysis, volume frequency analysis for high or low flows, coincident frequency analysis, balanced hydrograph analysis, curve combination analysis, fitting distribution analysis, and mixed population analysis. HEC-SSP software was utilized to calculate the flood frequency analysis. The annual highest observed flow rate between 2002 and 2020 was used as input data for the software. The software uses different distributions to analyze the expected peak flood of a specific return period. These distributions include the General Extreme Value, Log-Pearson 3, Normal, Gumbel-Max and Log-Normal distributions. To determine the most suitable distribution that fits the input data the KS test was used in the software, and then the distributions were ranked according to their GOF test. The method of estimating parameters for each distribution used in this software is standard product moments.

The software determined the most fitting distributions for the input data that were the identical distributions generated by the EasyFit software in the previous analysis. These distributions were the General Extreme Value (GEV), Log-Pearson 3, Normal, and Log-Normal distributions. Then using the HEC-SSP software, the expected peak flood discharge of each distribution with their exceedance probability ware analyzed, as illustrated in Figure 4.3. Exceedance probability is the inverse of the return period.
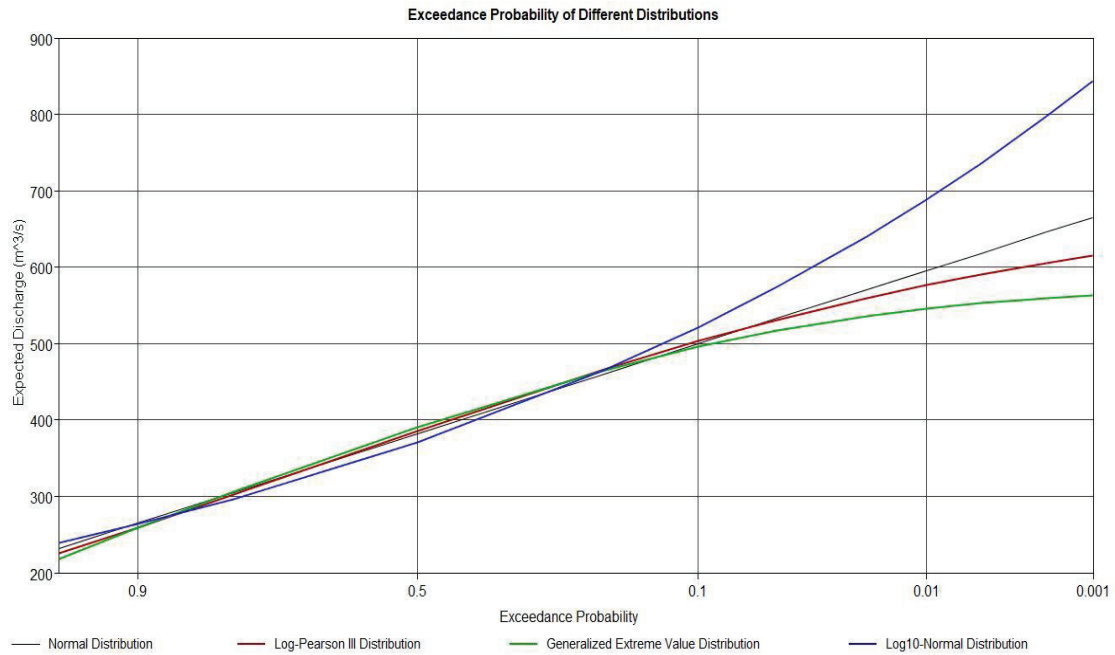
Figure 4.3. Peak Flood Discharge for Exceedance Probability Using Different Distributions

Based on the result of the software estimated peak discharge using the Log-Pearson Type III distribution with various return periods intervals 2,5, 10, 20, 50, 100, 200, 500 and 1000 years with the result of 385.5 m^3/s, 465.3 m^3/s, 503 m^3/s, 531.4 m^3/s, 559.8 m^3/s, 576.7 m^3/s, 590.6 m^3/s, 605.4 m^3/s, and 614.6 m^3/s, respectively, as shown in Figure 4.4. The corresponding peak discharge value of 500 years of return period for the Log-Pearson 3 distribution was used as the design discharge value in the HEC-RAS model. Table 4.3 summarizes the expected maximum flood discharges for different distributions with specified return periods for the study area.

Table 4.3. Expected Maximum Flood Discharges of each Distribution

Return Period (Year)	Expected Peak Discharge (m^3/s)			
	GEV	Log-Pearson Type III	Normal	Log-Normal
2	391	385.5	382.4	370.7
5	464.2	465.3	459.4	463.7
10	495.4	503	499.6	521.3
20	516.8	531.4	532.9	574.2
50	535.9	559.8	570.3	640.2
100	545.7	576.7	595.2	688.4
200	552.8	590.6	618	735.7
500	559.2	605.4	645.7	797.3
1000	562.6	614.6	665.1	843.6
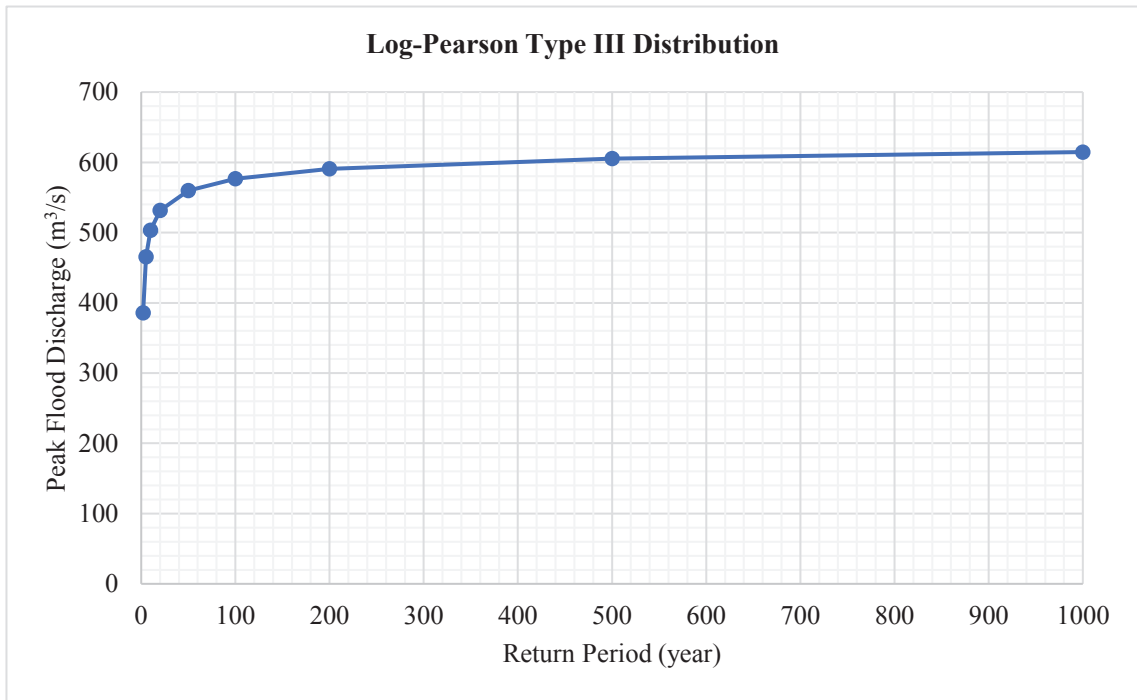
Figure 4.4. Peak Flood Discharge for Different Return periods Utilizing Log-Pearson 3 Distribution

4.5   Hydrological Modelling

4.5.1 Conceptual Framework

The general methodology of the hydrological model is summarized in Figure 4.5.
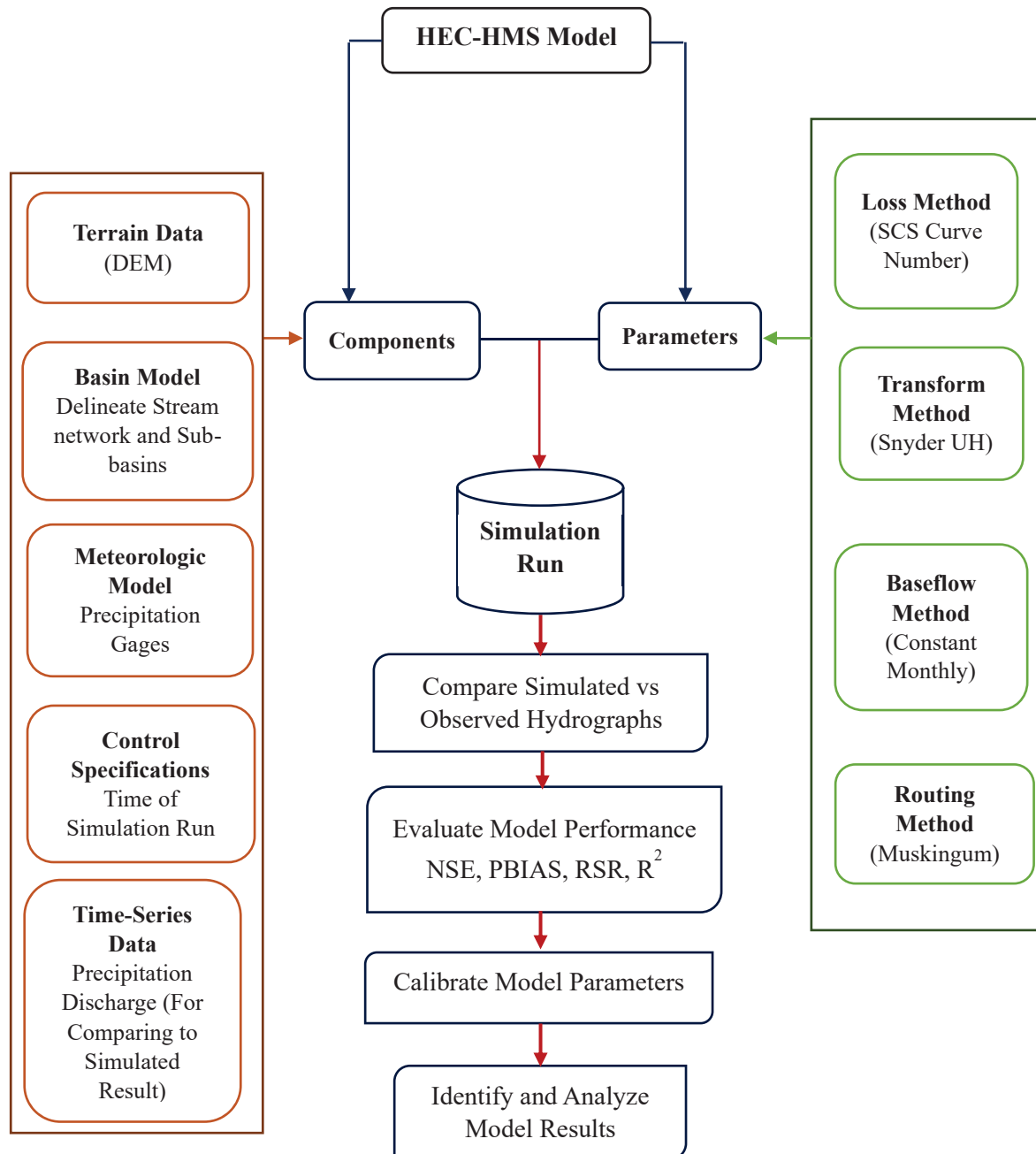
Figure 4.5. Flow chart showing the general framework of the HEC-HMS model

4.5.2 Model Overview

In this research, the HEC-HMS model was used for the hydrological modelling. The model simulates the entire hydrologic processes, such as rainfall-runoff processes of dendritic watershed designs. HEC-HMS model can be applicable in a broad scope of geographic areas to crack the broadest possible problems, including natural watershed or small urban rainfall runoffs, ample river basins, and flood hydrology. The model uses different hydrological analysis methods such as traditional hydrologic analysis methods (e.g., event infiltration, hydrologic routing and unit hydrographs) and others. Also, the model has advanced capabilities to provide for gridded rainfall-runoff simulation by using linear quasi-distributed rainfall-runoff transform (ModClark). The results of the HEC-HMS model are the primary inputs of the hydraulic model for flood simulation analysis (Olajuyigbe et al., 2012).

The essential component of the HEC-HMS model includes basin model, terrain data, meteorological model, time-Series data and control specifications manager. The latest version of the HEC-HMS model, released on 12 Jan 2022, contains the GIS tools necessary for delineating catchments. These tools include Coordinate System, Preprocess Sinks, Preprocess Drainage, Identify Streams, Break Points Manager, Delineate Elements, Merge and Split Elements and others. The GIS tools in the model facilitate that the user can perform all necessary analysis of catchment delineation required for the basin model without using other software such as QGIS or ArcMap GIS.

HEC-HMS model uses various parameters to simulate Rainfall-runoff simulation. Each parameter component has several available methods for modelling the essential elements of the hydrologic cycle. For example, some of the parameters and their methods available in the model are summarized in Table 4.4.

Table 4.4. Some of the HEC-HMS model Parameters and their processes.

Parameters	Some of the Methods
Losses (for calculating runoff volume)	SCS Curve Number, Green and Ampt, Deficit and Constant
Transform (for computing direct runoffs)	SCS Unit Hydrograph (UH), Clark UH, Snyder UH
Baseflow (for calculating baseflow)	Constant Monthly, Linear Reservoir, Recession
Routing (for modelling channel flow)	Lag, Muskingum, Normal Depth

Parameters and methods used in this research are SCS Curve Number for analyzing runoff volume, Snyder Unit Hydrograph for estimating direct runoffs, Constant Monthly for calculating the baseflow and Muskingum for channel routing.

4.5.2.1 Modelling Losses

SCS Curve Number (CN) procedure was selected to calculate the rainfall-runoff volume. This procedure is commonly used in hydrological models to develop flood hydrographs, and it is an event-based procedure. The Soil Conservation Service (SCS) Curve Number (CN) method was developed by the United States Department of Agriculture (USDA), especially the Department of Soil Conservation Service (SCS), which is recently called as Natural Resource Conservation Service (NRCS) (Mishra & Singh, 2003). SCS CN procedure differentiates with moderately fewer parameter requirements and achieves simple and accurate rainfall-runoff rates corresponding to given rainfall, land and soil data. The following equation gives the SCS CN method is as follows:

$$Q = \frac{(P - I_a)^2}{(P - I_a) + S} \tag{4.25}$$

Where Q is the accumulated rainfall-runoff at a time; P is the accumulated rainfall depth at a time; I_a is the initial abstraction (initial loss); and S is the potential maximum retention, a measurement of the capability of a watershed to abstract and retain storm precipitation. The empirical relationship between I_a and S is as follows:

$$I_a = 0.2S \tag{4.26}$$

The cumulative excess for a period interval is calculated as the change between the cumulative excess at the period's end and beginning. The potential maximum retention (S) value of a given curve number (CN) can be calculated using the following equation.

$$S = \begin{cases} \frac{1000}{CN} - 10 \ (foot - English \ System) \\ or \\ \frac{25400}{CN} - 254 \ (SI \ System) \end{cases} \tag{4.27}$$

The CN depends on soil properties such as type infiltration ability, and also it relies on the land use land cover and the depth of the water table.

4.5.2.2 Transform Method

Snyder Unit Hydrograph (UH) procedure was used to compute the direct rainfall-runoff in the HEC-HMS model. This method is based on standard unit hydrograph elements and watershed characteristics. The standard unit hydrograph elements are the peak direct runoff rate (q_p), the basin lag time (t_l) and effective rainfall duration (t_r). The relationship between t_l and t_r in a standard UH is given as follows:

$$t_l = 5.5t_r \tag{4.28}$$

Where the basin lag time t_l (hrs), and the peak discharge q_p (m³/s), are given by the following equations:

$$t_l = C_1 C_t (LL_c)^{0.3} \tag{4.29}$$

$$q_p = \frac{C_2 C_p A}{t_l} \tag{4.30}$$

Where L is the mainstream length from the outlet to the upstream in km, L_c is the distance from to a point on the stream nearest the centroid of the watershed area in km and $C_1 = 0.75$ (for SI units). The product of L and L_C measures the shape watershed, and C_t is a coefficient representing the watershed's slopes and storage characteristics. A is the basin area in km², and $C_2 = 2.75$ (for SI units). C_t and C_p are coefficients that represent the effects of storage and retention.

The HEC-HMS model requires setting the values of standard lag time t_l and the peaking coefficient C_p to compute the Snyder UH peak discharge and time of peak.

4.5.2.3 Routing Method

For this analysis, the Muskingum routing technique was used as a routing method for the reaches in the HEC-HMS model because it is typically used for flood routing in

the natural channels. The Muskingum routing method has two essential parameters, X and K. The Muskingum X is the weighting among inflow and outflow impact, and it varies from (0 to 0.5), where the Muskingum K is the journey period through the reach. The Muskingum value of X can be calculated using the following equation (Cunge, 1969):

$$X = \frac{1}{2}\left(1 - \frac{Q_0}{S_0 c \Delta x}\right)$$
(4.31)

Where Q_o is the unit-width flow from the inflow hydrograph, S_o is the channel bed slope, c is the flood wave speed (celerity), and Δx is the reach length. The Muskingum value of K is given as follows:

$$K = \frac{L}{V}$$
(4.31)

Where L (m) is the river's length, and V is the velocity of the inundation wave through the reach (m/s) and is obtained as follows:

$$V = \frac{Q}{A}$$
(4.32)

Where Q is the flood discharge (m³/s) and A is the cross-section area at the gauging station (m²). The following equation gives the Muskingum routing model:

$$Q_t = \left(\frac{\Delta t - 2KX}{2K(1-X)+\Delta t}\right) I_t + \left(\frac{\Delta t + 2KX}{2K(1-X)+\Delta t}\right) I_{t-1} + \left(\frac{2K(1-X)-\Delta t}{2K(1-X)+\Delta t}\right) Q_{t-1}$$
(4.33)

Where Q_t is the outflow from storage at a time t, K is the travel time of inundation wave in the reach, X is dimensionless weight, Δt is time increment, and Q_{t-1} is the outflow from storage at previous time t-1(m³/s).

4.5.2.4   Baseflow Method

The Constant monthly baseflow method was used in this analysis for suitability for the studied area. This method is intended mainly for continued simulation in subbasins, and it requires a good approximation of constant flow values for each month

of the year. The average of the minimum flow was taken as initial values before calibrating the model.

4.5.3   Model Setup

4.5.3.1   Defining the Basin Model

The purpose of defining the Basin model is to set up all basin components necessary for the hydrological model analysis. These include physical delineation of the watershed, defining subbasins, reaches, junctions, and catchment outlets.

In the first step, the basin model was created, and the terrain data was imported to the model. Then GIS tool in the HEC-HMS model was utilized to delineate the characteristics of the watershed, such as fill sinks, flow direction, flow accumulation, identifying streams, creation of outlet points and delineating elements. The delineated elements are Subbasins, Reaches and Junctions of the catchment. The whole catchment was divided into 16 Subbasins and two outlet points as calibration points, as shown in Figure 4.6. The locations of the outlet points were selected based on the locations of manual gauge stations available in the study area (Baledwayne city) and Bulo-Burti town. Table 4.5 summarize subbasin catchment characteristics in the Hiran region, including the study area.

Table 4.5. Physical characteristics of the catchment.

Subbasins	Area (km^2)	Basin Slope (%)	Longest Flow Path Length (km)
Sub1	183.8	4.3	42.2
Sub2	233.5	4.3	61.1
Sub3	198.9	6.1	71.0
Sub4	171.3	4.6	59.1
Sub5	209.9	4.0	59.2
Sub6	246.1	6.4	84.0
Sub7	202.0	5.0	65.9
Sub8	225.9	4.7	97.5
Sub9	144.9	5.5	44.0
Sub10	207.1	5.8	74.3
Sub11	85.0	5.2	18.5
Sub12	114.7	7.6	29.1
Sub13	192.0	4.0	43.6
Sub14	149.6	8.3	34.4
Sub15	199.3	4.8	72.9
Sub16	50.0	3.9	17.6
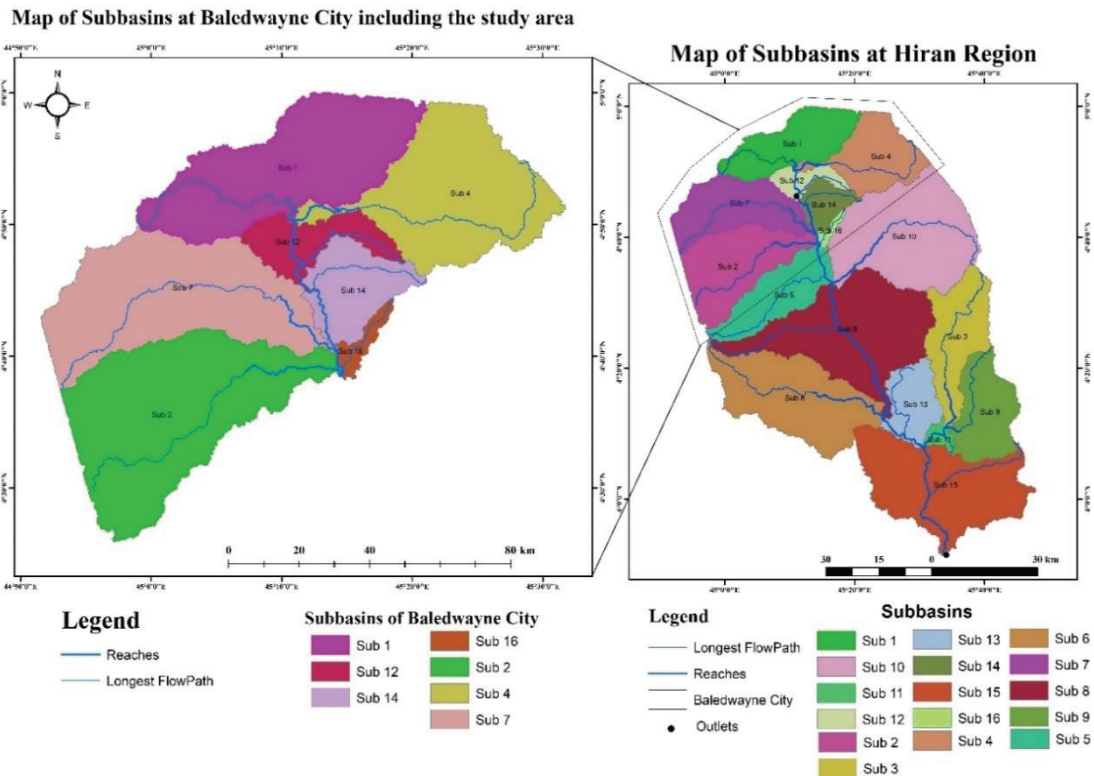
Figure 4.6. Map of Subbasins at the Hiran region, developed by the HEC-HMS model

4.5.3.2 Defining the Mereological Model

The meteorological is created to import the meteorological data in the HEC-HMS model. Observed 2019 daily rainfall data of both Baledwayne and Bulo-Burti stations were imported to the model. Also, the observed 2019 daily discharge of the Shabelle River of both stations was imported to the model to calibrate the outflow hydrograph of outlets. The HEC-HMS model was used to generate a rainfall-runoff hydrograph of the 2019 event in the study area. This event was selected based on two criteria: 1) In that year, the city experienced an extreme flood event, which locals expressed was the most significant flood event seen in the city. 2) Availability of observed meteorological data for both stations.

Parameters and methods were selected to compute the rainfall-runoff hydrograph of each subbasin and outlet in the model. SCS CN method was selected to compute the rainfall-runoff volume, whereas Snyder UH method for computing the direct rainfall-runoff as a transform parameter. Also, the Muskingum method was selected as a routing

parameter and the Constant Monthly as a baseflow parameter. In the first simulation, an initial value was for each parameter, and then their value was changed during the calibration process.

4.5.4   Evaluation of Model Performance

The degree of correctness, adaptability and durability are essential for evaluating the model's efficiency. The performance of the HEC-HMS model was evaluated based on the selected objective that assesses the level of fitness between the simulated and observed hydrograph at both stations. The performance of the HEC-HMS model was evaluated by optical calculation of the virtual and simulated observed hydrographs and a setting of objective processes that estimate the level of fit between the hydrograph observed and simulated.

These parameters were used to evaluate the performance of the HEC-HMS model, and they are Nash-Sutcliffe (NSE), percentage bias (PBIAS), coefficient of determination (R2), root mean square error normalized by the standard deviation (RMSE Std Dev) ratio (RSR), relative peak error (PE) and percentage error in peak flow (PEPF). The NSE indicates how the fitness of simulated versus observed hydrograph. The value of NSE ranges between infinity and 1.0, and the optimal value of NSE is equal to 1. However, values ranges between 0.0 and 1.0 are commonly regarded as good performance levels, while values < 0.0 indicates that the mean observed value is a better predictor than the simulated value, indicating unacceptable model results. PBIAS estimates the average bias of the simulated data to be smaller or larger than their observed data. The optimal value of PBIAS is equal to 0.0; however, low magnitude values mean accurate model simulation results. Positive values mean the model underestimation bias, whereas negative values show overestimation bias. The RMSE Std Dev RSR is used to evaluate the difference between observed and simulated hydrographs in the model. The values of RSR differ from the optimal value of 0.0, and if RSR is 0.0, the model results are perfect. The coefficient of determination (R^2) was utilized to test the capacity of the model to produce the sequence of the simulated hydrographs. The optimal value of R^2 is 1.0; however, values larger than 0.6 is generally regarded as acceptable model results. The model uses the following equations to calculate NSE, PBIAS and RSR values:

$$NSE = 1 - \left[\frac{\sum_{i=1}^{n} (Q_{obs,i} - Q_{sim,i})^2}{\sum_{i=1}^{n} (Q_{obs,i} - Q_{mean})^2} \right]$$ (4.34)

$$PBIAS = 100 \times \left[\frac{\sum_{i=1}^{n} (Q_{obs,i} - Q_{sim,i})}{\sum_{i=1}^{n} (Q_{obs,i})} \right]$$ (4.35)

$$RSR = \frac{\sqrt{\sum_{i=1}^{n} (Q_{obs,i} - Q_{sim,i})^2}}{\sqrt{\sum_{i=1}^{n} (Q_{obs,i} - Q_{mean})^2}}$$ (4.36)

In the equations, $Q_{obs,i}$ refers to the values of observed flow rate at the time step i, and $Q_{sim,i}$ refers to the values of simulated flow rate at the time step i. At the same time, Q_{mean} represents the mean values of observed flow rate where n is the number of observations.

The relative peak error (PE) and percentage error in peak flow (PEPF) were calculated to check the performance of the HEC-HMS model using the peak flow data. The optimal value of PE is 0.0; however, values less than 0.2 indicates the model performance is very good. At the same time, the general performance rating for recommended statistics of PEPF is between the range of very good to satisfactory < 20%, 30-40%, respectively. The following equations are used to calculate PE and PEPF.

$$RPE = \frac{|Q^{obs} - Q^{sim}|}{Q^{obs}}$$ 4.37

$$PEPF = 100 \, x \frac{|Q^{obs} - Q^{sim}|}{Q^{obs}}$$ 4.38

Where Q^{obs} and Q^{sim} are the observed and simulated peak flow values.

4.5.4.1 HEC-HMS Model Calibration

The model was calibrated by changing the values of parameters shown in Table 4.6. After assigning a value to each parameter, the model is simulated, and the model's

performance is estimated using performance parameters. Figure 4.7 illustrates the conceptual framework of the calibration method used in the model. The HEC-HSM model performance is quantified using these statistics and ranked as very good, good, satisfactory, or unsatisfactory using the guidelines in Table 4.7.

Table 4.6. The Calibration Parameter of the HEC HMS model.

Modelling	Method	Parameter	Range
Rainfall-runoff Volume	Curve Number	Initial Abstraction (mm)	0.1-100
		CN	1-100
Direct Rainfall-runoff	Snyder UH	Lag (hr)	0.1-100
		C_p	0.1-1
Base Flow	Constant Monthly	Monthly Constant values (m^3/s)	0-100
Routing	Muskingum routing	K (hr)	0.1-2
		X	0-0.5

Table 4.7. The performance rating of the HEC HMS model (Source: Moriasi et al., 2007).

Performance Rating	Statistics			
	NSE	PBIAS	RSR	R^2
Very Good	$0.75 < NSE \leq 1.0$	$PBIAS < \pm 10$	$0.00 < RSR \leq 0.50$	$0.65 < R^2 \leq 1.00$
Good	$0.65 < NSE \leq 0.75$	$\pm 10 \leq PBIAS < \pm 15$	$0.50 < RSR \leq 0.60$	$0.55 < R^2 \leq 0.65$
Satisfactory	$0.50 < NSE \leq 0.65$	$\pm 15 \leq PBIAS < \pm 25$	$0.60 < RSR \leq 0.70$	$0.40 < R^2 \leq 0.55$
Unsatisfactory	$NSE \leq 0.50$	$PBIAS \geq \pm 25$	$RSR > 0.70$	$R^2 \leq 0.40$
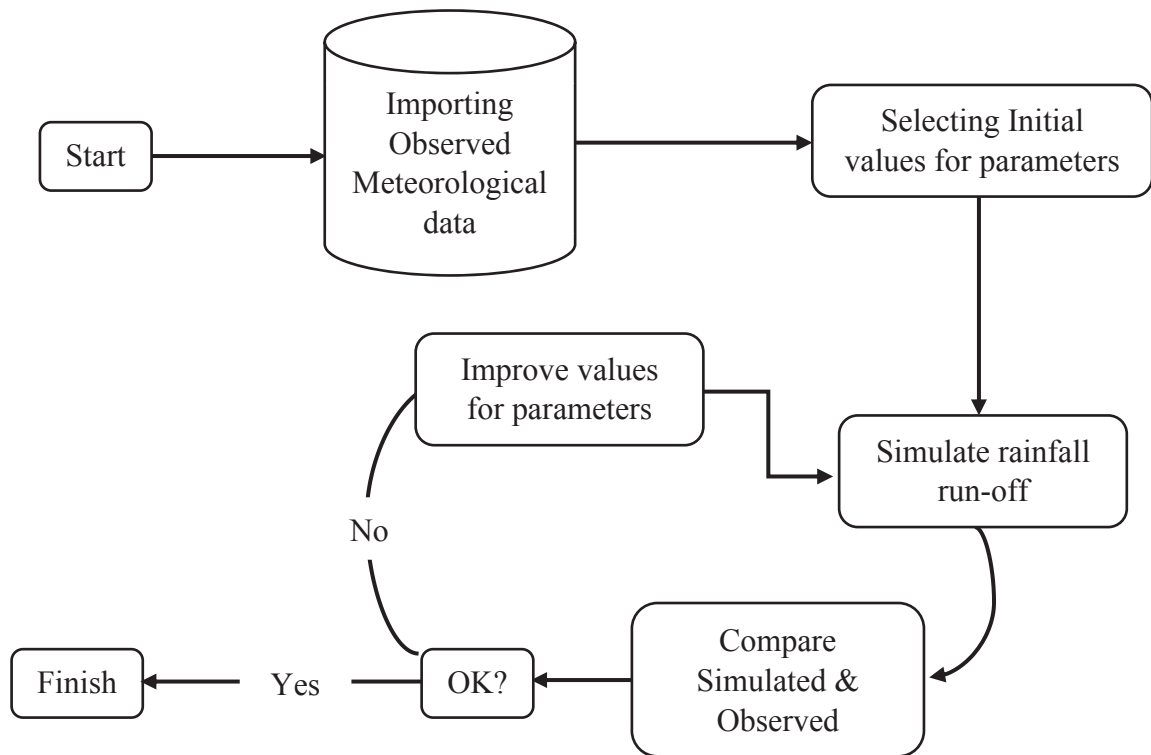
Figure 4.7. Calibration process of the HEC-HMS model

4.5.5 HEC-HMS Model Results

Calibrated results of the HEC-HMS model for both outlets at the stations in Baledwayne city and Bulo-Burti town are indicated in Figures 4.8 and 4.9. The simulated hydrograph of the 2019 event smoothly agrees with the corresponding observed hydrograph; however, due to insufficient discharge and precipitation data, specific peaks did not reflect smoothly to the observed hydrograph. The simulated hydrographs were obtained after the model performance was checked using these statistical parameters NSE, PBAIS, RSR and R^2. According to the objective of model performance, it was observed that the model results are acceptable. The statistical values of PBAIS, RSR and R^2 for the model calibration showed very good performance in assessing streamflow. At the outlets of Baledwayne and Bulo-Burti stations, the value NSE is found to be 0.896

and 0.916, respectively. A summary of the value of statistical parameters is indicated in table 4.8.

Table 4.8. The Calibration performance results of the HEC HMS model.

Summary of Calibrated Results at the Outlet Points	Results of Statistics				Model Performance Rank
	NSE	PBIAS (%)	RSR	R^2	
Baledwayne station (Study Area)	0.896	6.08	0.3	0.906	Very Good
Bulo-Burti station	0.916	2.44	0.3	0.923	Very Good

As shown in Table 4.8, the calibrated model results at the Baledwayne gauging station, the values of NSE, PBAIS, RSR and R^2 were found to be 0.896, 6.08, 0.3%, and 0.906, respectively. At the same time, calibrated model results at the Bulo-Burti gauging station, the values of NSE, PBAIS, RSR and R^2 were observed to be 0.916, 2.44, 0.3%, and 0.923, respectively. The relative peak error (PE) and percentage error in peak flow (PEPF) were calculated using Microsoft excel. The 5 events with the most extreme peak flow values at Baledwayne and Bulo-Burti stations were selected in this analysis as indicated in Tables 4.9 and 4.10. All the peak flow events in both stations were observed during the Deyr season.

Table 4.9. PE and PEFP at Baledwayne station (Study Area)

No	Qobs(m3/s)	Qsim(m3/s)	PE	PEPF (%)
1	470.01	349	0.26	26
2	470.01	347	0.26	26
3	470.01	403	0.14	14
4	470.01	459	0.02	2
5	470.01	456	0.03	3
Qaverg	**470.01**	**403**	**0.14**	**14**
Qmax	**470.01**	**414**	**0.12**	**12**

Table 4.10. PE and PEFP at Bulo-Burti station

No	$Q_{obs}(m^3/s)$	$Q_{sim}(m^3/s)$	PE	PEPF (%)
1	419	417	0.01	0.6
2	419	411	0.02	2.0
3	419	383	0.09	8.7
4	396	422	0.07	6.7
5	392	402	0.02	2.5
Qaverg	**390**	**407**	**0.005**	**0.5**
Qmax	**419**	**422**	**0.01**	**0.6**

Table 4.9 indicates the calculated values of PE and PEPF at Baledwayne station using 5 peak flow events. The average and maximum values of PE are 0.14 and 0.12, respectively. At the same time, the PEPF has a maximum value of 12%.

Table 4.10 demonstrates the obtained PE and PEPF values at the Bulo-Burti station using 5 peak flow events; the average and maximum values are also indicated in the table. The calculated maximum values of PE and PEPF are 0.01 and 0.6%, respectively.

According to obtained values shown in Tables 4.9 and 4.10, the average and maximum values of PE at both stations are less than 0.2; at the same time, their PEPF values are less than 20%. So, the performance rank of PE and PEPF in Baledwayne and Bulo-Burti stations is very good.

The performance rank of each NSE, PBAIS, RSR, R^2, PE and PEPF for both stations is very good according to their statistics values. Therefore, the general performance rating of the model for both stations was found to be very good, which indicates that the simulated hydrograph in the HEC-HMS model for this study is acceptable. The observed discharge of both stations is near to the simulated hydrographs of the model.
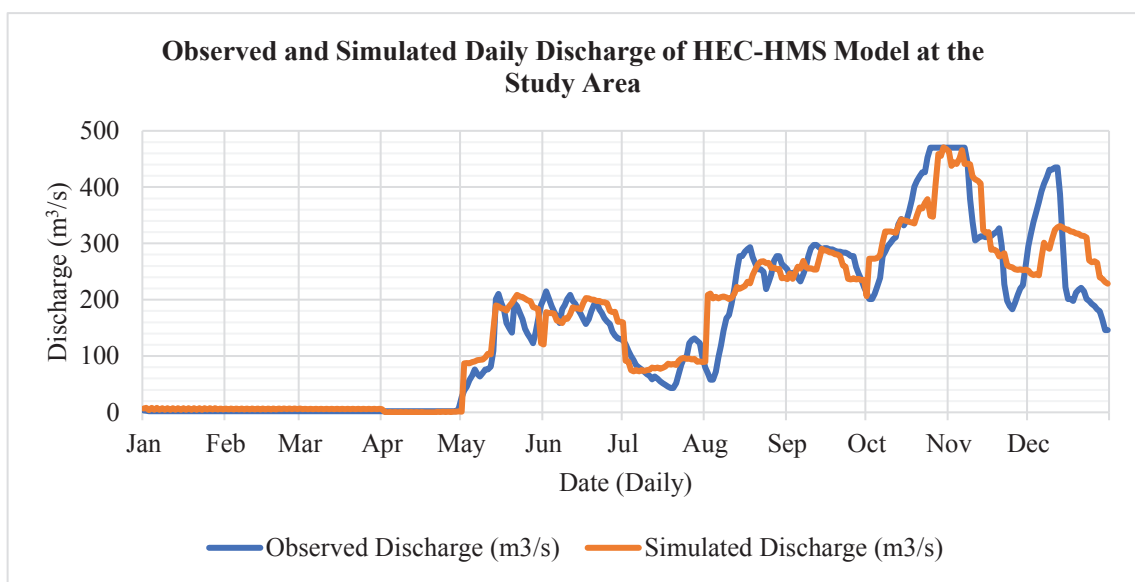
Figure 4.8. Observed and Simulated Discharges at Baledwayne (Study Area) station
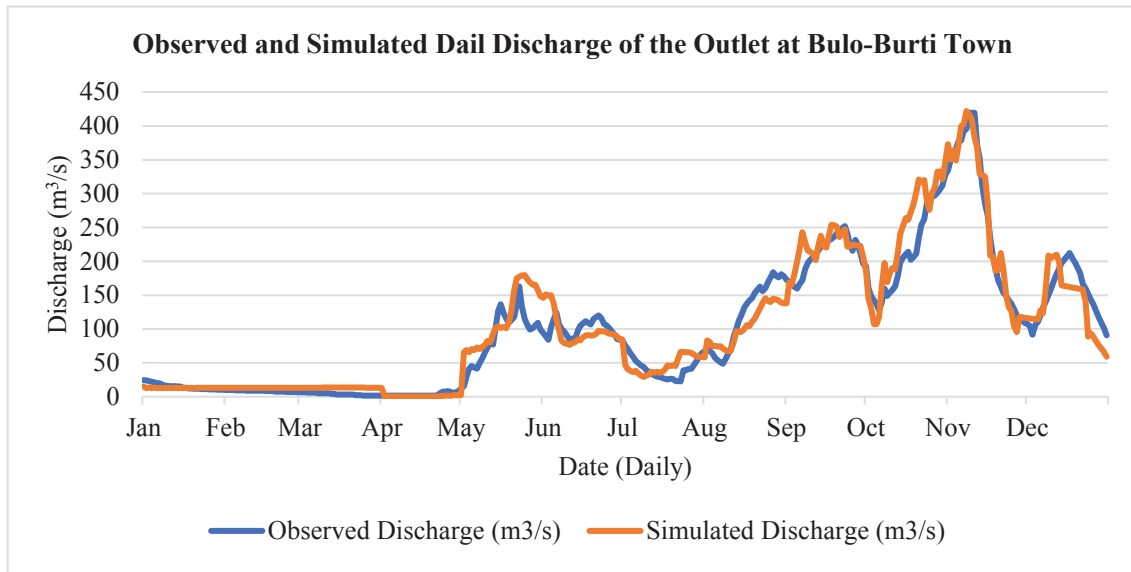
Figure 4.9. Observed and Simulated Discharges at Bulo-Burti station

The maximum simulated discharge at the Baledwayne station was 477.7 m³/s with a peak time of 30-Oct-2019; the corresponding observed peak flow rate is 470.1 m³/s with a peak time of 25-Oct-2019. Whereas the simulated peak discharge at the Bulo-Burti station was 422.0 m³/s with a peak time of 08-Nov-2019, the corresponding observed peak discharge is 419.4 m³/s with a peak time of 09-Nov-2019. The values of simulated peak discharge for both stations are close to the corresponding observed peak discharges. Therefore, the results demonstrate that the analysis is fine and can be taken for further analysis. Table 4.9 summarizes simulated and observed peak discharge for both stations.

Table 4.11. Summary of Calibrated Results at the Outlet Points.

Summary of Calibrated Results at the Outlet Points	Baledwayne station (Study Area)		Bulo-Burti station	
	Simulated	Observed	Simulated	Observed
Peak Flow Rate (m³/s)	477.7	470.1	422.0	419.4
Total Volume (MM)	5113.34	4813.91	438.07	426.97
Time of Peak Discharge	30-Oct-2019	25-Oct-2019	08-Nov-2019	09-Nov-2019

The linear correlation coefficient R^2 was analyzed using Microsoft Excel to check the relationship between the simulated and observed discharge for both stations, as shown in Figures 4.10 and 4.11. According to values of R^2 for both stations, it indicates a strong and positive relationship between the simulated and observed discharges. Therefore,

64

regarding the performance of the model criteria, the obtained model results for both stations are very good. Thus, the simulated rainfall-runoff hydrograph of the HEC-HMS model at the Baledwayne (Study Area) station will be used as the input inflow hydrograph for the hydraulic model.
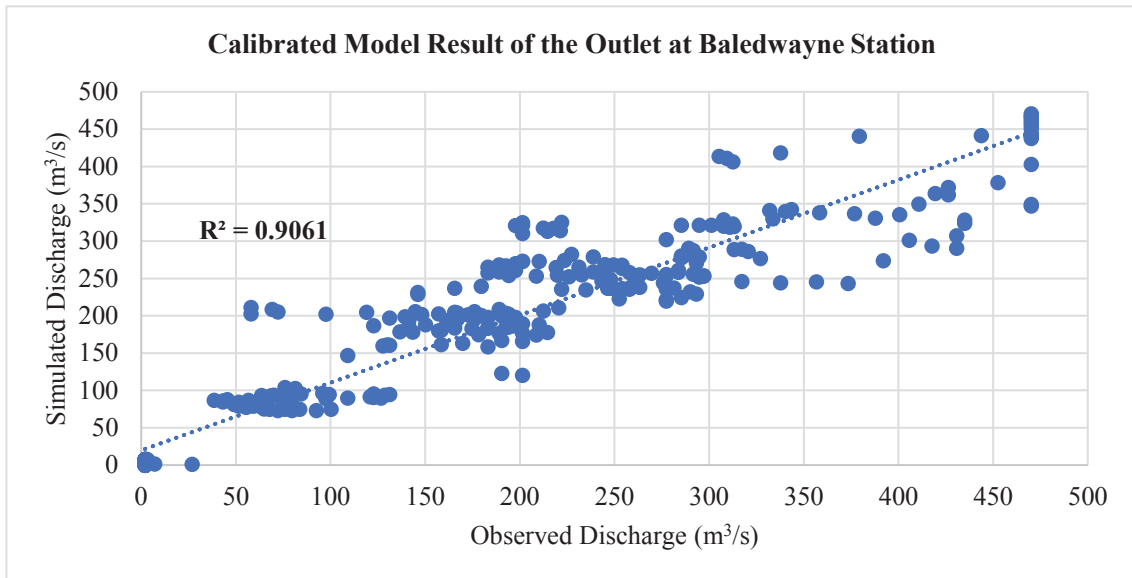
Figure 4.10. Correlation Between Observed and Simulated Discharge at Baledwayne (Study Area) station
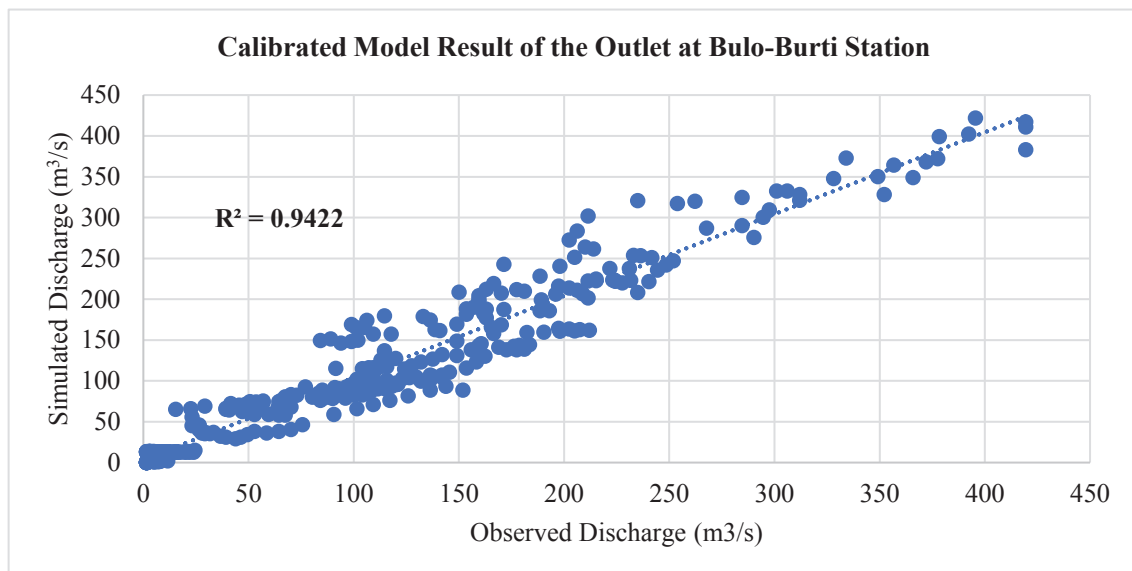
Figure 4.11. Correlation Between Observed and Simulated Discharge at Bulo-Burti station

4.6 Hydraulic Modelling

4.6.1 Conceptual Framework

The general methodology of the hydraulic model is summarized in Figure 4.12.

```
                    ┌──────────────────────────────────────┐
                    │  Hydraulic Modell Using HEC-RAS Model  │
                    └──────────────────────────────────────┘

┌─────────────────────┐              ┌─────────────────────────┐
│   Create Project    │─────────────▶│ Create Terrain Data Layer│
│  Set Unit and Define│              │     Using DTM Data       │
└─────────────────────┘              └─────────────────────────┘
                                                 │
                                                 ▼
┌─────────────────────┐              ┌─────────────────────────┐
│ Connect 1D&2D Geometry│◀───────────│  Create Base Geometry Data│
│ Using Lateral Structural│           │  1D Geometry (Main Channel)│
└─────────────────────┘              │  2D Flow Areas (Floodplains)│
                                     └─────────────────────────┘
        │
        ▼
┌─────────────────────┐              ┌─────────────────────────┐
│ Create Land Cover Layer│──────────▶│ Assign Manning's n Values and│
│ Using ESRI 2020 Land Cover│        │ Percentage of Impervious Using│
│        Data         │              │     Land Cover Layer     │
└─────────────────────┘              └─────────────────────────┘
                                                 │
                                                 ▼
┌─────────────────────┐              ┌─────────────────────────┐
│ Assign Boundary Conditions│◀───────│ Associate Geometry Data to│
│ (Flow Hydrograph and Normal│        │ Terrain and Land Cover Layers│
│        Depths)      │              └─────────────────────────┘
└─────────────────────┘
        │
        ▼
┌─────────────────────┐              ┌─────────────────────────┐
│ Perform Unsteady Flow│────────────▶│ Check Model Performance │
│    Simulation       │              │ (Inundation Map and Depth,│
│  (Deyr 2019 Flood)  │              │       River Level)       │
└─────────────────────┘              └─────────────────────────┘
                                                 │
                                                 ▼
┌─────────────────────┐   ┌─────┐    ┌─────────────────────────┐
│ Update Flow Hydrograph BC│◀─│ Ok │◀──│ Calibrate the Model Using│
│ Data and Perform Unsteady│  └─────┘   │       (n values)        │
│   Flow Simulation   │              └─────────────────────────┘
│  (500 years of Flood)│
└─────────────────────┘
        │
        ▼
        ┌─────────────────────────┐
        │ Process Generated Maps of Both Flood│
        │    Events Using ArcMap   │
        └─────────────────────────┘
```

Figure 4.12. Flow chart showing the general framework of the HEC-RAS model

4.6.2   Model Description

In this research, the HEC-RAS model was used for the hydraulic modeling. A combined 1D&2D hydraulic modeling of the model was used to develop first flood risk maps and then flood mitigation measures for Baledwayne City, Somalia. The HEC-RAS model was established as a component of the Hydrologic Engineering Center's "Next Generation" (NexGen) hydrologic engineering software by the US Army Corps of Engineers. The HEC-RAS model performs the following four river analysis components: 1D steady flow and water surface profile analyses, 1D & 2D unsteady flow simulation, 1D water quality computation, and partially or fully unsteady flow transportable boundary sediment transport analyses (1D and 2D). The essential element is that all those four components use a common geometric data model and standard geometric and hydraulic calculation routines. Additionally, to the four river computation elements, the model has several hydraulic design components that can be mustered after analyzing water surface profiles.

HEC-RAS model also has a mapping procedure (HEC-RAS Mapper) and a comprehensive spatial data integration. Using the HEC-RAS Mapper window, users can create, edit and visualize all geometry data and layers such as terrain, land cover, and soil layer. Also, it can be visualized and animate all simulation results of the model. The RAS Mapper has a powerful geospatial capability (USACE, 2022b).

HEC-RAS model requires several data inputs to perform and simulate the hydraulic modeling, and these input data depend on the objective of the analysis required. The main objective of this study is to examine a set of alternatives as remedial measures for flood management purposes to protect the Baledwayne city from Shabelle River flooding. The hydraulic modeling of this study starts with analyzing and generating the inundation map of the Deyr 2019 flood in the city, then compares different flood mitigation measures to determine the most appropriate flood mitigation measure for the Baledwayne city. So, the input data used for the HEC-RAS model are the DTM of the study area with a resolution of 10 m to extract the elevation profiles of geometry data in the study area, land cover, and others. Table 4.10 summarizes all the input data used in the model and their purposes.

Table 4.12. Outline of all the input data utilized in the HEC-RAS model.

No	Input Data	Purpose	Source
1	DTM of 10m resolution	As terrain layer to extract elevation profiles of all geometry data required for the analysis	SWALIM
2	2020 Land use the land cover of 10m resolution	For assigning Manning's Roughness Coefficients	Esri website
3	Simulated 2019 Discharge	It is used as an inflow hydrograph the upstream of the river for generating the inundation map of the Deyr 2019 flood in the city	From the output results of the Hydrological modeling using the HEC-HMS model
4	The peak discharge value of 500years of the return period	It is used as an inflow hydrograph upstream of the river to generate the inundation map of 500years of return period using different flood mitigation measures.	From the output results of the flood frequency analysis using the HEC-SSP model

4.6.3   Model Setup

In the RAS Mapper window, the projection file was imported to define the geographic coordinate system of the study area. The coordinate reference system or the projection of the study area is WGS_1984_UTM_Zone_38N.   After setting the projection, the terrain data was created using the same window and called "Base_Terrain", as illustrated in Figure 4.13. The DTM of the Baledwayne city (Study area) with 10 m resolution was used to create the terrain layer. The HEC-RAS model uses this layer to derive elevation profiles of all geometry data required in the analysis.
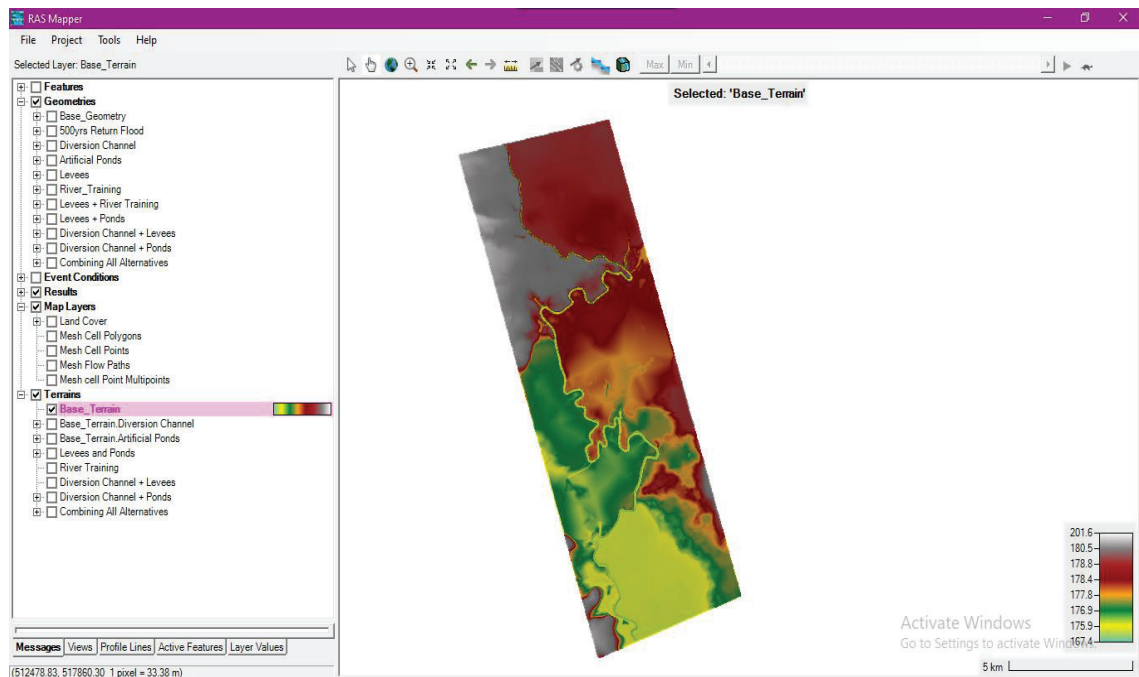
Figure 4.13. RAS Mapper window of the terrain layer at the Study Area

4.6.3.1 Developing 1D and 2D Geometry

The first step is to create the geometry data in the model, and this can be done using the Geometric Data window or RAS Mapper window, then associate them with the created terrain layer. After creating the new geometry, the model requires importing or creating the necessary geometric data. In the case of 1D geometry, the model requires elements: the river's centerline, bank lines, cross-sections, and flow paths which are utilized to assess the overbank reach lengths. Whereas in the case of 2D geometry, the model needs to specify the 2D Flow Areas. These elements, including the 2D Flow Areas, can be imported to the HEC-RAS model as a GIS format file or drawn using the RAS Mapper window.

The geometric data was created using the RAS Mapper window in this study. Then the centerline, bank lines, and flow paths of the Shabelle river at the study area were drawn using an editing tool in the RAS Mapper window of the model. The total length of the river centerline drawn in the 1D geometry of the study area is 13 803 km. The cross-sections of the Shabelle River at the study area were automatically generated using the Auto-Generate Cross Sections tool in the model. Each generated cross-sections have a width of 150 m, and the distance between two cross-sections is 300 m. A total of 130

cross-sections were generated in the entire study area, the detailed summary of cross-sections as shown in Appendix C.

The 2D Flow Areas or Floodplains in the study area were drawn using an editing tool in the RAS Mapper window of the model. The 2D Flow Areas in this study are divided into two areas, the left 2D flow area, which is the left side of the floodplain and the right 2D flow area, which is the right side of the floodplain. After drawing the 2D flow areas, the computational mesh cells were developed using the 2D Flow Area Editor. Individually cell in the 2D computational mesh has three elements: Cell Center, Cell Face Points and Cell Faces.

The Cell Faces are the boundaries of the cell, where the maximum number of cell faces allowed in a single cell is eight. The cell Faces in the 2D flow area act as detailed cross-sections and can be processed into detailed profile, elevation versus area, roughness and wetted perimeter relationships. The Cell center is the center of each cell, and in the HEC-RAS model, a single water surface elevation is calculated in the center of each cell. So, it is essential to select the most suitable mesh cell size to obtain accurate solutions with 2D flow areas. The mesh cell size in this study was selected to be 100 m x 100 m after many trials. Also, break-lines and refinement areas were used to refine the mesh cell size in some areas. The total number of cells generated in the left 2D flow area or left floodplain is 7380 cells, whereas in the right 2D flow area or right floodplain is 4584 cells.

In this study, 1D geometry is used for 1D modelling of the Shabelle River, whereas 2D Flow Areas are used for 2D modelling of the floodplains. It is required to connect 1D river reach and 2D flow area to combine both 1D and 2D modelling. There are several ways to connect 2D flow areas to the 1D river reach. This study used several lateral structures representing the levees in that region to connect the 1D river reach to the 2D flow areas, as shown in Figure 4.14. HEC-RAS model allows more than one lateral structure in one 2D flow area. After creating the lateral structures, the next step is to link 1D reach to the 2D flow area. It was selected Storage Area/2D Flow Area as the type of link between the 1D River Reach and 2D flow areas. The Lateral Structures (levees) automatically determine the location and intersection of the 1D cross-sections, and they

are used to model flow going over the levee. The Weir Equation method was selected for the overflow computation method. The type of structure used is Weir/Embankment.
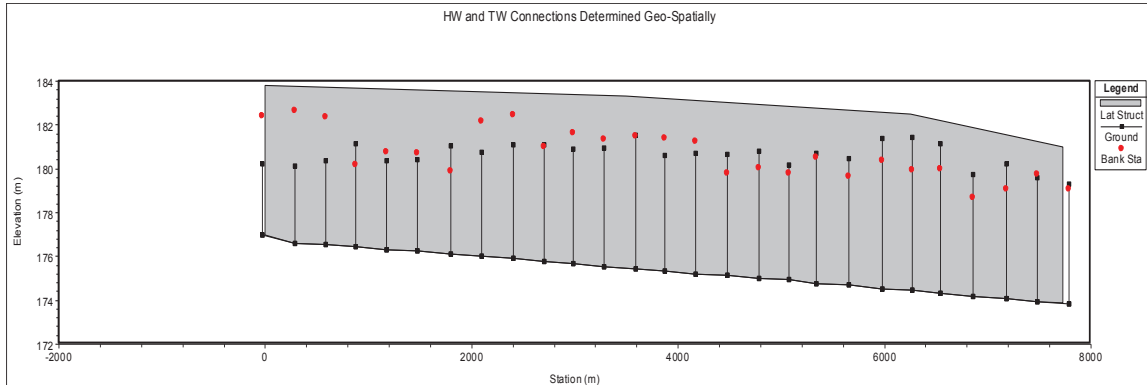
Figure 4.14. Lateral Structure of Reach Station 38975 at the Upstream of Left Overbank Floodplain of the Study Area

Six lateral structures were utilized to connect 1D river reach to 2D flow areas. Four lateral structures (levees) connect the river's right overbank to the right 2D flow area. Also, two lateral structures (levees) are connected the Left overbank of the river to the Left 2D flow area. The combined 1D&2D geometric data used in this study is shown in Figure 4.15.
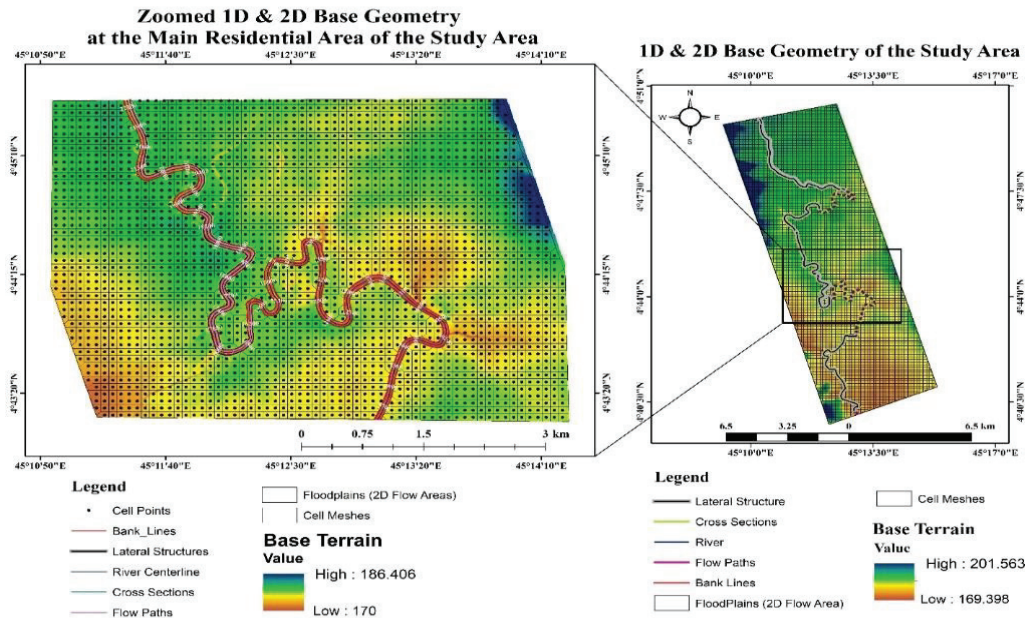
Figure 4.15. Combined 1&2D Base Geometry of the Study Area

4.6.3.2 Manning's Roughness Coefficient

One of the most significant parameters in the hydrological analyses is the Manning's Roughness Coefficient (n). It is generally utilized to estimate flow rate and flood water elevations (Coon 1995). Also, n is one of the essential parameters for analyzing the stormwater drainage system, canal and flow in conduit pipes. The accurateness of the simulated streamflow mainly depends on the value of n. Many factors affect the value of n that contribute to flow resistance. These include the riverbed irregularity of the channel, the shape and geometry of the channel, vegetation and other obstruction on the channel, and boundary and surface roughness of the channel. So, it is not easy to obtain the number of n in natural channels and floodplains. The values of n vary from one place to another in both channel and floodplains, and the leading cause is the terrain surface and land cover. There are many guidelines and tables for selecting the values of manning's roughness coefficient for both natural channels and floodplains. Arcement & Schneider (1989) proposed tables and guidelines for selecting n values corresponding to different conditions for natural channels and floodplains. This study has used these guidelines of manning's roughness coefficient values.

The HEC-RAS model allows assigning manning's n values and percentage impervious based on the land cover layer which must have spatially changing n values within 2D flow areas. The ESRI 2020 land cover with a resolution of 10 m in the study area was used to create a land cover layer in the RAS Mapper window. Then it is associated with the previous combined 1D&2D geometry data set. The study area was divided into eight polygons based on the land cover type, and then it was assigned Manning's n values and percentage impervious of each polygon. The classification polygons in the land cover layer were used to define the accurate area for the main channel.

4.6.3.3 Boundary Conditions

Boundary conditions are an essential element of hydraulic modelling, and they define the starting point of the simulation of the model. There are several boundary conditions available in the HEC-RAS model, and they depend on the type of simulation required to perform. Since this study performs a combined 1D&2D unsteady simulations,

the Flow Hydrograph was used as the upstream boundary condition while the Normal Depth was utilized as the downstream boundary conditions.

In this study, two different Flow Hydrographs were used separately to generate two different flood maps: An inundation map of the Deyr 2019 flood event and the inundation map of 500 years of the flood. First, a simulated 2019 discharge hydrograph from the output results of the HEC-HMS model was utilized as a Flow Hydrograph boundary condition for generating the inundation map of the Deyr 2019 flood in the city, as shown in Figure 4.16. Second, the peak discharge hydrograph from the output results of the HEC-SSP model was used as a Flow Hydrograph boundary condition for generating the inundation map of 500 years of the flood, as shown in Figure 4.17.

Inflow hydrograph 2019 boundary condition has a peak discharge of 477.7 m³/s, and this boundary condition is used in this chapter to generate the inundation map of the Deyr 2019 inundation event in the study area. In contrast, the inflow hydrograph of a 500-year flood boundary condition has a peak flow rate of 605.4 m³/s and was used in chapter five to generate the inundation map of the 500-year flood event in the study area.
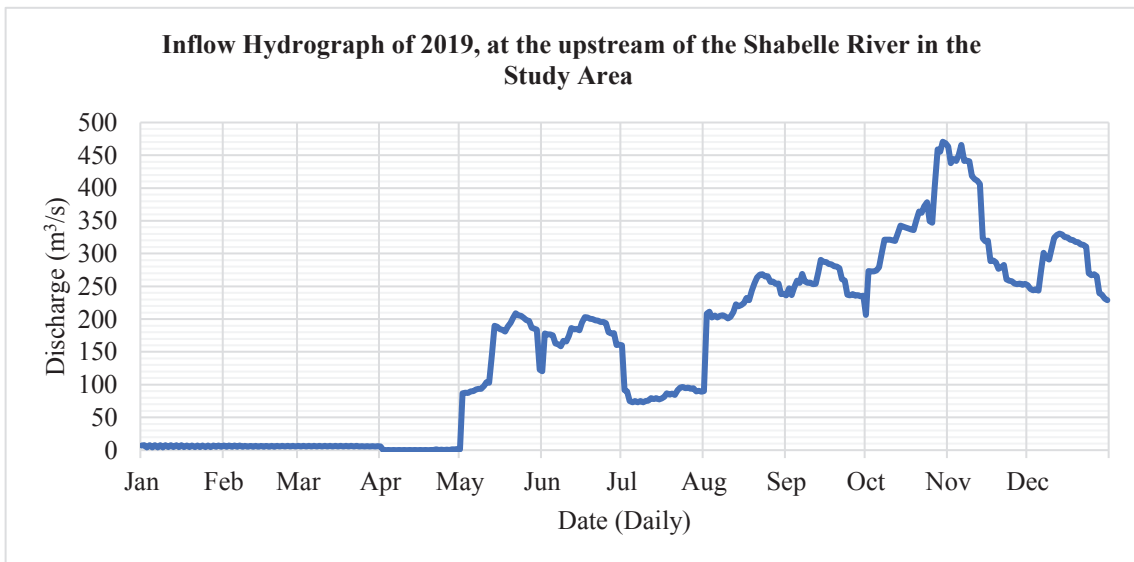
Figure 4.16. Inflow Hydrograph of 2019, at the Study Area
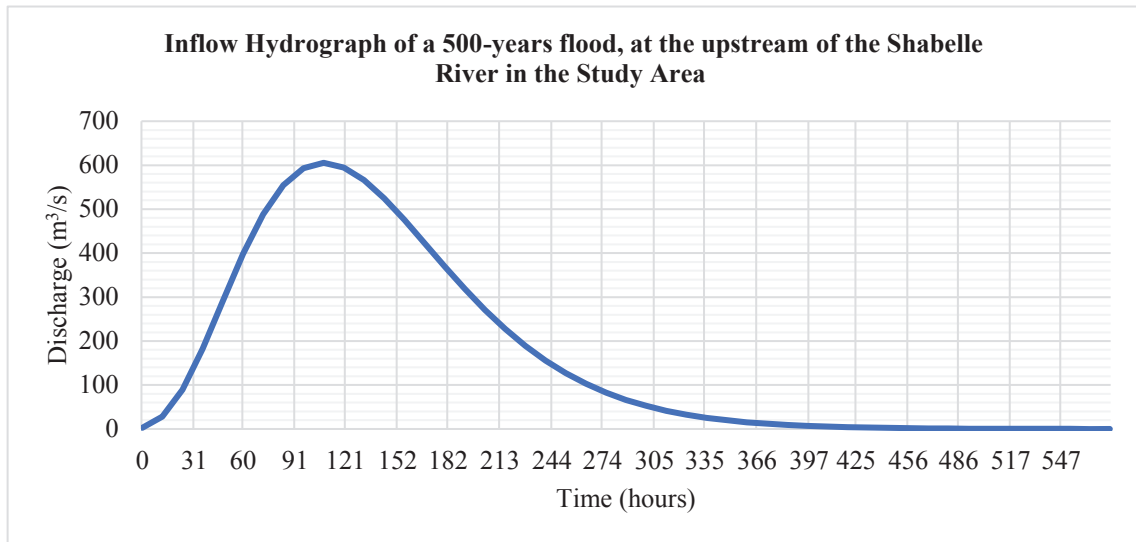
Figure 4.17. Inflow Hydrograph of a 500-years flood at the Study Area

The normal depth boundary condition was utilized as a downstream boundary condition of the Shabelle River and the 2D flow areas. This boundary condition applies Manning's equation to calculate a stage for each calculated flow, and it requires values of the friction slope, which is the slope of the energy grade line. In this study, the value of the friction slope was obtained by measuring the average bed slope of the Shabelle river in the profile plot window in the model. The frictional slope used for the downstream boundary condition (BC) of the Shabelle River is 0.00015. The friction slopes used in the 2D flow areas in the study area are 0.002 for the Right and 0.00015 for the Left 2D flow areas.

4.6.3.4   Unsteady Flow Simulation

The unsteady flow computational in the HEC-RAS model utilizes the hydraulic calculations of geometry data such as cross-section, weirs and 2D mesh cells to solve the unsteady flow equations (continuity and momentum equations). After entering the boundary conditions in the model, the unsteady flow computation was performed to calculate the hydraulic parameters of flow, such as flow velocity and flow depth. There are three equations available in the HEC-RAS model to perform 2D unsteady flow routing. These equations are the Diffusion Wave equation, the Shallow Water Equations using Eulerian-Lagrangian Method (SWE-ELM) and Shallow Water Equations using Eulerian Method (SWE-EM). The default equation in the model (Diffusion Wave

74

equations) was used in this study to predict the flow moving over the 2D Flow areas. This equation has more tolerant numerically than the SWE equation. Also, it has the advantage of using larger time steps and still obtaining numerically stable and accurate solutions. The following formula can be used as the numerical stability condition:

$$c = \frac{V\Delta T}{\Delta X} \leq 1.0 \ (with \ a \ maximum \ c = 1.0) \tag{4.39}$$

Where c is the Courant numbers, V is the flood wave velocity, ΔT is the computational time step, and ΔX is the average cell size. The following equations are continuity and momentum equations of the 1D model:

$$\frac{\partial A}{\partial t} + \frac{\partial Q}{\partial x} = 0 \tag{4.40}$$

$$\frac{\partial A}{\partial t} + \frac{\partial}{\partial x}\left(\beta \frac{Q^2}{A}\right) + gA\frac{\partial z}{\partial x} + gAS_f = 0 \tag{4.41}$$

Where A is the wet cross-section area; t signifies time; Q is the discharge; x is the Cartesian coordinates; β is the momentum correction factor; g is gravity acceleration; Z is the water head for free-surface flow, and Sf is the friction slope. HEC-RAS unsteady computation option and tolerance used in this study is shown in Figure 4.18.
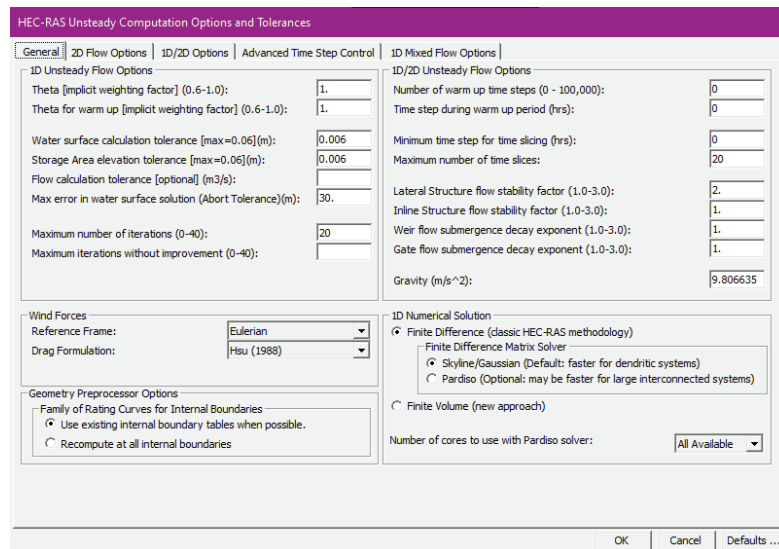
Figure 4.18. Unsteady Computation Options of the HEC-RAS Model

After performing the unsteady flow simulation, all detailed output results can be visualized in the RAS Mapper; however, some output results, such as the inundation map

and depth and water surface elevation map, were exported to ArcGIS. The ArcMap 10.8 software was used to process the output maps of the HEC-RAS model.

4.6.3.5   Overview of Model Performance and Calibration

The model performance was checked by comparing the observed inundation map of Deyr 2019 to the corresponding simulated inundation map in the study area. However, due to the lack of data, the inundation depth in the floodplains of the model was compared to collected images during flooding and observed flood depth marks after the flooding. During this study, site observation to collect necessary data was conducted. During that time, interviews with witnesses, landowners and experts of the local community in the study area were conducted to ensure the extent and depth of the Deyr 2019 flood event, which locals described as the most extreme flood event recorded in the Baledwayne city (Study Area). Also, it was compared the observed water levels to the simulated water levels at the Shabelle River in the study area to evaluate the model's performance.

Calibration of the model is adjusting model parameters to enhance the model's performance. The manning's roughness coefficient n for both 1D and 2D flow areas was used as a calibration parameter in the model to reproduce an acceptable accuracy of simulated results. The model simulation was run several times and compared to observed data; each time, a different value of Manning's n was used. The calibrated values of Manning's n were acceptable. Then, these Manning's coefficients were used in the unsteady flow simulation of the 500 years flood to develop mitigation measures.

4.6.4   HEC-RAS Model Results

4.6.4.1   Evaluating Model Performance and Calibration

This study used the HEC-RAS model to develop flood mitigation measures for Baledwayne city, Somalia. Combined 1D and 2D geometry data were used to analyze the unsteady flow simulation of the study area, which has a total area of 117.13 km^2. Besides geometry data, the land cover layer of the study area was created to assign the Manning's n values of each land cover type. Then the layer was associated with geometry data. After

setting up the model, the unsteady flow was performed to simulate the Flood Deyr 2019 event in the study area using the diffusive wave equation.

The model's performance was evaluated by comparing the extent and depth of the simulated map to the corresponding observed map. Also, the maximum simulated daily river level of the Shabelle River was compared to the observed river level of the study area. The model was calibrated by altering n values to enhance the performance of the model. Several simulations were performed to generate an acceptable inundation map compared to the observed data.

In this study, the ESRI 2020 land cover of the study area was used to assign the n values and the percentage of impervious. The study area was divided into seven types of land cover; each land cover was assigned a specific Manning's n value. Figure 4.19 illustrates the types of land cover and their calibrated n values used in this study. The most abundant type of land cover in the study area is Agricultural lands, with a total area of 63.72 km^2, or 54.4% of the study area. The calibrated n values and the percentage of impervious assigned to this land cover were 0.06 and 3%, respectively. The residential areas cover 14.2% of the study area, and it was assigned an n value of 0.08. The land cover types with calibrated Manning's n values and the percentage of impervious utilized in this study were summarised in Table 4.11.

Table 4.13. Types of Landcover with the calibrated Manning's n values at Baledwayne City (Study Area).

No	Type of Land Cover	Area (km^2)	Percentage (%)	Manning's n	Percentage Impervious (%)
1	Agricultural lands (Rainfed and irrigated agriculture crops)	63.72	54.4	0.06	3
2	Trees (e.g., dense vegetation and wood, wooded vegetation)	3.72	3.18	0.05	3
3	Scrub and Shrub (e.g., sparse shrubs and savannas grass)	30	25.61	0.04	1.5
4	Urban and Residential Areas	16.63	14.2	0.08	75
5	Bare Ground (e.g., exposed rock or soil and dunes)	0.26	0.22	0.015	15
6	Waterbody (Shabelle River valley)	2.75	2.35	0.045	100
7	Grassland (e.g., open savanna and pastures)	0.05	0.04	0.035	3
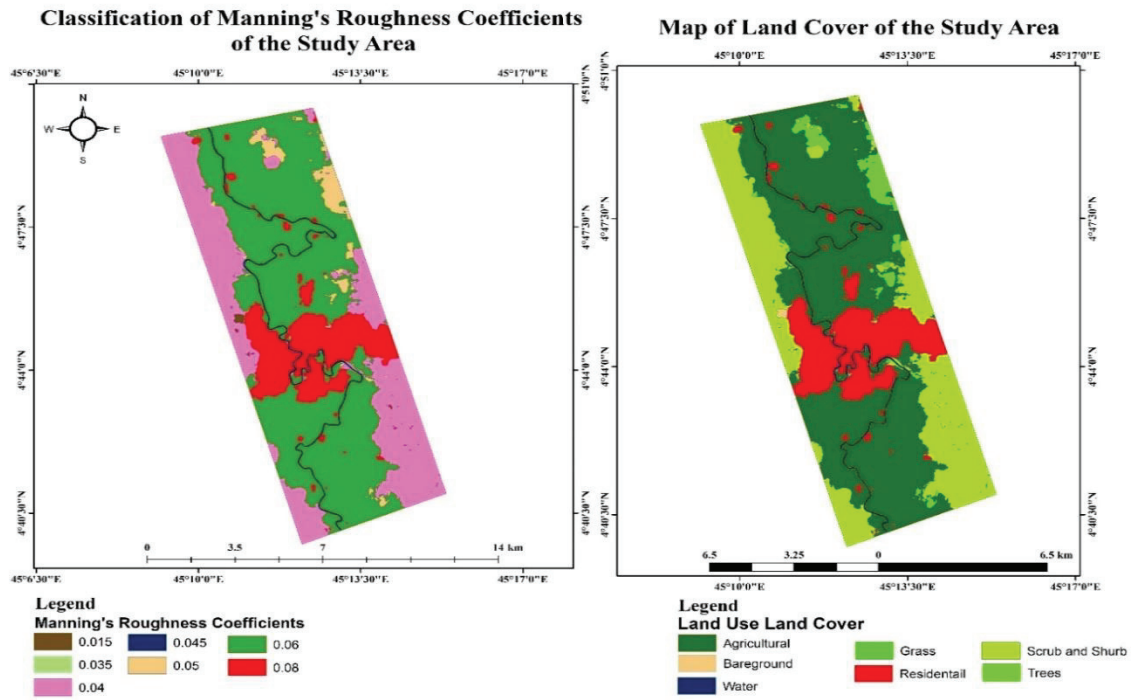
Figure 4.19. Land Cover and Manning's Roughness Coefficients at the Study Area

The inundation map of the Deyr 2019 flood event in the study area was simulated using the calibrated n values shown in table 4.1. Figure 4.20 shows the map extent of the simulated and observed inundation of the Deyr 2019 event flood. According to the observed map, 69.91% of the study area was inundated during the Deyr 2019 event flood, whereas the simulated inundation map shows that 77.00% of the study area was flooded. The maximum observed inundation depth at the downstream of the city was roughly between 0.80 m - 1.0 m, as shown in Figures 4.21 a and b; the corresponding simulated maximum inundation depth to that area was between 0.80 m to 1.10 m. Besides the extent and depth of inundation maps, the Shabelle River level of the study was evaluated and compared to the observed river levels.

Figure 4.22 illustrates the observed and simulated river level though whole the year. The Deyr season in the city starts from the beginning of September to the first week of December, and it is a rainy season, the river level increases and causes flooding. During the Deyr season of 2019, the river level at the upstream of the study area reached 8.35 m leading to extreme flooding. The simulated maximum river level corresponding to the observed river level was 8.44 m. Also, Figure 4.22 shows the river's High-Risk level and

Bank Full level of the Shabelle River in the study area, which are 7.5 m and 8.3 m, respectively. According to Simulated and Observed River levels, the Shabelle River overflows and exceeds the Bank Full level during the Deyr season, as indicated in Figure 4.22. Furthermore, the correlation coefficient R^2 was analyzed using Microsoft Excel to measure the relationship between the observed and simulated river levels at the upstream of the study area. The observed value of R^2 was 0.868, indicating a strong relationship, as shown in Figure 4.23.
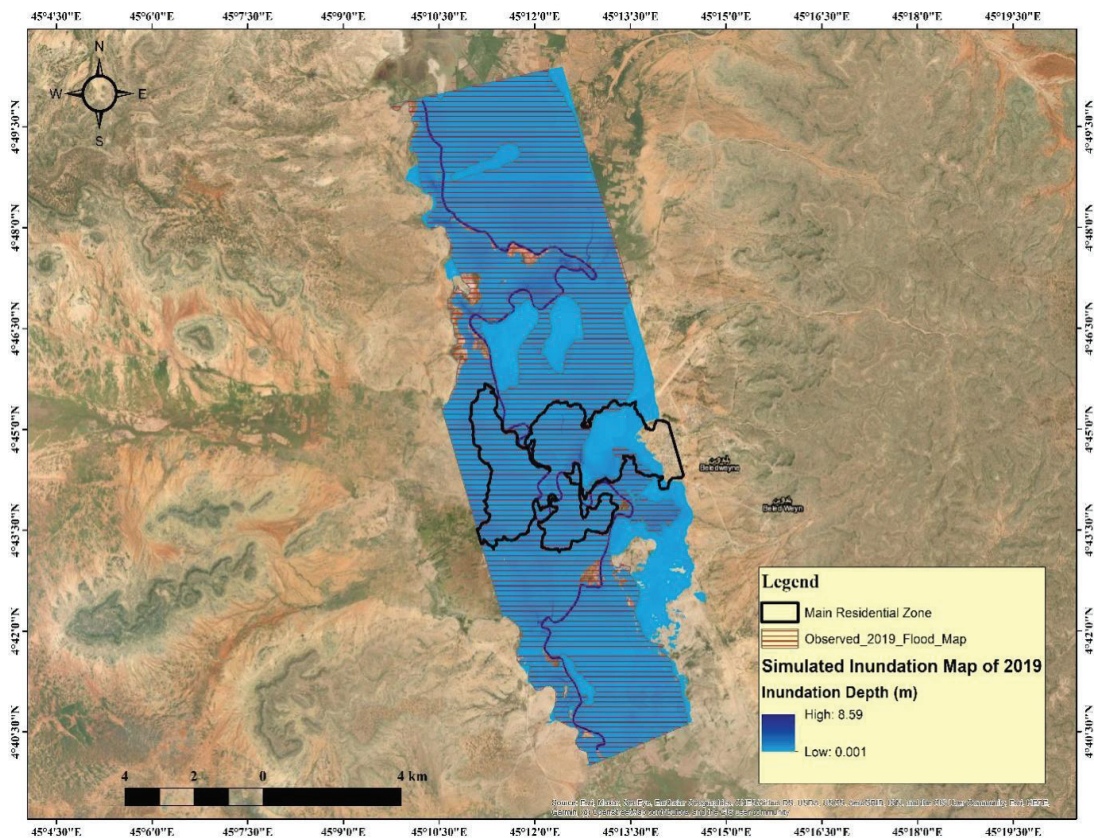
Figure 4.20. The Inundation map extent Observed vs Simulated of Deyr 2019 flood at the Study Area

Figure 4.21 (a). The Observed Inundation depth of the Deyr 2019 flood at the main hospital
in the city
(Source: Abdi Ahmed Hussein, 2019)

Figure 4.21 (b). The Observed flood depth mark of the Deyr 2019 flood at
downstream in the city
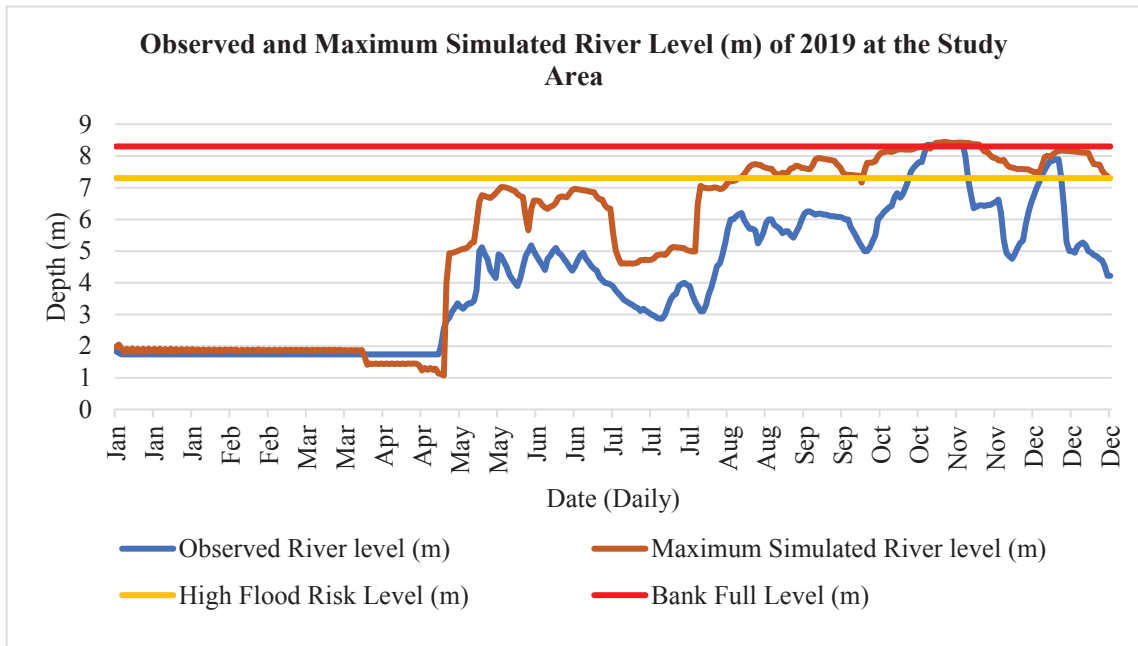
Figure 4.22. Observed and Simulated River Level at upstream of the Shabelle River during the Deyr 2019 flood in Study Area
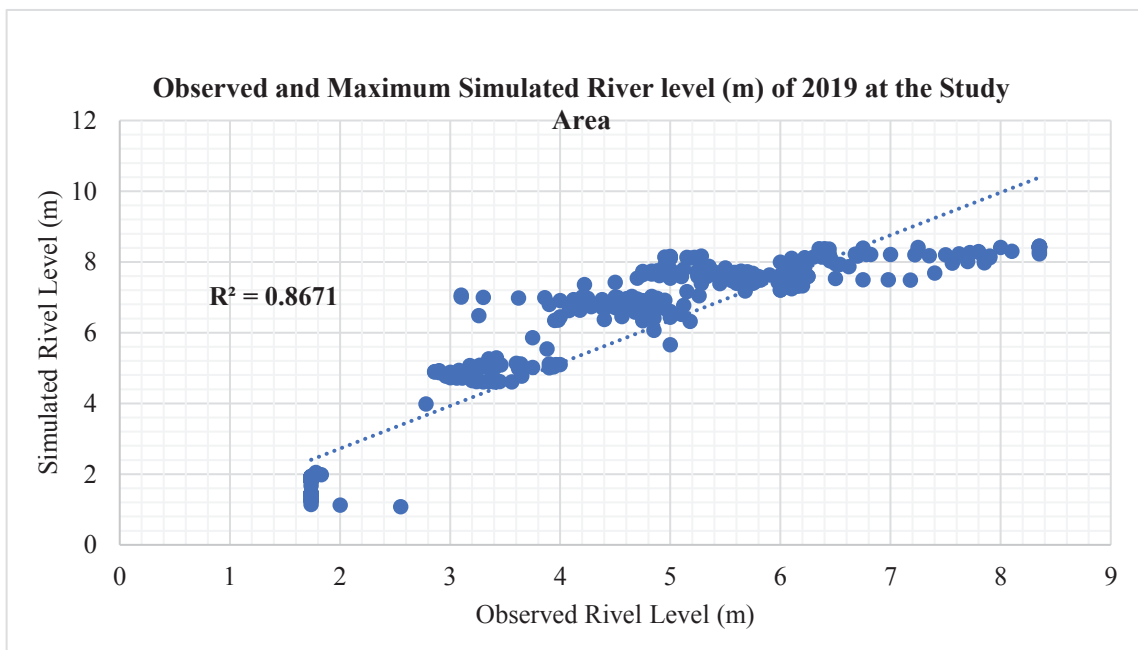
Figure 4.23. Correlation Between Observed and Simulated River Level at upstream of the Shabelle River during the Deyr 2019 flood in Study Area

According to the model's performance results, the simulated inundation map of the Deyr 2019 flood event is accepted and close to the observed map. Furthermore, the correlation between the simulated and observed river levels indicates a strong

relationship. So, chapter five uses a calibrated and validated model result to simulate a 500-years flood return period.

4.6.4.2 Inundation Map of Deyr 2019 Flood Event

Shabelle River divides the study area into Left and Right sides. So, the 2D flow areas in this study are the Left floodplain with a total area of 69.23 km^2 and the Right floodplain with a total area of 41.55 km^2, as indicated in Figure 4.24. The Left floodplain is almost had a flat slope, which increases the extent of inundation, whereas the Right floodplain contains highland, which decreases the extent of inundation.
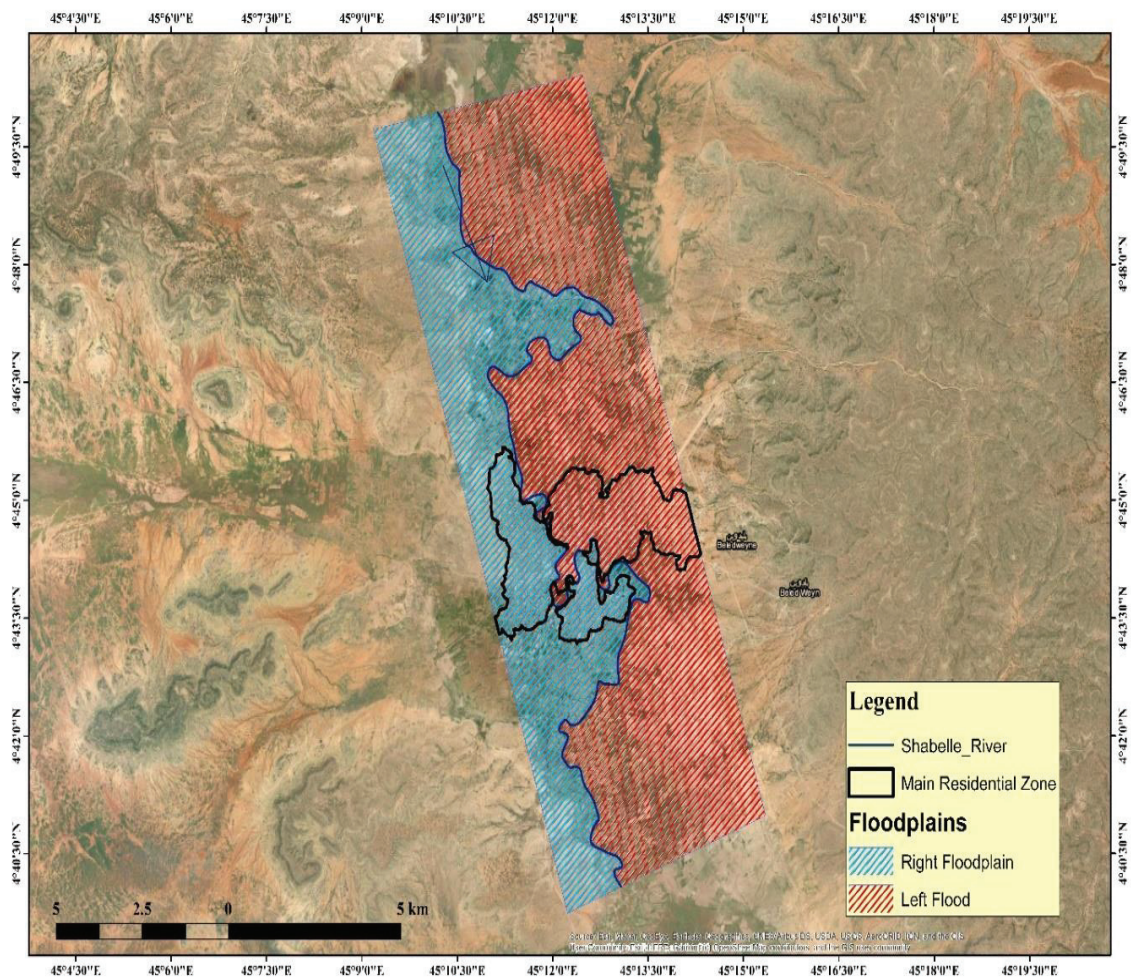
Figure 4.24. The 2D Flow Areas (Floodplains) in the Study Area

The Shabelle River flooded more than 85.7% of the Left floodplain and more than 62.5% of the Right floodplain in the study area during the Deyr 2019 flood event, as indicated in Figure 4.25. However, the maximum flood depth in the Left floodplain was between 1.00 m and 1.50 m, whereas the Right floodplain has a maximum inundation depth ranging between 0.90 m and 1.70 m. The difference between the Left and Right floodplains is mainly due to the land formation of the Baledwayne city (Study area). The river level at the downstream of the study areas reaches up to 8.6 m, indicating that the river exceeded its full bank level.
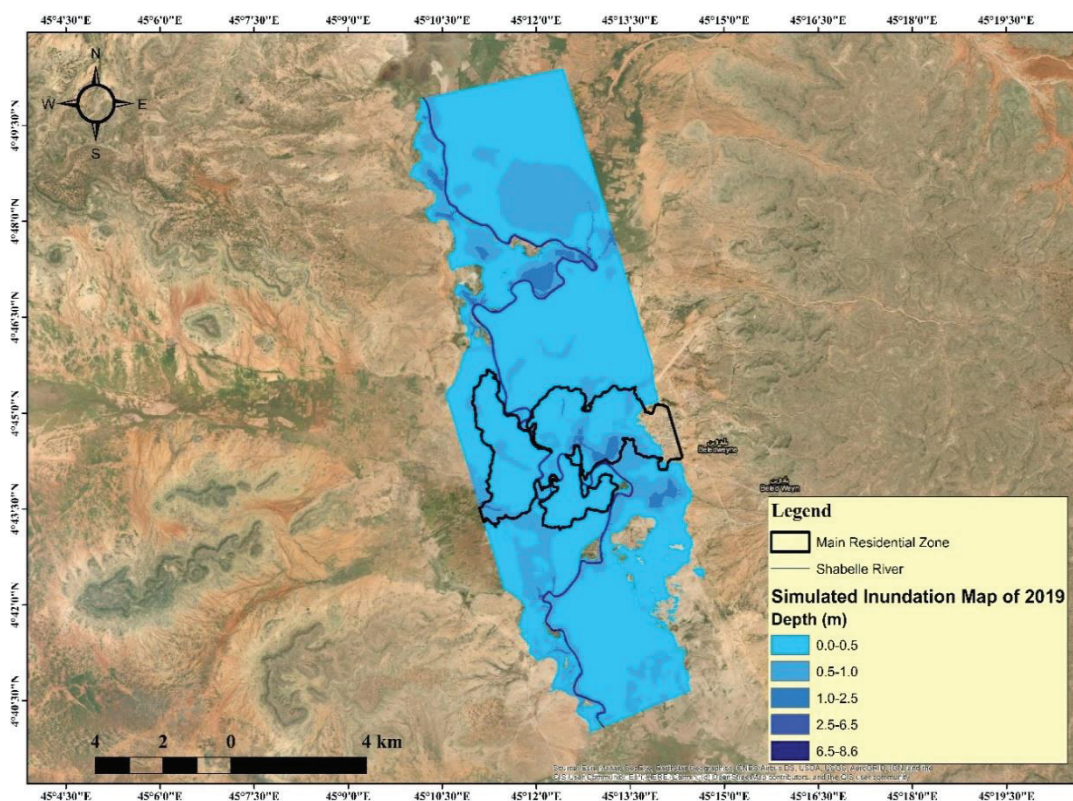
Figure 4.25. The Deyr 2019 Flood-Simulated Depth and inundation Extent in the Study Area

Figure 4.26 indicates the velocity of the flood in the study area. The maximum velocity in the Shabelle River ranges between 1.30 m/s and 1.70 m. The flood velocity in the Left floodplains ranges between 0.01 m/s to 0.05 m/s in most areas; however, small areas reach up to 0.50 m/s. The flood velocity in the Right floodplain ranges between 0.01 m/s and 0.31 m/s in most areas, but in some locations, the flood's velocity reaches 0.70 m/s.
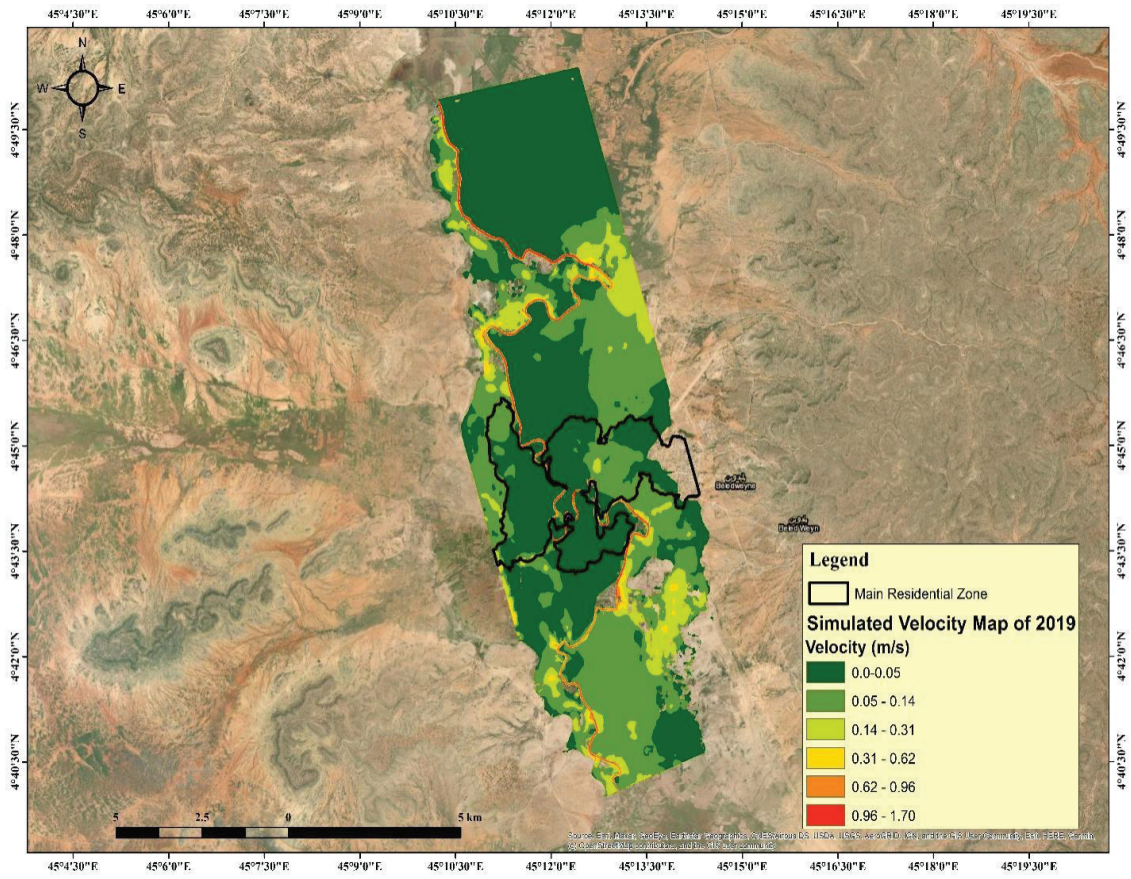
Figure 4.26. The Flood Velocity Map Simulated the Deyr 2019 Flood Event in the Study Area

CHAPTER 5

FLOOD MITIGATION MEASURES

5.1 Introduction

This study used the HEC-RAS model to develop flood mitigation measures for Baledwayne city (Study Area). Except for the Flow hydrograph boundary condition, the calibrated model parameters used in Chapter Four to simulate an inundation map of the Deyr 2019 flood event were also used in this analysis. The peak discharge value of 500 years of the return period from the output result of the flood frequency analysis using the HEC-SSP model was used as a flow hydrograph boundary condition for generating the inundation map of 500 years of the flood, as shown in Figure 5.1. The inflow hydrograph of 500 years has a peak flow rate of 605.4 m³/s, whereas the simulated peak discharge of 2019 illustrated in Figure 4.15 has 477.7 m³/s.
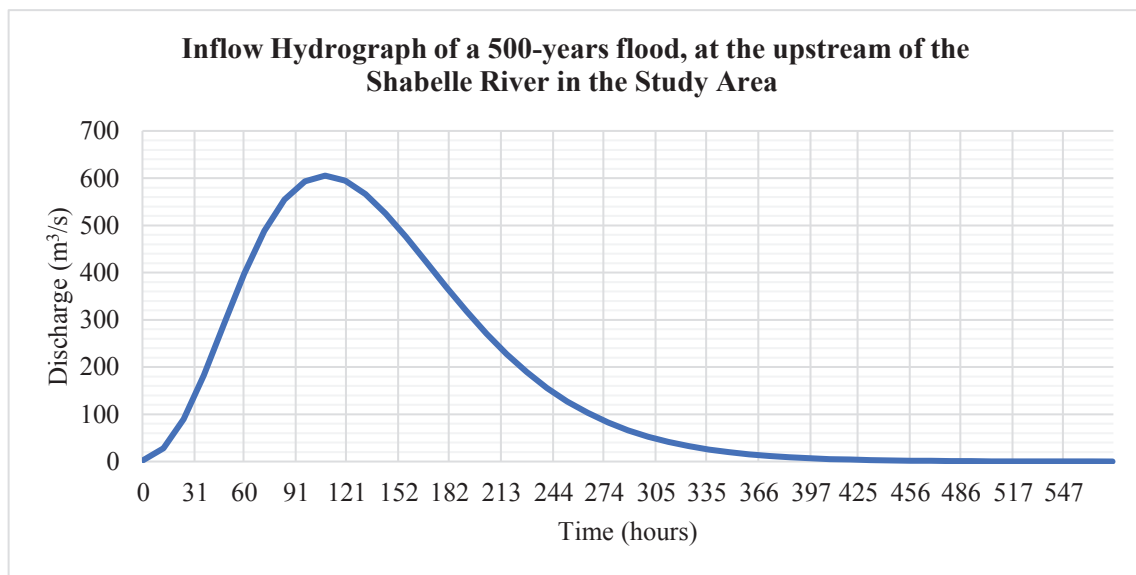
Figure 5.1. Inflow hydrograph of a 500-years flood at the Study Area

5.2 Modelling The Inundation Map of A 500-Years Flood

Unsteady flow simulation of a 500-year flood was generated using the calibrated value of Manning's (n) and other parameters used in the previous simulation; and the peak discharge hydrograph of the 500-year flood as inflow hydrograph boundary condition. The simulated 500-year flood return period was compared to the simulated Deyr 2019 flood event, as shown in Figure 5.2. The simulated 500-year flood event indicated that the inundation map increased compared to the 2019 flood event. Figure 5.2 indicates that the flood extent map of the 500-year return period reaches a total area of 88.56 km^2, which means that the flooded water submerged almost all of the city. In the Left floodplain of the study area, the flooded area during the simulated 500-year flood inundation map is almost the same compared to the simulated 2019 flood event. At the same time, the flooded area increased by about 3.25 km^2 on the right floodplains during the simulated 500-year flood inundation.

Figure 5.2 also shows that the flood depth increased in the simulated 500-year flood. The river level reached at the downstream of the study areas reaches up to 8.78 m, whereas the corresponding river level for simulated the Deyr 2019 flood event was 8.6 m. Also, the flood depth in floodplains was increased; in the left floodplain, the maximum flood depth increased from 1.00 m-1.50 m to 1.30 m-1.80 m, whereas on the right floodplain, the maximum flood depth raised from 0.90 m-1.70 m to 1.30 m-1.95 m in some locations.

Each alternative developed in this study was compared to the generated map of a 500-year flood event to develop the most appropriate mitigation measures that protected the Baledwayne city during the peak discharge of a 500-year flood.
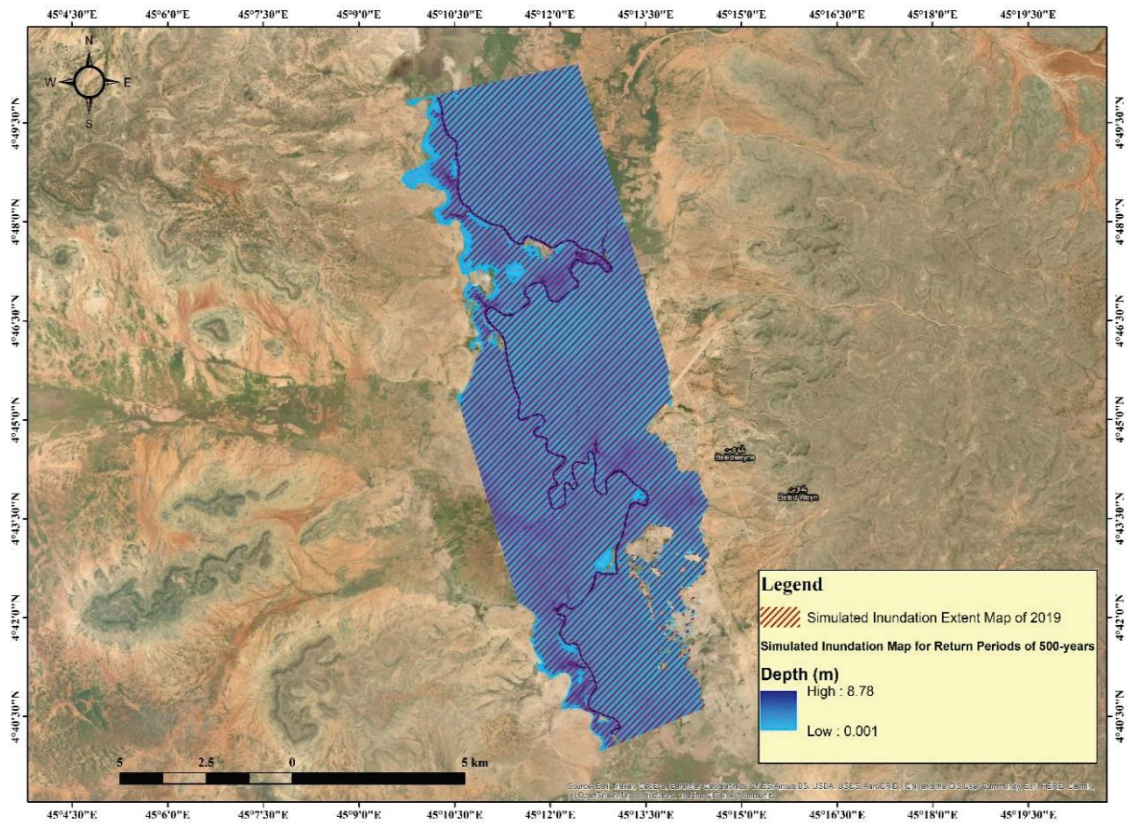
Figure 5.2. The inundation map simulated Deyr 2019 flood and a 500-year flood in the Study Area

5.3 Overview of Flood Mitigation Measures

Flooding can be defined as one of the most frequent natural tragedies. Last decade Baledwayne city experienced consecutive flood events, which led to the loss of life and economics. Generally, it is unattainable to eliminate the impact of flooding, though it can reduce the wear and effects of floods by implementing practical flood mitigation measures. Flood hazard reduction means decreasing the magnitude of overflow or exposure of the impacted area.

Flood Mitigation measures are divided into structural and non-structural mitigation measures. Non-structural mitigation measures are typically cheaper and easy to implement compared to structural mitigation measures. These mitigations include land use planning and soil management, flood forecasting, perception and awareness, emergency systems, and flood insurance. Structural mitigation plans are traditionally known practices of flood mitigation, and they have been used in corporations with general

flood managing approaches in most flood plain areas. Some structural mitigation measures are complex and massive structures, while others are simple. Structural mitigation includes the construction of flood levees or embankments, dams, floodwalls, artificial ponds, channel improvements, diversion schemes, reservoirs, river training works, and others.

Combining structural and non-structural mitigation measures is common to efficiently reduce the effect and damage of floodings. Determining the most appropriate mitigation measure needs an exhaustive study of possible risks and damages and comparative costs and advantages of various mitigation measures.

5.4 Selecting and Identifying Mitigation Measures

Baledwayne city is listed as one of the most vulnerable to floods in Somalia. The Baledwayne City Flood Committee mentioned that 1961 was the first flood event recorded in the city, and then 1981 was the second event recorded in the city. The flood events increased last decade and reached two or three flood events in a single year. The Deyr season 2019 flood event was the most extreme flood that the city experienced, as the local community mentioned. The consecutive flood caused massive damage to the city, leading to a gap in human growth which halted the community's development in the economic and educational sectors. Several projects of flood mitigations were going on in the city; however, all those were relief and emergency projects instead of permanent projects to protect the city from repeated flooding.

In 2017, some of the city's community volunteered and discussed how to deal with the repeated floods in the city, which every year affect the lives of the people causing death, displacement and damage to properties. Then, they formed the Baledwayne City Flood Committee, which consisted of some scholars and businessmen of the city. The Committee's main task started during the extreme flood of Deyr 2019. They initially analyzed and implemented relief mitigation measures to protect the flooding water from the city. After flooded water decreased and dried out, many efforts and projects were started to strengthen the mitigations implemented by the Committee. Also, new projects were started with the consultant of the Baledwayne City Flood Committee to protect the city from flooding, and different institutions and NGOs implemented those projects.

In 2020 GIZ funded a Sustainable Water Resource Management Programme in Somalia/Integrated Water Resource Management project implemented by the Ministry of Energy and Water Resources of Somalia (MoEWR). The location of the project was the study area, and its objective included rehabilitation of flood-prone priority areas, removal of trees, and sand deposits, diversion works and smoothening of relief slopes. During the preliminary study of that project, the researcher was part of a technical team that visited the city to do site observations. During that period, the researcher met and discussed with the Baledwayne City Flood Committee ongoing projects of flood mitigation measures in the city and visited all sites to see ongoing works and discussed with locals how floods affected them. Several flood mitigation projects were going on in the different parts of the city, such as the construction of levees, rehabilitation of the Warabole diversion channel, and detention ponds. It became possible to meet engineers and experts implanting those projects. Figures 5.3 (a), (b) and (c) illustrate some ongoing and executed projects during site observation in the study area.

This study examined mitigation measures implemented and ongoing in the study area regarding an event having a return period of 500 years flood to develop the most suitable measures to protect Baledwayne city from flooding of the Shabelle River. The analyzed remedial measures are the Warabole diversion channel located in the downstream of the river, detention ponds in the upstream of the floodplains, improvement of the river channel, and levees structures on both sides of the river. Each of the above remedial measures was investigated one by one and combined into two mitigations. Also, it was analyzed by integrating all those mitigations into complex mitigation measures to develop the most appropriate remedial measures.

Figure 5.3 (a): Constructed Levees along the side of Shabelle River in the Study Area

Figure 5.3 (b): Constructed Detention Pond at the upstream in the Left floodplain in the Study Area

Figure 5.3 (c): Ongoing rehabilitation of the Warabole diversion channel at the downstream in the Right floodplain in the Study Area

5.5   Developing Flood Mitigation Measures

5.5.1   Alternative 1: Assessment of Warabole Diversion Channel

Diversion channels are mainly artificial channels developed to divert excess water to prevent flooding, land sliding and erosion. Warabole Channel is located on the west side of Baledwayne city, as shown in Figure 5.4. The channel was constructed by the Somalia Democratic Republic mainly for irrigation and flood control purposes. The length of the Warabole channel is about 4 km, starting at the city's west side and ending at Gamberlawe outside of the city. After the collapse of the Somalia Democratic Republic government in 1991, the channel was not maintained or rehabilitated. So, the channel's function stopped, and most channels were covered by sand. Also, areas of the channel were illegally used for farming and building purposes. After Deyr 2019 flood event, it was suggested to rehabilitate the channel and reconstruct its gates.
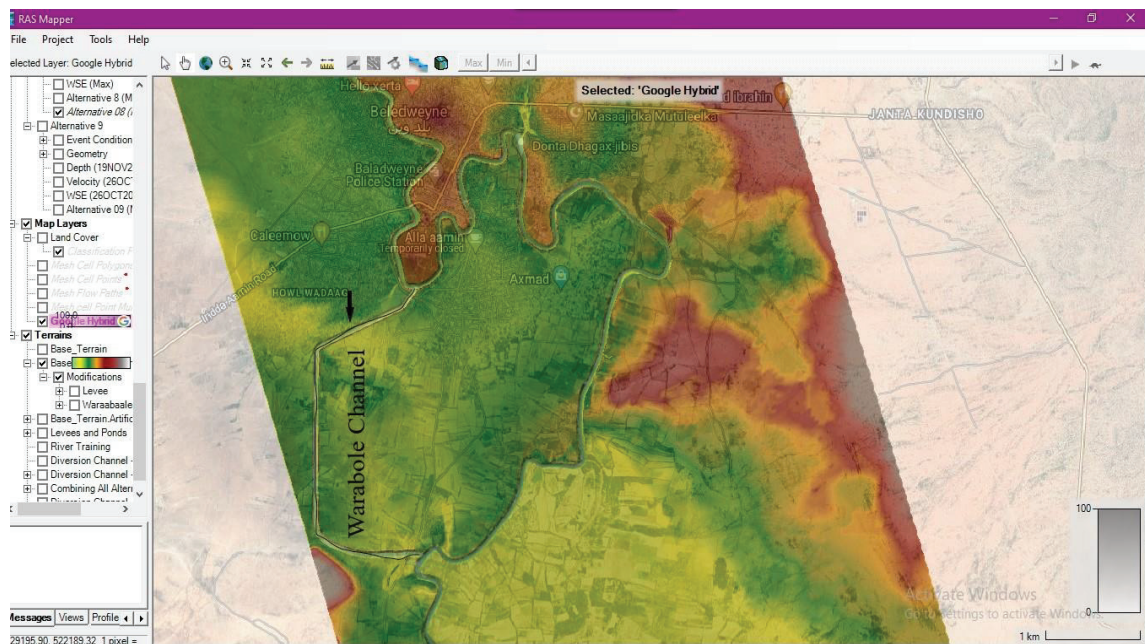
Figure 5.4. Warabole diversion channel at the downstream in the Right floodplain in the Study Area

This study examined the contribution of the current Warabole Channel without gates to protect the city from the flood of the Shabelle river using the peak flow rate of a 500-year flood event. Since there is no exact data on the dimension of the channel except its length, which is 4 km, after several trials dimensions, the bed width of 25 m and top width of 50 m and depth of 5 m was used as a final dimension of the channel, as shown in Figure 5.5. A levee dike was constructed on the channel's left side to prevent the overflow of the channel when it reaches its maximum depth. Figure 5.5 indicates the dimension of the Warabole channel, and its levee structure used in this analysis. The channel was designed by modifying the underly terrain used in the previous Deyr 2019 flood event simulation. A 500-year flood event was simulated using the modified terrain layer to assess how the channel contributes mitigation of this flood event.
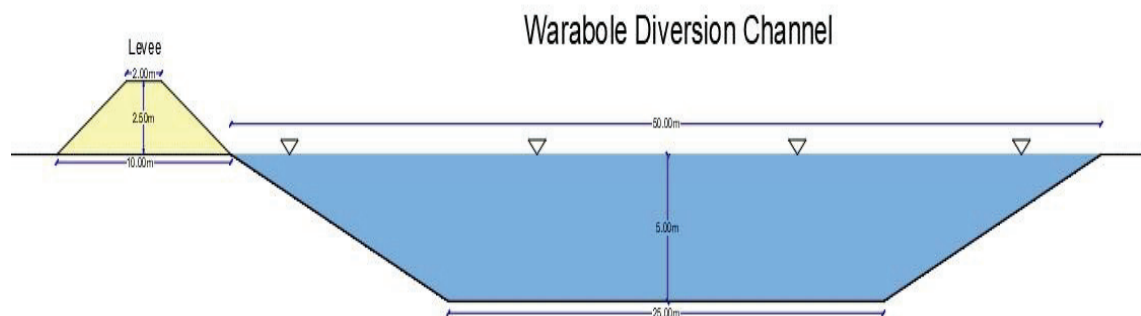
Figure 5.5. The Design of Warabole Diversion Channel and its Levee Structure Used in this Analysis

It was observed that the total flooded area decreased from 88.56 km^2 to 86.97 km^2. The inundation reached about 59.53 km^2 (86%) of the area in the left floodplain, almost the same as a 500-year flood event. At the same time, 27.45 km^2 (66.1%) of the area in the right floodplain of the study area. according to the simulated inundation map, the proposed channel does not affect the left floodplain of the study area, and the inundation extent remains. However, there is a slight change in the right floodplain of the study area; the inundation extent decreased from 29.21 km^2 to 27.45 km^2. The maximum simulated flood depth in the left floodplain is 1.50 m in small areas located in the downstream of the city. In comparison, the right floodplain has a maximum simulated inundation depth of 1.70 m in an area located in the upstream of the city. There is no notable difference in river level at the downstream of the study areas after applying alternative 1. Figure 5.6

illustrates the inundation map extent and depth after applying alternative 1 (Construction of Warabole channel).

It is concluded that this alternative is insufficient to protect the study area against a 500-years flood event and it has a minor contribution.
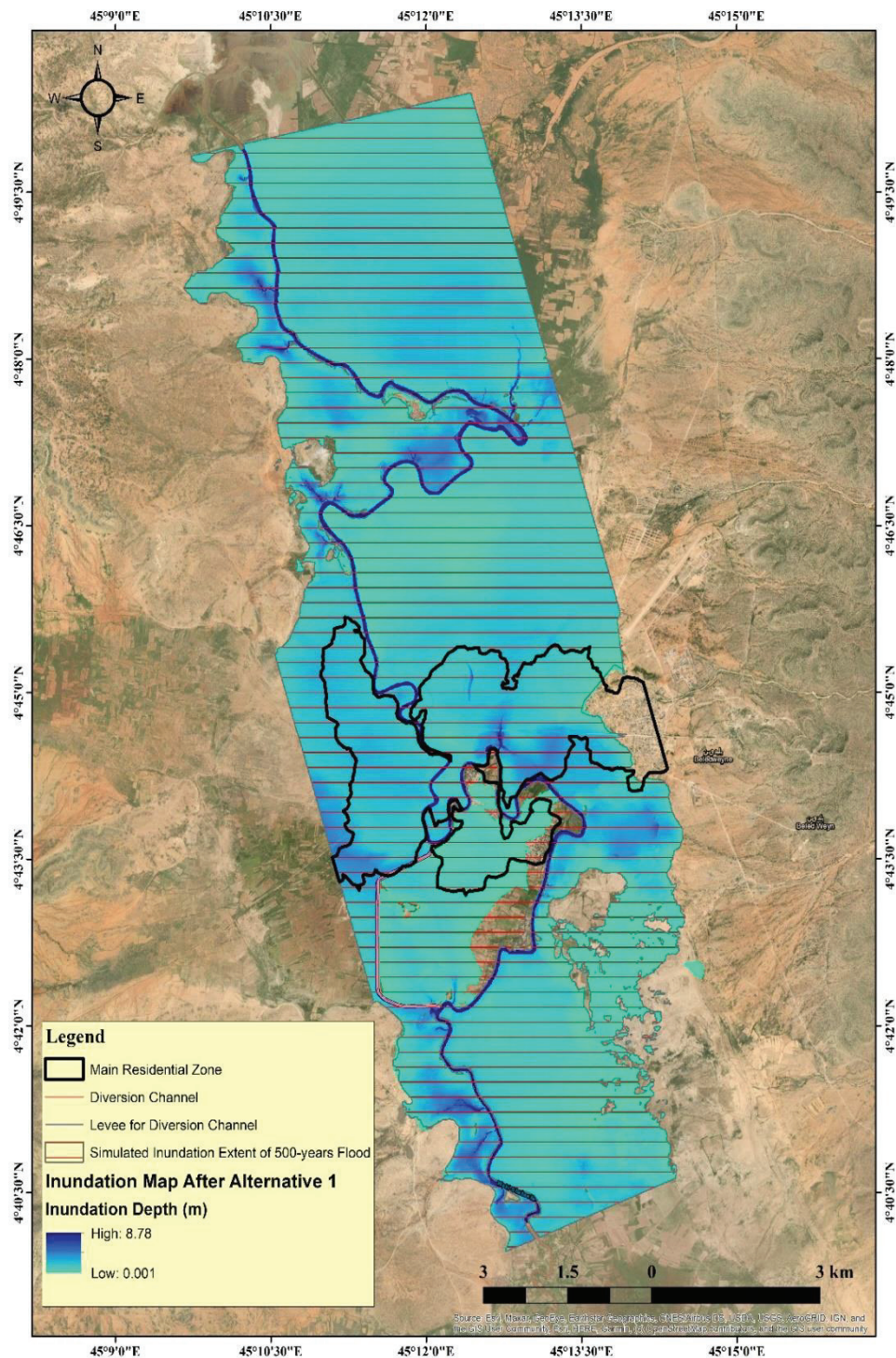
Figure 5.6. The Inundation Map Generated After Alternative 1

5.5.2 Alternative 2: Assessment of Detention Ponds

Detention ponds are commonly used for flood mitigation measures and are designed to hold temporary water before it enters the mainstream. This study analyzed the contribution of the constructed detention ponds to protect the city from the flood of the Shabelle River using the peak discharge of a 500-year flood event. A levee dike was constructed in the upstream parts of the Left and Right floodplains in order to block overflow from reaching the city during flooding. So, the area behind levees was used as detention ponds to protect the city from flooding the Shabelle river. The Levees were developed by modifying the underly terrain used in the previous Deyr 2019 flood event simulation. A 500-year flood event was simulated using the modified terrain layer to evaluate how the detention ponds mitigate this flood event.

The location of the proposed levees for the detention pond was based on the constructed Hiilo-Kili levees dike in the study area in 2019. However, the dimension of the proposed levees used in this alternative was obtained after several trials to obtain the most proper dimensions to protect the study area against peak discharge of a 500-years flood event. Figures 5.7 (a) and 5.6 (b) indicate the dimension of the proposed levees on both floodplains used in this analysis.
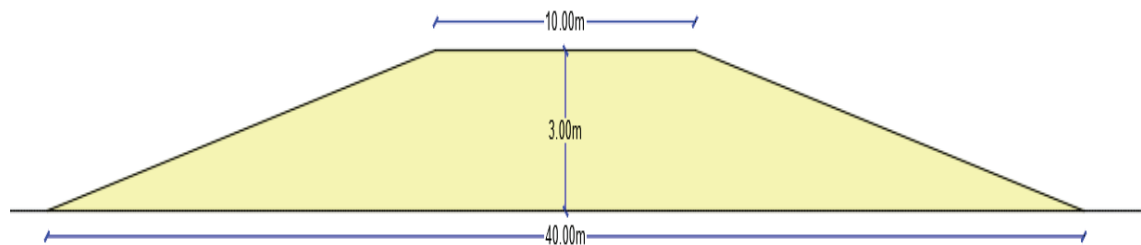
Figure 5.7 (a). The Design of Levee Structure for Left Detention Pond in the Study Area
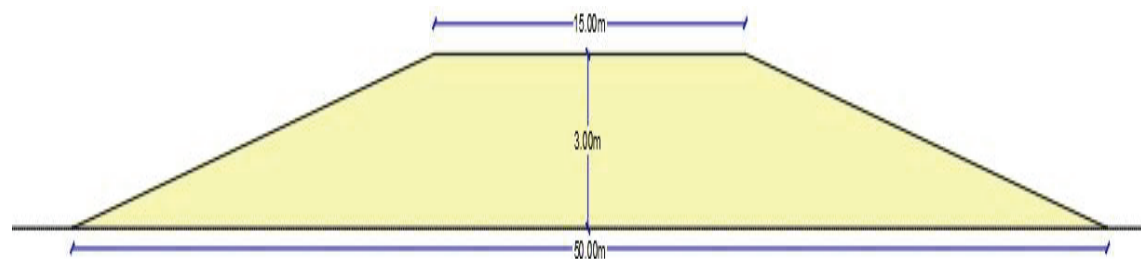
Figure 5.7 (b). The Design of Levee Structure for Right Detention Pond in the Study Area

It was detected that the total flooded area decreased from 88.56 km^2 to 31.47 km^2. The Shabelle River flooded into an area of 19.997 km^2 (28.89%) of the area inside of the left detention pond in the Left floodplain. At the same time, the total area flooded in the Right floodplain of the study area is 11.48 km^2 (27.62%) of the area in that floodplain, as shown in Figure 5.8. The maximum simulated water depth in the detention pond on the Left floodplain is between 2.0 m and 2.7 m. In comparison, the detention located in the Right floodplain has a maximum simulated water depth ranging from 2.5 m to 3.5 m. So, inundation water reached downstream of the Right floodplain in the study area, and the overflowed water has a maximum depth of 0.20 m. Almost all the excess water of the river was held in the detention ponds, so the river level raised 0.3 m at the upstream of the study areas after applying Alternative 2.

According to the simulated inundation map, shown in Figure 5.8, the proposed levee of the detention pond in the Left floodplain blocked the flooded water and held it in the detention ponds during the peak discharge of a 500-year flood, so the downstream of the study area, including the residential areas, is protected. However, the proposed levee of the detention pond in the Right floodplain did not block all the water and overflowed.

The obtained results indicated that the proposed levee of the detention pond in the Left floodplain is a risk of overflow since this detention pond has a high-water depth. Meanwhile, the proposed levee of the detention pond in the Right floodplain overflowed during the peak discharge of a 500-year flood. So, it is concluded that this alternative only is a risk to rely on as a mitigation measure to defend the study area against the peak discharge of a 500-year flood event.

Figure 5.8. The Inundation Map Generated After Alternative 2

5.5.3 Alternative 3: Assessment of Levees (Dikes)

Levees or dikes are usually earthen structures designed to control the overflow of a river. This study examined the contribution of the constructed levees along the Shabelle River to protect the city from the river's flood using the peak discharge of a 500-year flood event. One of the main reasons behind the repeated flood event in the city is a lack of regulation and management of the Shabelle River basin. After the collapse of the Somalia Democratic Republic government in 1991, the embankments or dikes of the Shabelle river in the study area did not receive any rehabilitation or maintenance, and it was getting worse. Also, farmers illegally opened the embankments and dikes of the river to irrigate their agricultural land, which increased the flooding.

In this alternative it was developed lateral structures (levees), which have a total length of about 8 km along the left side of the river and about 11 km along the right side of the river in the study area. The location of the levees was selected based on the main breakage points of the river in the study area; also, it was blocked open points, which can lead overflow of the river by modifying the underly terrain used in the previous Deyr 2019 flood event simulation.

During this analysis, the levee structure was initially assigned to the dimensions of constructed levees in the study area, which are 1 m of top width, 5 m of bottom width and a height of 2 m. It was observed that the above dimensions are insufficient, so several trials were applied to obtain the most proper dimensions to protect the study area against peak discharge of a 500-years flood event. Figure 5.9 shows the dimension of the proposed levees structures on both sides of the river used in this alternative.
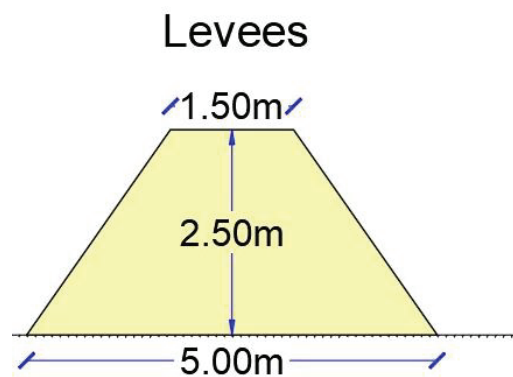
Figure 5.9. The Design of Levee Structure along both sides of Shabelle River in the Study Area

It was observed that the total flooded area decreased from 88.56 km^2 to 75.14 km^2. The Shabelle River overflowed into 47.87 km^2 (69.15%) of the area in the left floodplain. At the same time, the total area flooded in the Right floodplain of the study area is 27.27 km^2 (65.63%) of the area in that floodplain, as shown in Figure 5.10. The maximum simulated water depth in the Left floodplain is between 0.5 m and 1.0 m; however, a small area in downstream of the left floodplain inundation depth reached 1.80 m. The Right floodplain has a maximum simulated water depth ranging from 0.90 m to 1.50 m. The water level in the river reached 9.39 m downstream in the study area after applying alternative 3.

According to the simulated inundation map shown in Figure 5.10, the proposed levees along the river on the left side decreased the flooded area by 16.61% during the peak discharge of a 500-year flood. However, the proposed levee along the river on the right side made little progress, less than 2 km^2, and it can be said that the inundation map extent is almost the same as the simulated inundation map of a 500-year flood. Since the proposed levees on both sides of the river did not prevent the river's overflow during the peak flow rate of a 500-year inundation event it is concluded that this alternative is insufficient and a risk to rely on as a mitigation measure to defend the study area against the peak discharge of a 500-year flood event.

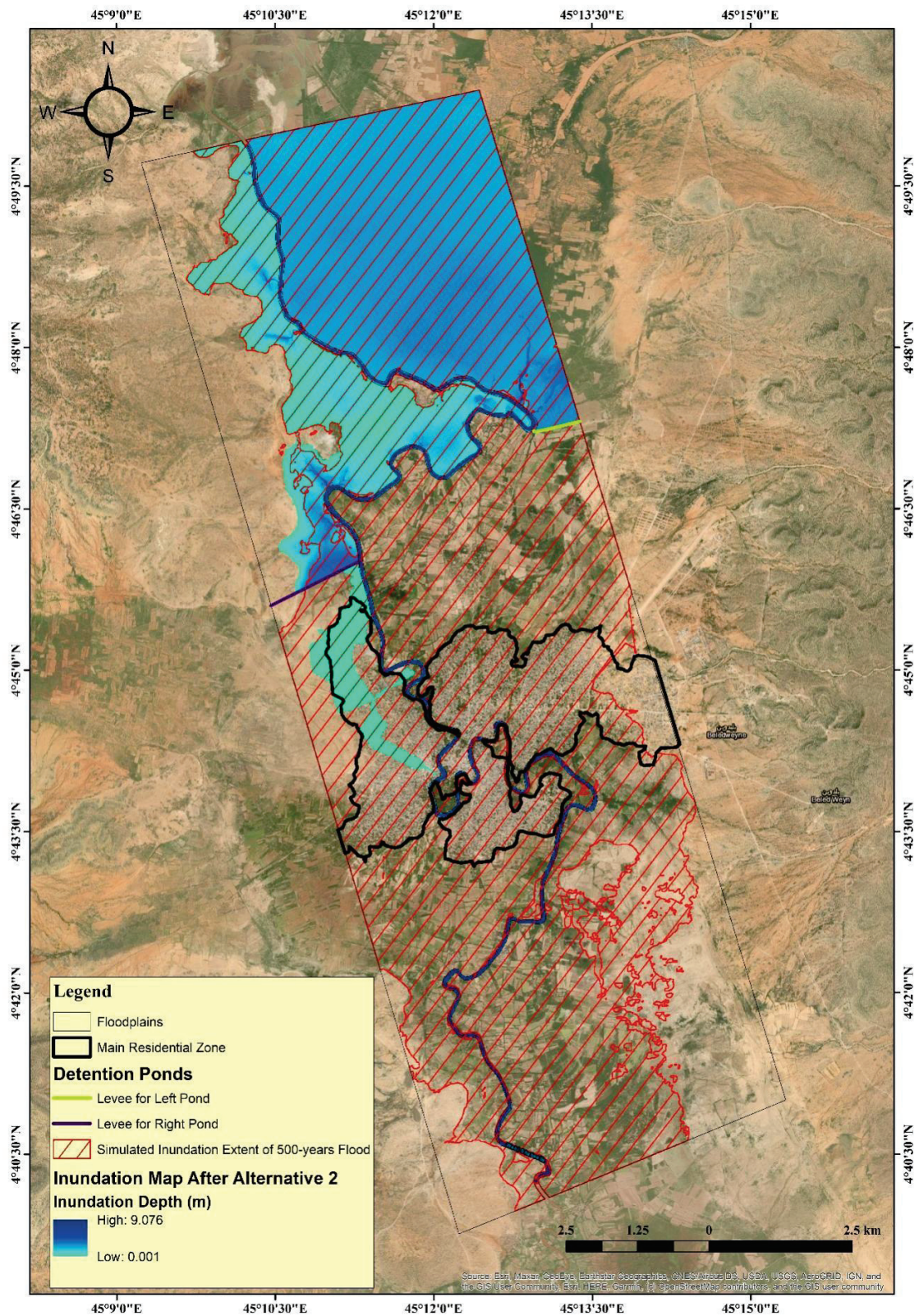Figure 5.10. The Inundation Map Generated After Alternative 3

5.5.4 Alternative 4: Improving (Restoration) the Shabelle River

River dredging is the process of removing debris and sediments from the bed of rivers. This process is commonly used to maintain the channel's capacity and prevent floods by improving the river. Shebelle River in the study area did not receive any rehabilitation, which decreased the river's capacity due to sediments and debris filling the channel bed, as the local community mentioned. This alternative investigated the contribution of improving Shabelle river to protect the city from the river's flood using the peak discharge of a 500-year flood event. The river was improved by modifying the underly terrain used in the previous Deyr 2019 flood event simulation. During the modification of the river, it was investigated all cross-sections of the river developed in chapter four to increase the depth of cross-sections containing low depth. Since there is no historical data on the river's depth in the study area, several trail depths were applied. Finally, the depth of Shabelle River in the study area was increased by roughly 1 m; also, the river banks were modified to protect the study area against peak discharge of a 500-years flood event.

It was observed that the total flooded area decreased from 88.56 km^2 to 87.54 km^2 which is negligible progress. Shabelle River overflowed into 60.33 km^2 (87.14%) of the area in the Left floodplain. At the same time, the total area flooded in the Right floodplain of the study area is 27.22 km^2 (65.51%) of the area in that floodplain, as shown in Figure 5.11. The maximum simulated water depth in the Left floodplain is between 1.20 m and 1.50 m, slightly different from the flood depth of a simulated 500-year flood, which was between 1.30 m and 1.80 m. The Right floodplain has a maximum simulated water depth ranging from 0.70 m to 1.20 m, different from the flood depth of a simulated 500-year flood, which was between 1.30 m and 1.95 m. The water level in the river reached 9.81 m in the downstream of the study area after applying Alternative 4.

According to the simulated inundation map illustrated in Figure 5.11, improving the river did not make notable progress, and the inundation map extent is almost the same as the simulated inundation map of a 500-year flood. However, the flood depth decreased significantly in both floodplains, especially the Right floodplain. Since the proposed improvement of the river did not reduce the flooding during the peak discharge of a 500-

year flood event, this alternative is inadequate to defend the study area against the peak discharge of a 500-year flood event and also has a minor contribution, so it is a risk to rely on as a mitigation measure.

Figure 5.11. The Inundation Map Generated After Alternative 4

5.5.5 Alternative 5

This alternative investigated the contribution of combing detention ponds and levees along the Shabelle river to protect the city from the river's flood using the peak discharge of a 500-year flood event. The previous dimensions of both mitigations were tried to reduce; however, the reduced dimensions did not show progress. So, the exact dimensions used in alternatives two and three were used when combining them.

It was observed that the total flooded area decreased from 88.56 km^2 to 30.974 km^2 which is good progress. Shabelle River overflowed into 19.94 km^2 (28.80%) of the area inside of the left detention pond. At the same time, the total area flooded in the Right floodplain of the study area is 11.036 km^2 (26.56%) of the area in that floodplain, as shown in Figure 5.12. The maximum simulated water depth in the detention pond on the Left floodplain is between 0.70 m and 1.0 m, significantly different from the flood depth after using Alternative 2 only, which was between 2 m and 2.7 m. In comparison, the detention located in the Right floodplain has a maximum simulated flood depth ranging from 2.5 m to 3.5 m, and this is almost the same as alternative two. So, inundation water reached downstream of the Right floodplain in the study area, and the overflowed water has a maximum depth of 0.10 m. The river level reached 9.79 m at the upstream of the study areas after applying Alternative 5.

According to the simulated inundation map of the combination of Alternatives 2 and 3, shown in Figure 5.12, the dike of the detention pond in the Left floodplain blocked the flooded water and held it in the detention ponds during the peak discharge of a 500-year flood, so the downstream of the study area, including the residential areas, is protected. However, the proposed levee of the detention pond in the Right floodplain did not block all the water, although overflowed water depth behind the levee of this detention pond is less than 0.21 m. After the combination of Alternatives 2 and 3, it was observed that there was a significant reduction in the flood depth in the left detention pond; however, there is no change in the right detention pond.

The obtained results indicated that the levee for the detention pond in the Right floodplain overflowed during the peak discharge of a 500-year flood, and there is still a probability of failure since this detention pond has a high-water depth. So, it is concluded that this alternative with the above design measurements may be a risk to rely on as a mitigation measure to defend the study area against the peak discharge of a 500-year flood event.
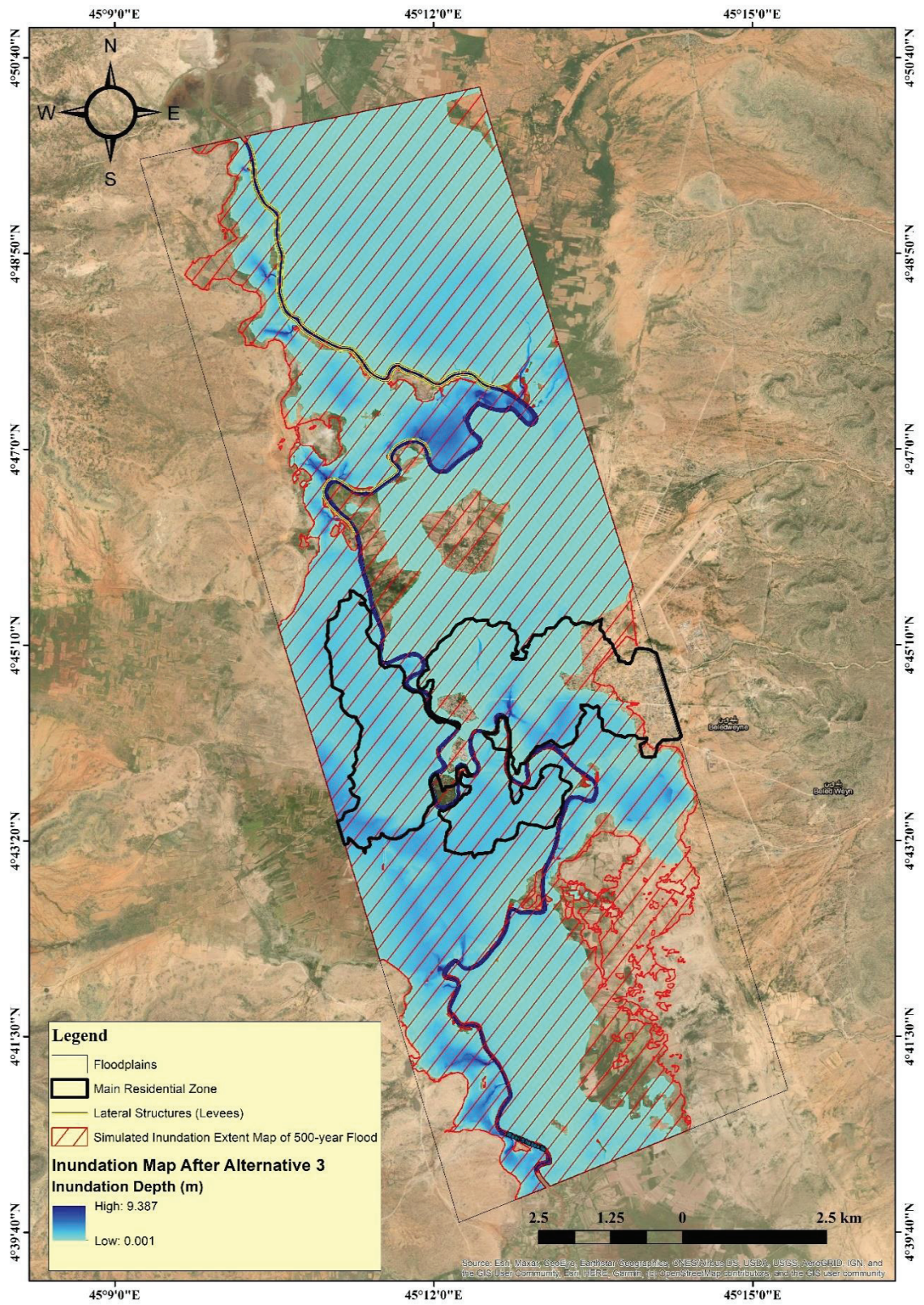

Figure 5.12. The Inundation Map Generated After Alternative 5

5.5.6 Alternative 6

This alternative assessed the construction of levees (dikes) along both sides of the Shabelle river and the improvement of the river by dredging it to increase its capacity. So, this alternative is the combination of Alternatives 3 and 4. Several trails were applied to identify the appropriate dimensions of each alternative component; however, it was concluded to use previous dimensions as the final dimensions in this alternative.

The simulated results indicate that the total inundated area decreased from 88.56 km^2 to 72.73 km^2, which is minor progress. The River overflowed into an area of 49.80 km^2 (71.94%) of the area in the Left floodplain. At the same time, the total area flooded in the Right floodplain of the study area is 22.93 km^2 (55.19%) of the area in that floodplain, as shown in Figure 5.13. The maximum simulated flood depth in the Left floodplain is between 0.70 m and 1.0 m, significantly different from the flood depth after using Alternative 4 only, which was between 1.20 m and 1.50 m. The Right floodplain has a maximum simulated flood depth ranging from 0.50 m to 1.0 m, slightly different from the overflow depth after using Alternative 4 only, which was between 0.70 m to 1.20 m. The river level reached 10.825 m at the upstream of the study areas after applying Alternative 6.

According to the simulated flood map of the combination of Alternatives 3 and 4, shown in Figure 5.13, the extent of the flood was reduced in the Left floodplain in the study area; however, there is a little progress in the Right floodplain of the study area. It is crucial to mention that after the combination of Alternatives 3 and 4, the flood depth in the main residential zone of the study decreased significantly. The maximum flood depth in the residential area of both floodplains was less than 0.50 m.

The obtained results indicate that the inundation extent still is significant, and most of the study area, including the residential zone, is inundated during the peak discharge of a 500-year flood. Hence, it is concluded that this alternative is insufficient and a risk to depend on as a mitigation measure to defend the study area against the peak discharge of a 500-year flood event.
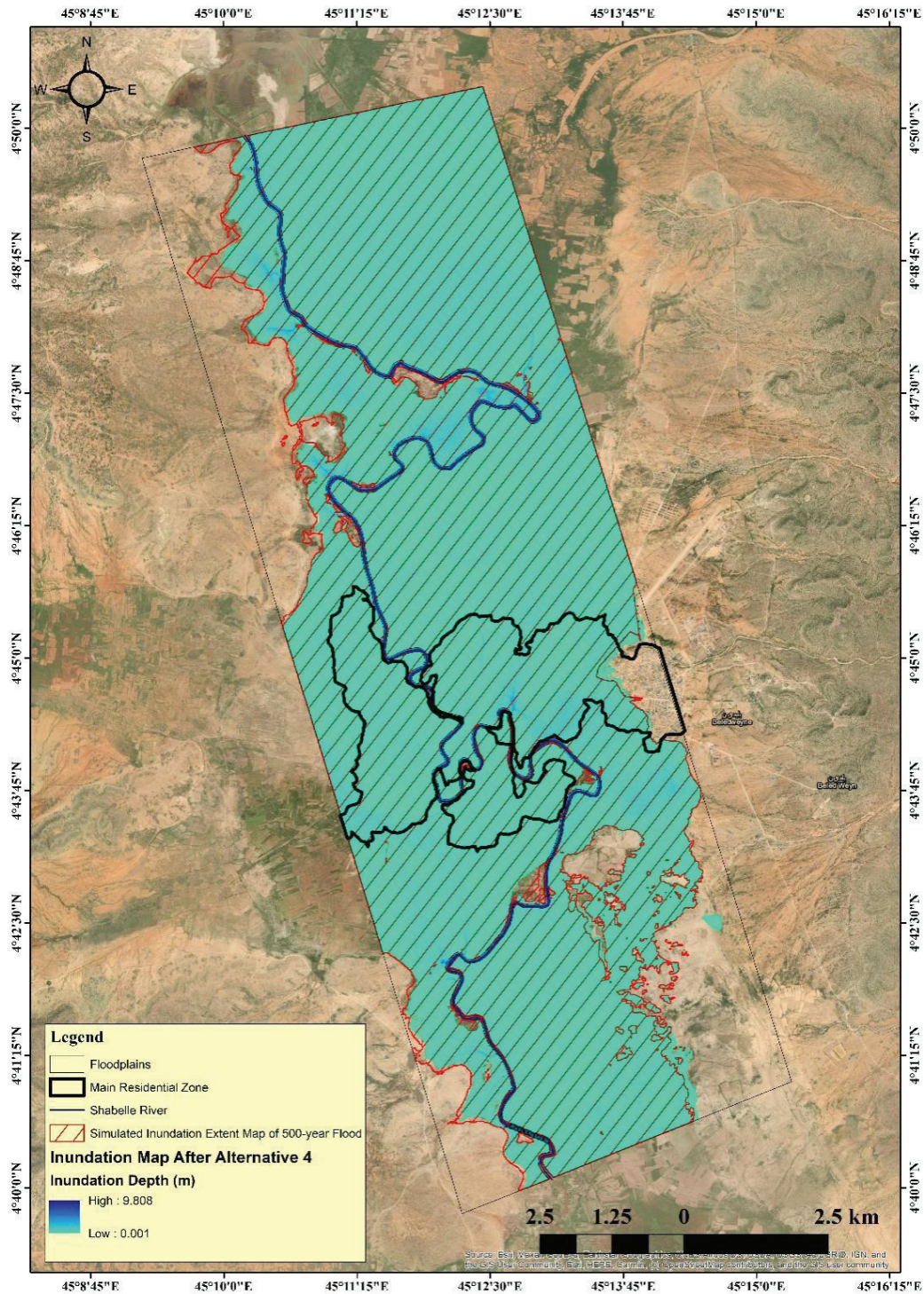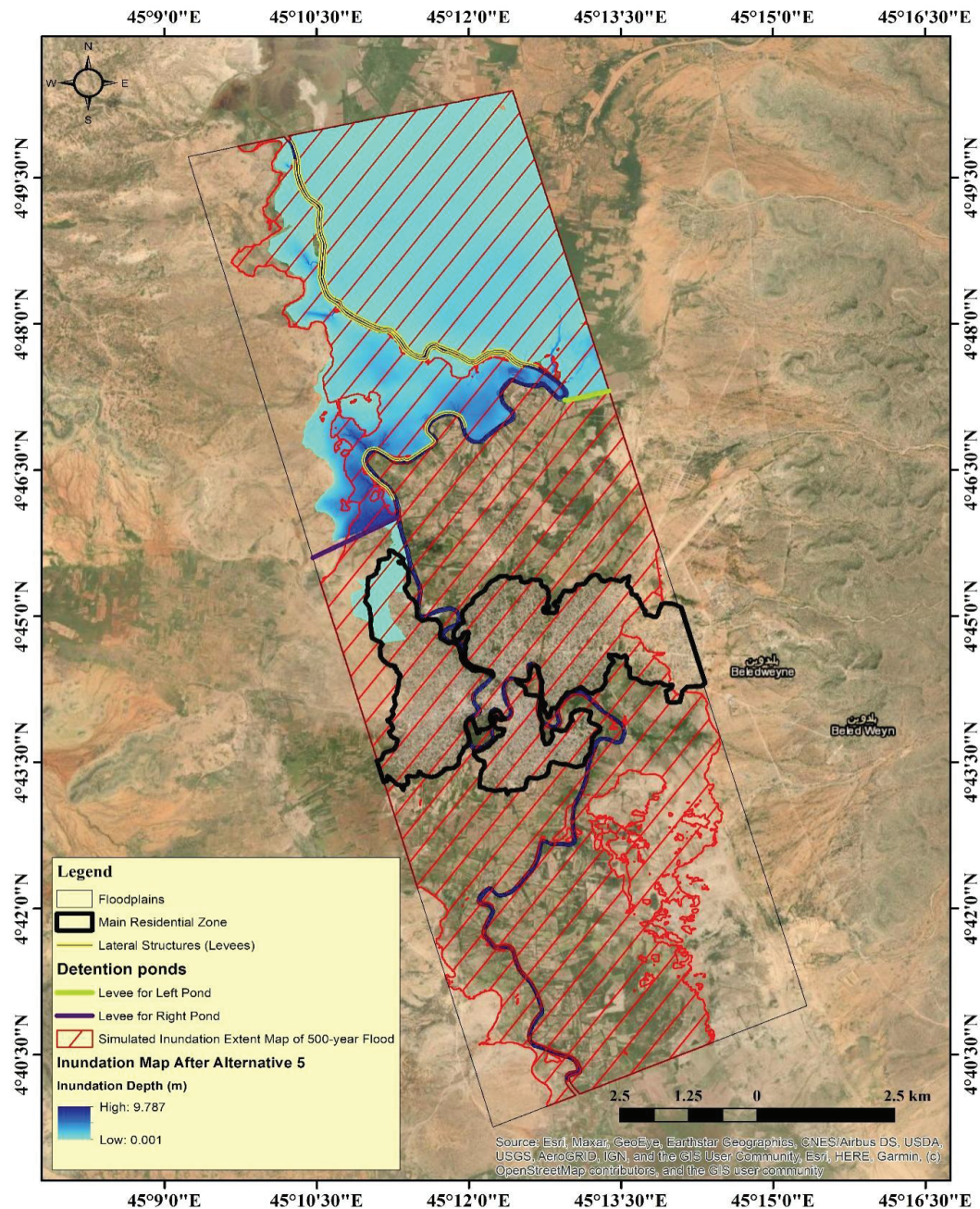
Figure 5.13. The Inundation Map Generated After Alternative 6

5.5.7 Alternative 7

This alternative analyzed the contribution of combining Alternatives 1 and 3 to protect the city from the river's flood using the peak discharge of a 500-year flood event. Rehabilitation of the Warabole diversion channel and the construction of levees (dikes) along both sides of the Shabelle river were assessed by this alternative. Modifying the dimensions of the Warabole channel and its levee structure was initially tried; however, no tangible progress was founded, so both the levee (dike) along the river and Warabole channel, including its levee structure, were given the previous dimensions in Alternatives 1 and 3.

The obtained results show that the total flooded area dropped from 88.56 km^2 to 67.71 km^2, which is a good improvement. Shabelle River flooded into an area of 52.50 km^2 (75.84%) of the area in the Left floodplain. At the same time, the total area flooded in the Right floodplain of the study area is 15.21 km^2 (36.61%) of the area in that floodplain, as shown in Figure 5.14. The highest simulated flood depth in the Left floodplain is between 0.80 m and 1.0 m, significantly different from the flood depth after using Alternative 1 only, which was a maximum flood depth of 1.50 m in some areas. The Right floodplain of the study area has a maximum inundation depth ranging from 0.70 m to 1.0 m, which is remarkably different from the inundation depth after using Alternative 1 only, which was the highest flood depth of 1.70 m in some areas. The river level reached 9.62 m at the upstream of the study areas after using Alternative 7.

Regarding the inundation map generated after the combination of Alternatives 1 and 3, illustrated in Figure 5.14, the extent of the flood was significantly reduced in the Left floodplain in the study area; however, the progress in the Right floodplain of the study area is little compared to that in the Left floodplain. It is fair to mention that the Warabole channel and its levee protected the areas behind it in the Right floodplain, as shown in Figure 5.14; this includes the residential zone of the study area; also, the combination of Alternatives 1 and 3 decreased the flood depth in both floodplains. According to the results, the flood extent is still enormous in the Left floodplain, and the river was inundated in some urbanized areas in the Right floodplain.

So it is finalized that this alternative is insufficient to protect the study area against the peak discharge of a 500-year flood event.

Figure 5.14. The Inundation Map Generated After Alternative 7

5.5.8 Alternative 8

This alternative examined the contribution of combining Alternatives 1 and 2 to protect the city from the river's flood using the peak discharge of a 500-year flood event. The previous sizes of both mitigations were tested to decrease; however, the reduced dimensions did not show progress. So, the same dimensions used in Alternatives 1 and 2 were used when combining them. The obtained results indicate that the total inundated area decreased from 88.56 km^2 to 44.71 km^2, which is good progress. Shabelle River overflowed 30.52 km^2 (44.08%) of the area inside the left detention pond and 14.19 km^2 (34.16%) of the area in the Right floodplain in the study area, as indicated in Figure 5.15. The maximum simulated flood depth in the detention pond on the Left floodplain is between 1.0 m and 1.20 m, significantly different from the flood depth of Alternative 2, which has a maximum flood depth between 2.0 m and 2.7 m. The detention pond in the Right floodplain of the study area has a maximum flood depth ranging from 2.0 m to 2.5 m, which is remarkably different from the inundation depth after using Alternative 2 only, which has the highest flood depth ranging from 2.5 m to 3.5 m. However, the inundation area increased in the downstream of the Right floodplain in the study area compared to Alternative 2; also, the flood depth raised from 0.2 m to 0.35 m in that area. The maximum river level reached 9.754 m at the upstream of the study areas after using Alternative 8.

According to the inundation map generated after the combination of Alternatives 1 and 2, shown in Figure 5.15, all overflowed water was held by the left detention pond, and the levee for that detention pond blocked the flooded water during the peak discharge of a 500-year flood, so the downstream of Left floodplain on the study area, including the residential areas, are protected. However, the proposed levee of the detention pond at the Right floodplain did not block all the water, and inundation reached the downstream of the study area, including residential areas. It is fair to state that the levee in the right detention pond overflows before the river water enters the Warabole diversion channel; this is mainly due to the depth of the diversion channel, which is 5 m, and it is not practical to increase the depth.

According to the results, the levee on the right detention pond overflowed during the peak discharge of a 500-year flood, and inundation water reached downstream of the study area. Also, there is a risk of failure of that levee since the water depth in the right

detention pond is high. Meanwhile, the Warabole diversion channel did not contribute mitigation of the peak discharge of a 500-year flood. So, it is concluded that this alternative is insufficient and a risk to rely on as a mitigation measure to protect the study area against the peak discharge of a 500-year flood event.
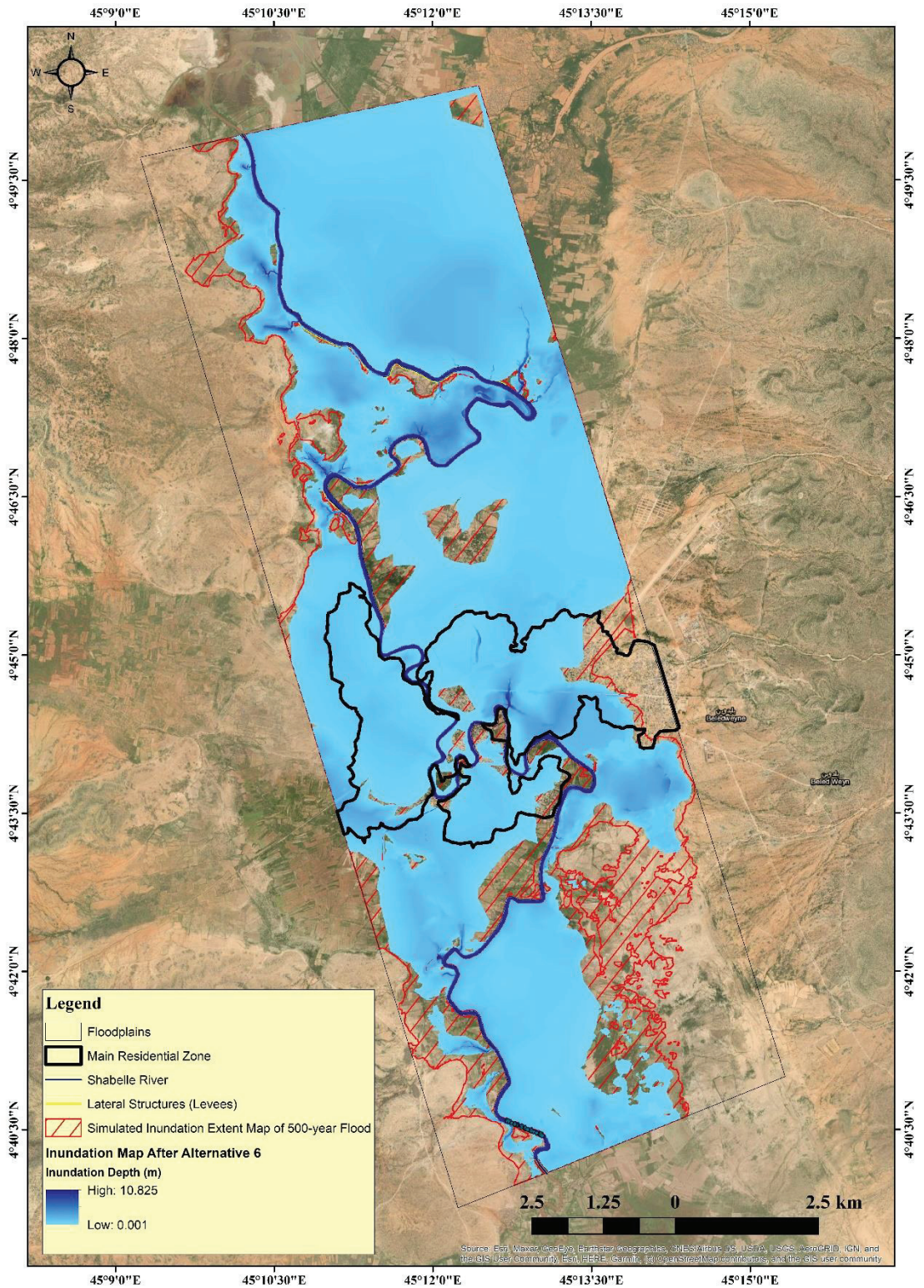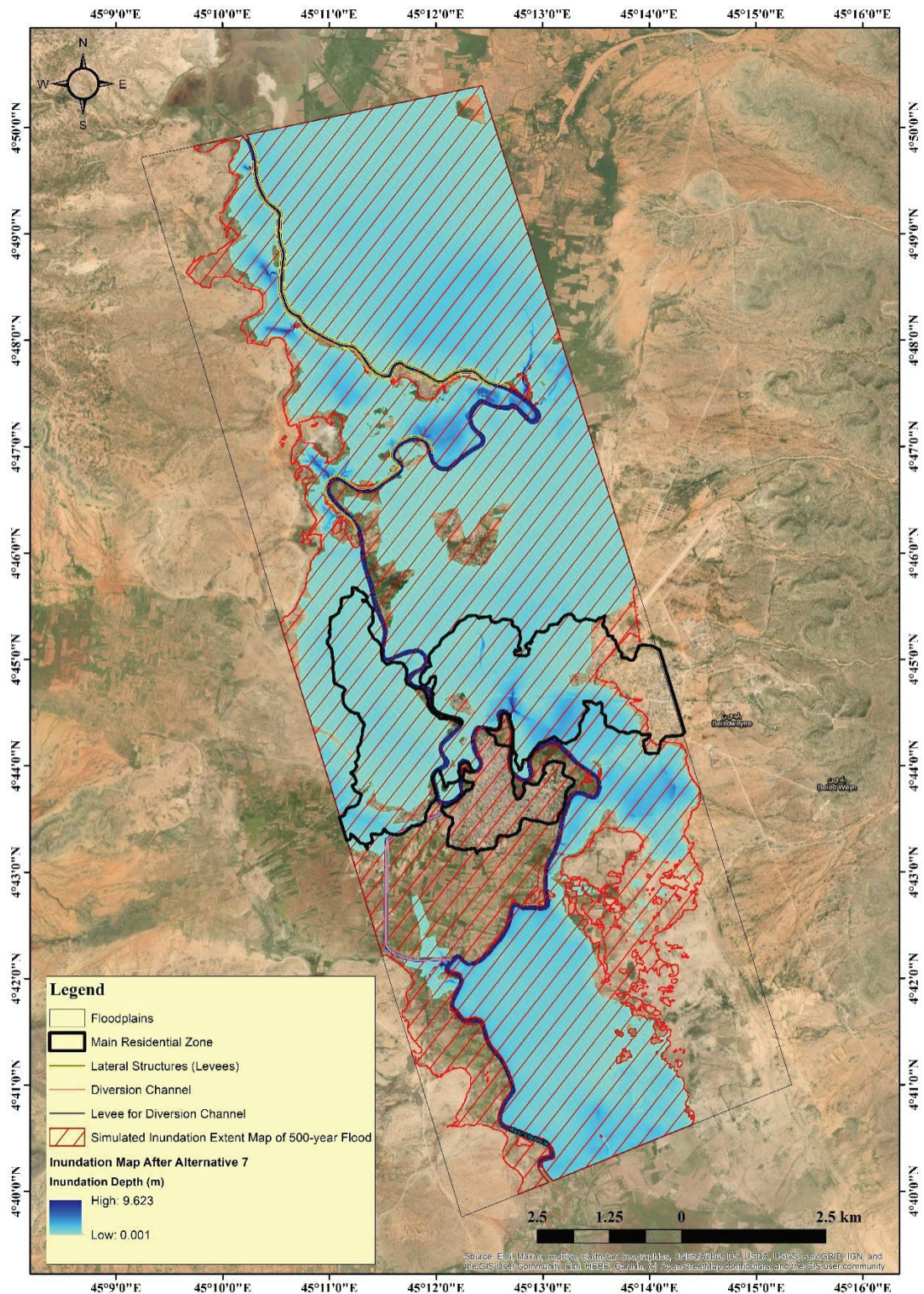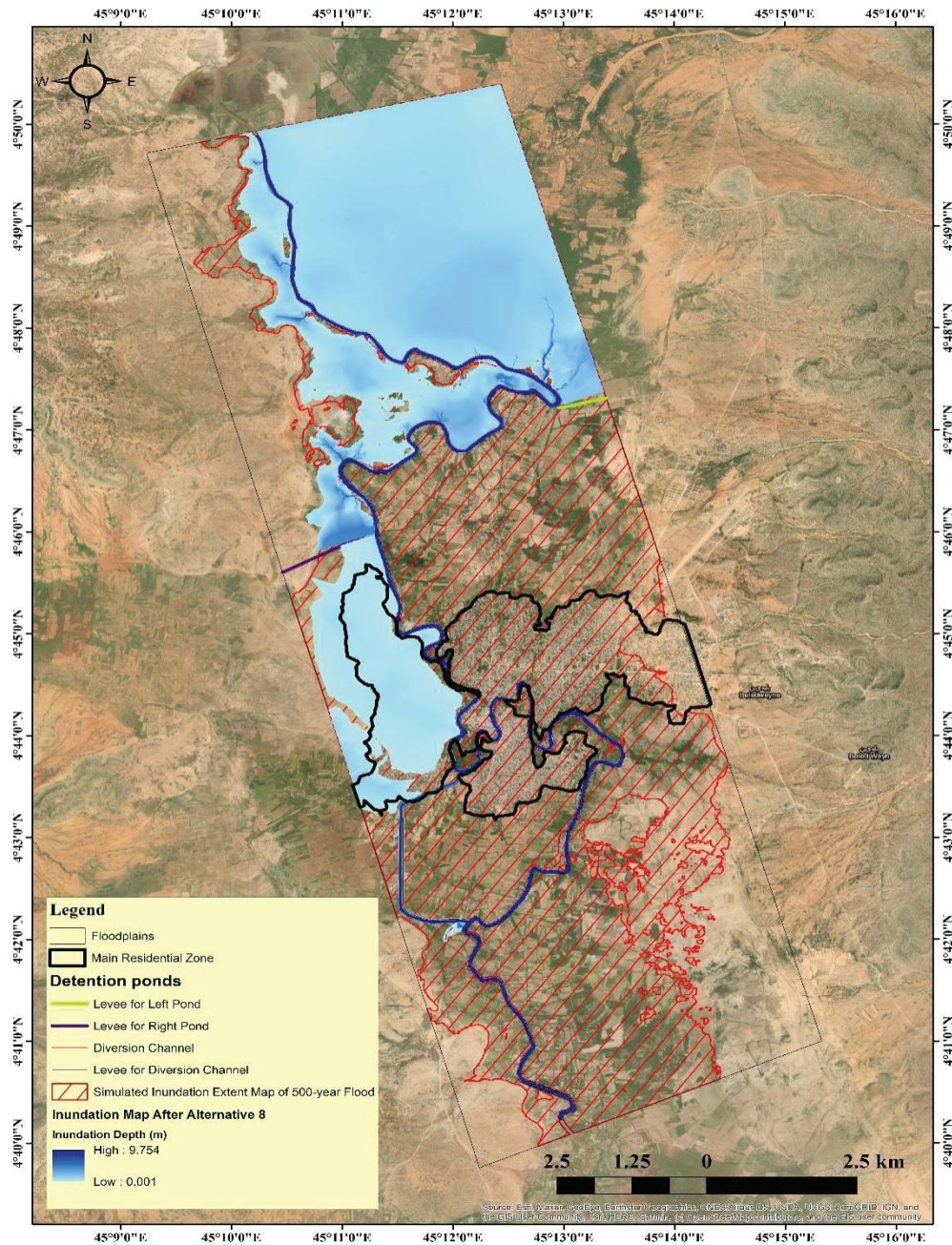

Figure 5.15. The Inundation Map Generated After Alternative 8

5.5.9 Alternative 9

This alternative investigated the contribution of combing Alternatives 1, 2, 3, and 4 to protect the city from the river's flood using the peak discharge of a 500-year flood event. The previous dimensions of both mitigations were tried to be reduced; however, the reduced dimensions of a detention pond and levee (dikes) along the river did not indicate progress, so the exact dimensions used in Alternatives 2 and 3 were used. The Warabole diversion channel's depth is reduced to 3 m, where the improvement river is done by dredging rough 0.3 m and adjusting the river banks.

The obtained results indicate that the total flooded area dropped from 88.56 km^2 to 27.87 km^2, which is excellent progress. The flooded area in the left detention pond in the Left floodplain is 19.91 km^2 (28.76%) of the area inside that detention pond, whereas in the right detention pond is 7.96 km^2 (19.16%) of the area in the Right floodplain in the study area, as illustrated in Figure 5.16. The maximum simulated flood depth in the detention pond located on the Left floodplain is between 0.70 m and 1.0 m, almost the same as the previous alternative five. The detention located in the Right floodplain has a maximum flood depth ranging from 2.0 m to 2.5 m; this is significantly less than the maximum simulated depth in the alternative five, which was between 2.5 m and 3.5 m. The river level reached 9.75 m at the upstream of the study areas after applying Alternative 9.

Regarding the inundation map generated after the combination of Alternatives 1, 2, 3, and 4, illustrated in Figure 5.16, the extent of the flood was significantly reduced in both floodplains in the study area; the levees of detention ponds held all the water, so, the downstream of the study area including the urbanization zones was protected during the peak discharge of a 500-year flood event. Also, it is fair to mention that the flood depth in both detention ponds decreased, so the chance of failure and overflowing levees of detention ponds was reduced. The Warabole diversion channel was used in case of emergency and to speed up the process of returning water held in the detention pond to the river.

According to the simulated results, in a concussion, this alternative is the most appropriate mitigation measure to protect the Baledwayne city against the peak discharge of a 500-year flood event.
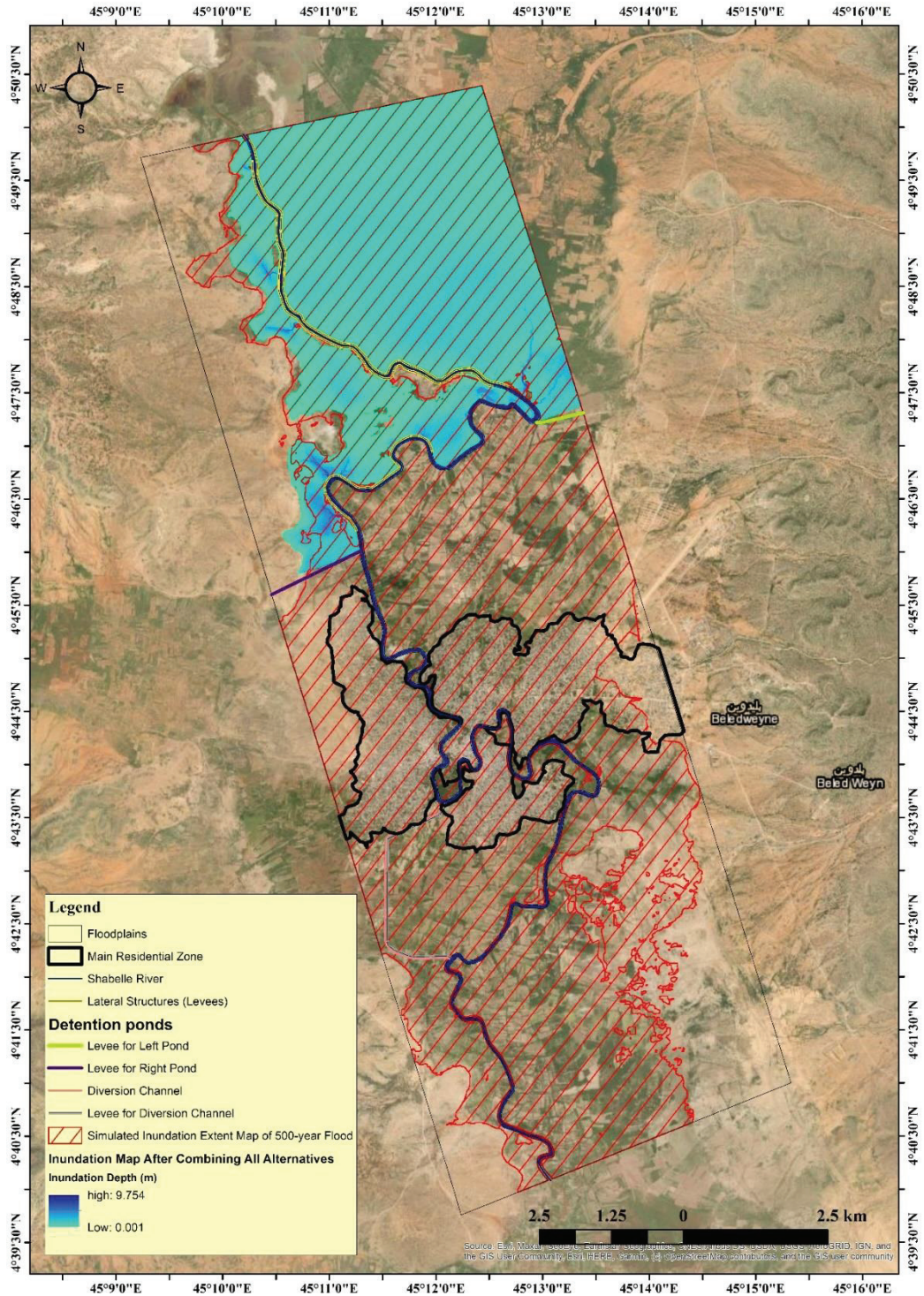
Figure 5.16. The Inundation Map Generated After Alternative 9

5.6 Discussion of Results

This study utilized the HEC-RAS model to develop different flood mitigation measures for Baledwayne city. Calibrated model setup and parameters used in Chapter Four to simulate an inundation map of the Deyr 2019 flood event were also used in this analysis, except for the flow hydrograph boundary condition. In this chapter, the peak discharge of a 500-year flood obtained from flood frequency analysis was used as a flow hydrograph boundary condition to generate the inundation map of a 500-year flood.

After the generation of the inundation map of a 500-year flood, different mitigation measures were analyzed using the same inflow hydrograph to protect the study area against the peak discharge of a 500-year flood event. Four mitigation measures were analyzed in this study area, and which are rehabilitation of the Warabole diversion channel, construction of Levees (Dikes) along the Shabelle river, construction of a Detention Ponds in the upstream of both floodplains in the study area, and finally, improving the river channel to increase its depth and remove the sediments and debris. All those mitigations were selected because they were the study area's ongoing and executed mitigation projects.

Initially, the four mitigations were analyzed separately, then combined into mitigation, and finally, the combination of all mitigations was analyzed to develop the appropriate mitigation measure for protecting the Baledwayne city against the peak discharge of a 500-year flood event. Table 5.1 summarizes all simulation results of generated maps in this chapter. Reducing the inundation extent and depth of generated map of a 500-year flood was a target, and each developed alternative was compared to that target to protect the study area against the peak discharge of a 500-year.

A total of nine alternatives were examined during this analysis. According to the obtained results from generated maps indicating the inundation extent and flood depth, alternative nine, which was the combination of Alternatives 1, 2, 3, and 4, made excellent progress, and all flooded water was held in its detention pond. Also, the maximum flood depth simulated in the detention ponds is low compared to other alternatives. This alternative protected the downstream of the study area, including the residential zone, during the peak discharge of a 500-year flood. So, in conclusion, Alternative 9 is the

appropriate mitigation measure to protect the Baledwayne city against the peak discharge of a 500-year flood event.

Table 5.1. Summary of results generated inundation maps.

Generated Inundation Map	Total Flooded Area (km²)	Flooded Area on the Left Floodplain (km²)	Flooded Area on the Right Floodplain (km²)	Maximum Flood Depth (m)	
				Left Floodplain	Right Floodplain
Simulated inundation map 500-year flood	88.56	59.37	29.21	1.30 - 1.80	1.30 - 1.95
Alternative 1 (Diversion Channel)	86.97	59.53	27.45	1.20 - 1.50	1.30 - 1.70
Alternative 2 (Detention Pond)	31.47	19.997 (In the Detention Pond)	11.48	2.0 - 2.7 (In the Detention Pond)	2.5 - 3.5 (In the Detention Pond)
Alternative 3 (Levees or Dikes)	75.14	47.87	27.27	1.0 - 1.8	0.90 - 1.50
Alternative 4 (Improving the River)	87.54	60.33	27.22	1.20 - 1.50	0.70 - 1.20
Alternative 5 (Combining Alternatives 2&3)	30.97	19.94 (In the Detention Pond)	11.04	0.70 - 1.0 (In the Detention Pond)	2.5 - 3.5 (In the Detention Pond)
Alternative 6 (Combining Alternatives 3&4)	72.73	49.80	22.93	0.70 - 1.0	0.50 - 1.0
Alternative 7 (Combining Alternatives 1&3)	67.71	52.50	15.21	0.80 - 1.0	0.70 - 1.0
Alternative 8 (Combining Alternatives 1&2)	44.71	30.52 (In the Detention Pond)	14.19	1.0 - 1.20 (In the Detention Pond)	2.0 - 2.5 (In the Detention Pond)
Alternative 9 (Combining Alternatives 1 up to 4)	27.87	19.91 (In the Detention Pond)	7.96 (In the Detention Pond)	0.70 - 1.0 (In the Detention Pond)	2.0 - 2.5 (In the Detention Pond)

Table 5.2 was organized as the best-worst Alternatives used in this investigation to protect the Baledwayne during a peak discharge of a 500-year flood. According to generated maps, Alternative 9 was selected as the overall best alternative in terms of reducing the flood map extent and drop of flood depth in the detention ponds; this

alternative also protected the entire urbanized zone in the study area. In this analysis, the worst alternative was observed to be Alternative 4, which was improving the Shabelle river channel; this alternative almost has no contribution to mitigating the flood.

Table 5.2. Summary of overall best-worst alternatives.

Generated Inundation Map	Total Flooded Area (km²)	Flooded Area on the Left Floodplain (km²)	Flooded Area on the Right Floodplain (km²)	Maximum Flood Depth (m)	
				Left Floodplain	Right Floodplain
Simulated inundation map 500-year flood	88.56	59.37	29.21	1.30 - 1.80	1.30 -1.95
Alternative 9 (Combining Alternatives 1 up to 4)	27.87	19.91 (In the Detention Pond)	7.96 (In the Detention Pond)	0.70 - 1.0 (In the Detention Pond)	2.0 - 2.5 (In the Detention Pond)
Alternative 5 (Combining Alternatives 2&3)	30.97	19.94 (In the Detention Pond)	11.04	0.70 - 1.0 (In the Detention Pond)	2.5 - 3.5 (In the Detention Pond)
Alternative 2 (Detention Pond)	31.47	19.997 (In the Detention Pond)	11.48	2.0 - 2.7 (In the Detention Pond)	2.5 - 3.5 (In the Detention Pond)
Alternative 8 (Combining Alternatives 1&2)	44.71	30.52 (In the Detention Pond)	14.19	1.0 - 1.20 (In the Detention Pond)	2.0 - 2.5 (In the Detention Pond)
Alternative 7 (Combining Alternatives 1&3)	67.71	52.50	15.21	0.80 - 1.0	0.70 - 1.0
Alternative 1 (Diversion Channel)	86.97	59.53	27.45	1.20 - 1.50	1.30 - 1.70
Alternative 3 (Levees or Dikes)	75.14	47.87	27.27	1.0 - 1.8	0.90 - 1.50
Alternative 6 (Combining Alternatives 3&4)	72.73	49.80	22.93	0.70 - 1.0	0.50 - 1.0
Alternative 4 (Improving the River)	87.54	60.33	27.22	1.20 - 1.50	0.70 - 1.20

Besides that, Alternative 9 is the most suitable mitigation measure; however, it is costly to implement such a vast project in the study area. So, this study suggests other options from the analyzed alternatives as a plan B and C, as shown in Table 5.3. The table was organized as the first recommended alternative at the top of the list. The selection and criteria of listing the alternatives in Table 5.3 were based on which alternative protects

most of the urbanized zone in the study area during the peak discharge of a 500-year flood and has less cost to implement.

Alternative 5, which was the integration of Alternative 2 and 3, appeared in the top list. This alternative is not costly compared to others on the list and entirely protects the study area's urbanization zone in the Left floodplain. In contrast, the river flooded into small areas in the Right floodplain. However, the depth of the flooded water in the urbanized zone in that floodplain is low. So, it is recommended to increase the height of the Levees in this alternative to increase their efficiency and reduce the risk of overturning those Levees in detention ponds in both floodplains. According to Table 5.3, Alternative 9 is at the bottom of the list since it requires enormous funds to implement.

Table 5.3. Recommended Alternatives in this study.

Alternative	Status of the Main Urbanized Zone of Study Area after Applying the Alternative		Recommendations
	Left Floodplain	Right Floodplain	
Alternative 5 (Combination of Alternatives 2&3)	Fully Protected	Small areas of the main city that the river flooded with very low flood depth.	It is recommended to increase the height of the Levees along the river and the Levees of both Detention Ponds, especially the Levee of the Right detention pond.
Alternative 2 (Detention Ponds)	Fully Protected	Small areas of the main city that the river flooded with considerable flood depth	It is strongly suggested to increase the height of the Levees of both Detention Ponds and blockage all breaking points of the Shabelle river.
Alternative 9 (Combination of Alternatives 1 up to 4)	Fully Protected	Fully Protected	Decreasing the size of the Warabole diversion channel is recommended to decrease the implementation cost.

CHAPTER 6

SUMMARY, CONCLUSIONS AND RECOMMENDATIONS

6.1   Summary

Flooding is a common disaster in Somalia that affects thousands of people every year. Baledwayne city (study area) is among the areas with the highest risk of riverine and flash flooding in the country. The worst flood event in the study area occurred between October and the beginning of November 2019, when the Shebelle River overflowed and submerged more than 85% of the Baledwayne city. This study examines different alternatives as remedial measures for flood control to shield the city from Shabelle River flooding.

Initially, all required data was collected, such as the hydrometeorological data of both Baledwayne and Bule-Burti stations, including 2019 daily gauged precipitation and discharge to generate the simulated rainfall-runoff of both stations. The homogeneity of those collected data was tested utilizing Rainbow software. Also, the 30 m resolution of DEM for the Hiran region, the 10 m resolution of DTM and the land cover data of the study area were collected. Furthermore, it was collected the river level and observed inundation map of the Deyr 2019 to compare to the corresponding simulated inundation in the study area using the HEC-RAS model.

According to the results of Rainbow software, the homogeneity of the collected hydrometeorological data set of Baledwayne and Bulo-Burti stations is good and homogenous. So, the data set is used for other analyses in this study.

The flood frequency distribution was analyzed using the observed maximum annual discharge of the Shabelle River at Baledwayne station, and the data in this analysis ranged from 2002 to 2020. At first, the EasyFit software was used to choose the probability distribution that best fits the data set, and then the HEC-SSP model was utilized to calculate the flood frequency estimation of distributions fitted to the data. The Log-Pearson Type III distribution was observed to the best distribution that fits to the data set. The peak discharge value of 500-years of return period for the Log-Pearson III

distribution, which is 605.4 m^3/s, was used as the design discharge value in the HEC-RAS model.

In this study, the HEC-HMS model was used for the hydrological modelling to generate a rainfall-runoff hydrograph of the 2019 event in the study area for the calibration purpose of the model. The model uses various parameters to simulate rainfall-runoff simulation. The parameters and methods used in this research are the SCS Curve Number for analyzing the volume, the Snyder Unit Hydrograph for estimating direct runoffs, the Constant Monthly method for calculating the baseflow and the Muskingum method for channel flow routing. The DEM of the Hiran region was used to delineate the characteristics of the watershed; also, daily precipitation data of both Baledwayne and Bulo-Burti stations were used as inputs to the model. The simulated rainfall-runoff hydrographs of both stations were compared to their corresponding observed daily discharges. Then the model's performance was evaluated by visual calculation of the virtual simulated and observed hydrographs and a set of objective functions that assess the level of fit between the hydrograph simulated and observed. These parameters were used to evaluate the performance of the HEC-HMS model: NSE, PBIAS, R^2, RMSE Std Dev, PE and PEPF. Finally, the HEC-HMS model was calibrated by changing the values of model parameters to enhance the model's performance.

In the calibration process of the model, the simulated rainfall-runoff hydrographs for both stations were forced to be close to their corresponding observed discharges. The simulated rainfall-runoff hydrograph of the HEC-HMS model at the Baledwayne (Study Area) station was used as an inflow hydrograph boundary condition in the HEC-RAS model to generate the inundation map of the Deyr 2019 flood event.

The HEC-RAS model was used for the hydraulic modelling. A combined 1D&2D hydraulic modelling of the model was used to develop different mitigation measures to protect Baledwayne City, Somalia. The DTM of the study area is used as an input of the model to create the terrain layer, whereas the land cover of the study area was used to assign the Manning's (n) values corresponding to each land cover. The Flow hydrograph and Normal depth boundary conditions were used to simulate unsteady flow simulation of the study area.

At first, the inundation map of the Deyr 2019 flood event was generated using the simulated 2019 discharge hydrograph from the output results of the HEC-HMS model as a Flow Hydrograph boundary condition in the HEC-RAS model. The model's performance was evaluated by comparing the extent and depth of the simulated map to the corresponding observed map. Also, the maximum simulated daily river level of the Shabelle River was compared to the observed river level of the study area. To enhance the model's performance, manning's roughness coefficient (n) for both 1D and 2D flow areas was altered, and several simulations were performed to generate an acceptable inundation map compared to the observed data.

The Calibrated model setup and parameters utilized to generate the inundation map of the Deyr 2019 flood event, except the inflow hydrograph boundary condition, were also used to generate the inundation map of a 500-year flood in the study area. The peak discharge of a 500-year flood obtained from flood frequency analysis was used as an inflow hydrograph boundary condition to generate the inundation map of a 500-year flood.

After the generation of the inundation map of a 500-year flood, various mitigation measures were examined using the same inflow hydrograph to defend the study area against the peak discharge of a 500-year flood event. Four mitigation measures were examined in this study area and which are rehabilitation of the Warabole diversion channel, construction of Levees (Dikes) along the Shabelle river, construction of a Detention Ponds in the upstream of both floodplains in the study area, and finally, improving the river channel to increase its depth and remove the sediments and debris. All those mitigations were selected because they were the study area's ongoing and executed mitigation projects.

6.2   Conclusions

According to the observed map, 69.91% of the study area was inundated during the Deyr 2019 event flood, whereas the simulated inundation map shows that 77.00% of the study area was flooded. The maximum observed flood depth at the downstream of the city was roughly between 0.80 m - 1.0 m, and the corresponding simulated maximum inundation depth to that area was between 0.80 m to 1.10 m. The observed river level at the upstream of the study area was 8.35 m, whereas the maximum simulated river level was 8.44 m.

Regarding the model's performance results, the simulated inundation map of the Deyr 2019 flood event is accepted and close to the observed map.

Calibrated model setup and parameters used to simulate an inundation map of the Deyr 2019 flood event were also used to generate the inundation map of 500 years flood, except for the flow hydrograph boundary condition. The peak discharge hydrograph from the output results of the HEC-SSP model was used as a Flow Hydrograph boundary condition during this analysis.

After the generation of the inundation map of a 500-year flood, different mitigation measures were analyzed using the same inflow hydrograph to protect the study area against the peak discharge of a 500-year flood event. A total of nine alternatives were examined during this analysis. According to the generated maps, Alternative 9 was the combination of all alternatives and made excellent progress compared to other alternatives. The combined alternatives in Alternative 9 are rehabilitation of the Warabole diversion channel, construction of detention ponds at the upstream of both floodplains, levees and dikes along the Shabelle river and improving the river.

The obtained result after using Alternative 9 indicates that the total flooded area dropped from 88.56 km^2 to 27.87 km^2, and all this flooded area is inside the detention ponds. The maximum simulated flood depth ranged from 2.0 m to 2.5 m, and it was observed from the detention pond on the Right floodplain; this is significantly less than the maximum simulated depth in the alternative five, which was between 2.5 m and 3.5 m. After using alternative nine, the flood extent and depth in both detention ponds

significantly decreased; also, the downstream of the study area, including the urbanization zones, was protected during the peak discharge of a 500-year flood event. So, in conclusion, Alternative 9 is the appropriate mitigation measure to protect the Baledwayne city against the peak discharge of a 500-year flood event.

The analyzed alternatives were arranged as the best-worst alternatives in Table 5.2 to find out the overall best and worst alternative. According to generated maps of examined alternatives, Alternative 9 was selected as the overall best alternative in terms of reducing the flood map extent and drop of flood depth in the detention ponds; this alternative also protected the whole urbanized zone in the study area. In this analysis, the worst alternative was observed to be Alternative 4, which was improving the Shabelle river channel; this alternative almost has no contribution to mitigating the flood.

Besides that, Alternative 9 is the most appropriate mitigation measure; yet, it is costly to execute such an expansive project in the study area. So, this study presents other options from the analyzed alternatives as a plan B, and C. Table 5.3 was ranked as the preferably recommended alternative at the top of the list. The preference and criteria of ranking the alternatives in Table 5.3 were based on which alternative protects most of the metropolitanized zone in the study area during the peak discharge of a 500-year flood and has a little cost to execute the scheme.

Alternative 5, which was the combination of Alternative 2 and 3, appeared in the top list. This alternative is less expensive than others on the list and completely protects the study area's urbanization zone in the Left floodplain. In contrast, the river flooded into small areas in the Right floodplain. However, the depth of the flooded water in the urbanized zone in that floodplain is low. It is recommended to increase the height of the Levees in this alternative to increase their efficiency and reduce the risk of overturning those Levees in detention ponds in both floodplains. Alternative 9 appeared at the bottom of Table 5.3, though it is the most suitable mitigation measure analyzed in this research; however, it requires enormous funds to execute such a big project.

6.3 Recommendations

The following appropriate recommendations are suggested for the forthcoming study:

➤ This analysis utilized the most dependable open sources of satellite data for DEM and DTM of the study area; it is suggested to carry out site measurements of geometry data to resemble the contrast and validity of the study.

➤ The DTM data used for hydraulic modelling is limited to a thin strip along the Shabelle River. So, it is advised to carry observed geometry data to enlarge the study area since the city is expanding.

➤ This study analyzed riverine flooding in the study area; however, Baledwayne city sometimes encountered other types of flooding, such as flash flooding. It is recommended to analyze the magnitude of other floodings.

➤ Differences in climate, land cover& land use were not evaluated in this analysis, so examining the influences of those modifications is strongly suggested.

➤ Establishing more hydrological and meteorological stations in the basin is strongly recommended to obtain better results.

REFERENCES

Abdi Ahmed Hussein. (2019). *{DAAWO SAWIRADA} Fatahaada Wabiga shabeelle Oo Sameysay Howlahii isbitaalka Guud ee Baladweyne.* https://www.hiiraanweyn.net/2019/10/daawo-sawirada-fatahaada-wabiga-shabeelle-oo-sameysay-howlahii-isbitaalka-guud-ee-baladweyne/

ADPC & UNDP. (2005). *Integrated flood risk management in Asia*. ADPC. http://repo.floodalliance.net/jspui/44111/1380

Alabbad, Y., Yildirim, E., & Demir, I. (2022). Flood mitigation data analytics and decision support framework: Iowa Middle Cedar Watershed case study. *Science of The Total Environment*, *814*, 152768.

Basnyat, D. (2009). *Hydraulic Analysis of Rivers Juba and Shabelle in Somalia Basic Analysis for Irrigation and Flood Management Purposes*. https://doi.org/10.13140/RG.2.2.12795.36643

Benson, M. A. (1968). Uniform flood-frequency estimating methods for federal agencies. *Water Resources Research*, *4*(5), 891–908.

Buishand, T. A. (1982). Some methods for testing the homogeneity of rainfall records. *Journal of Hydrology*, *58*(1), 11–27. https://doi.org/https://doi.org/10.1016/0022-1694(82)90066-X

Calver, A., Stewart, E., & Goodsell, G. (2009). Comparative analysis of statistical and catchment modelling approaches to river flood frequency estimation. *Journal of Flood Risk Management*, *2*(1), 24–31.

Chow, V. T., Maidment, D. R., & Mays, L. W. (1988). *APPLIED HYDROLOGY*. McGraw- Hill Book Company, New York.

CRED. (2015). *The human cost of natural disasters: a global perspective.* https://www.emdat.be/index.php

Cunge, J. A. (1969). On the subject of a flood propagation computation method (Musklngum method). *Journal of Hydraulic Research*, *7*(2), 205–230.

DFID. (2004). *Adaptation to climate change : Making development disaster-proof.*

https://reliefweb.int/report/world/adaptation-climate-change-making-development-disaster-proof

Dottori, F., Szewczyk, W., Ciscar, J.-C., Zhao, F., Alfieri, L., Hirabayashi, Y., Bianchi, A., Mongelli, I., Frieler, K., Betts, R. A., & Feyen, L. (2018). Increased human and economic losses from river flooding with anthropogenic warming. *Nature Climate Change*, *8*(9), 781–786. https://doi.org/10.1038/s41558-018-0257-z

ECHO. (2019). *Vietnam - Flood in central region (DG ECHO, government, media) (Echo Daily Flash of 22 October 2019)*. https://reliefweb.int/report/viet-nam/vietnam-flood-central-region-dg-echo-government-media-echo-daily-flash-22-october

FAO-SWALIM. (2016). *Disaster management plan for the Juba and Shabelle basins in Somalia* (Issue January). https://www.faoswalim.org/content/w-27-disaster-managemnet-plan-juba-and-shabelle-basins-somalia

FAO-SWALIM. (2019). *Flood Monitoring Tool, Statistics Per Season*. https://floods.faoswalim.org/dashboard/?category2=2019&category=Deyr

FAO. (2020). *Gu 2020 Rainfall Performance (March to June 2020)* (Issue July). https://reliefweb.int/report/somalia/gu-2020-rainfall-performance-march-june-2020-issued-22-july-2020

FAOSWALIM. (n.d.). *Manual Rainfall Stations: MRS_HIBEL - Beledwayne*. https://climseries.faoswalim.org/rainfall/data/mrs/MRS_HIBEL

FAOSWALIM. (2019). *Soil_100K_S_FAOSWALIM*. https://spatial.faoswalim.org/layers/geonode:Soil_100K_S_FAOSWALIM#/

FloodList. (2019). *USA – 3 Dead as Rivers Reach Record Highs in Iowa and Nebraska*. https://floodlist.com/america/usa/iowa-nebraska-floods-march-2019

FSNAU. (2019). *Focus on 2019 Post-Deyr Season Early Warning*. https://fsnau.org/in-focus/focus-2019-post-deyr-season-early-warning

Gadain, H. M. and Jama, A. M. (2009). *Flood Risk and Response Management. Technical Report No W-15 produced under "Support to the Sustainable Management of the Shebelle and Juba Rivers in Southern Somalia Project"* (Issue

December). http://www.faoswalim.org/subsites/frrmis/index.php

Govt. Djibouti & UNCT Djibouti. (2019). *Djibouti Flash Update #1 - Humanitarian impact of flooding 24 November 2019*. https://reliefweb.int/report/djibouti-flash-update-1-humanitarian-impact-flooding-24-november-2019

Guha-sapir, D., Hoyois, P., & Below, R. (2015). *Annual Disaster Statistical Review 2015 The numbers and trends*. https://www.cred.be/downloadFile.php?file=sites/default/files/ADSR_2015.pdf

Gure, A. (2018). *Somalia Flood Update Devastating Floods Overwhelm Parts of Somalia* (Issue May). https://www.faoswalim.org/content/devastating-floods-overwhelm-parts-somalia

Haltas, I., Yildirim, E., Oztas, F., & Demir, I. (2021). A comprehensive flood event specification and inventory: 1930–2020 Turkey case study. *International Journal of Disaster Risk Reduction*, *56*, 102086. https://doi.org/https://doi.org/10.1016/j.ijdrr.2021.102086

Hamidifar, H., & Nones, M. (2021). Global to regional overview of floods fatality: the 1951--2020 period. *Natural Hazards and Earth System Sciences Discussions*, *2021*, 1–22. https://doi.org/10.5194/nhess-2021-357

Heidari, A. (2009). Structural master plan of flood mitigation measures. *Natural Hazards and Earth System Sciences*, *9*(1), 61–75.

Hu, P., Zhang, Q., Shi, P., Chen, B., & Fang, J. (2018). Flood-induced mortality across the globe: Spatiotemporal pattern and influencing factors. *Science of the Total Environment*, *643*, 171–182.

IFRC. (2022). *Brazil: Floods Emergency Plan of Action (EPoA) DREF Operation n° MDRBR010*. *December*. https://reliefweb.int/report/brazil/brazil-floods-emergency-plan-action-epoa-dref-operation-n-mdrbr010

ISRIC - World Soil Information. (2020). *World soil distribution*. https://www.isric.org/explore/world-soil-distribution

Jha, A. K., Bloch, R., & Lamond, J. (2012). *Cities and flooding: a guide to integrated urban flood risk management for the 21st century*. World Bank Publications.

Karra, K., Kontgis, C., Statman-Weil, Z., Mazzariello, J. C., Mathis, M., & Brumby, S. P. (2021). Global land use / land cover with Sentinel 2 and deep learning. *2021 IEEE International Geoscience and Remote Sensing Symposium IGARSS*, 4704–4707. https://doi.org/10.1109/IGARSS47720.2021.9553499

Kron, W. (2005). Flood Risk = Hazard • Values • Vulnerability. *Water International*, *30*(1), 58–68. https://doi.org/10.1080/02508060508691837

Menne, B., Murray, V., & Organization, W. H. (2013). *Floods in the WHO European Region: health effects and their prevention*. World Health Organization. Regional Office for Europe.

Mensah, H., & Ahadzie, D. K. (2020). Causes, impacts and coping strategies of floods in Ghana: A systematic review. *SN Applied Sciences*, *2*(5), 1–13.

Merz, B., Blöschl, G., Vorogushyn, S., Dottori, F., Aerts, J. C. J. H., Bates, P., Bertola, M., Kemter, M., Kreibich, H., Lall, U., & Macdonald, E. (2021). Causes, impacts and patterns of disastrous river floods. *Nature Reviews Earth & Environment*, *2*(9), 592–609. https://doi.org/10.1038/s43017-021-00195-3

Mishra, S. K., & Singh, V. (2003). *Soil conservation service curve number (SCS-CN) methodology* (Vol. 42). Springer Science & Business Media.

MOP. (2020). *Somalia National Development Plan 2020 to 2024*. http://mop.gov.so/wp-content/uploads/2019/12/NDP-9-2020-2024.pdf

Moriasi, D. N., Arnold, J. G., Van Liew, M. W., Bingner, R. L., Harmel, R. D., & Veith, T. L. (2007). Model evaluation guidelines for systematic quantification of accuracy in watershed simulations. *Transactions of the ASABE*, *50*(3), 885–900.

Munich, R. E. (2000). Topics 2000: Natural catastrophes-the current position. Munich RE. *Munich Reinsurance Company.*

Mutua, Francis M. – Balint, Z. (2009). *Analysis of the General Climatic Conditions to Support Drought Monitoring in Somalia. Technical Report No W-14, FAO-SWALIM Nairobi, Kenya*. http://www.faoswalim.org/resources/site_files/W-14 Analysis of General Climatic Conditions in Somalia in Support of Drought Monitoring.pdf

National Disaster Risk Management, & Commission (NDRMC). (2020). *Floods in Shebelle zone, 26 April 2020. April*, 1–3. https://reliefweb.int/attachments/624581fd-9580-3160-a529-edd774feb3bd/national_flood_alert_1_002.pdf

Nfor, J., Tamfuh, P. A., Magha, A., Guedjeo, C. S., Aka, P., Tamfuh, A., Tangan, A., Bitom, D., Nfor, J., Tamfuh, P. A., Magha, A., & Guedjeo, C. S. (2019). ASSESSMENT OF COMMUNITY'S PERCEPTION OF FLOOD DISASTERS IN THE BAMENDA MUNICIPALITY, NORTH-WEST CAMEROON. *South Asian Journal of Development Research*, *766*, 9–23.

OCHA. (2018). *Flood Response Plan Somalia* (Issues 15 May-15 August). https://www.humanitarianresponse.info/sites/www.humanitarianresponse.info/files/documents/files/somalia_flood_response_plan_may_-_august_2018_0.pdf

OCHA. (2019). *OCHA Somalia Flash Update #4 Humanitarian impact of flooding | 6 November 2019* (Issue November). https://reliefweb.int/report/somalia/ocha-somalia-flash-update-4-humanitarian-impact-flooding-6-november-2019

OCHA. (2020). *FLOOD RESPONSE PLAN SOMALIA* (Issue June). https://reliefweb.int/report/somalia/somalia-flood-response-plan-june-2020

Olajuyigbe, A. E., Rotowa, O. O., & Durojaye, E. (2012). An assessment of flood hazard in Nigeria: The case of mile 12, Lagos. *Mediterranean Journal of Social Sciences*, *3*(2), 367.

P.W, M. (2007). *Climate of Somalia. Technical Report No W-01, FAO-SWALIM, Nairobi, Kenya.* http://www.faoswalim.org/content/w-01-climate-somalia

Patrick, S. (2011). *Weak links: fragile states, global threats, and international security*. Oxford University Press.

Raes, D., Willems, P., & Gbaguidi, F. (2006). RAINBOW–A software package for hydrometeorological frequency analysis and testing the homogeneity of historical data sets. *In Proceedings of the 4th International Workshop on Sustainable Management of Marginal Drylands. Islamabad, Pakistan*, *2731*(January), 12.

Rumsby, B. T. (1991). *Flood frequency and magnitude estimates based on valley flood*

morphology and floodplain sedimentary sequences: the Tyne Basin, NE England. Newcastle University.

Samantaray, S., & Sahoo, A. (2020). Estimation of flood frequency using statistical method: Mahanadi River basin, India. *H2Open Journal*, *3*(1), 189–207.

Schipper, L., & Pelling, M. (2006). Disaster risk, climate change and international development: scope for, and challenges to, integration. *Disasters*, *30*(1), 19–38. https://doi.org/https://doi.org/10.1111/j.1467-9523.2006.00304.x

Sebhat, M. Y., & Wenninger, J. (2014). Water balance of the Juba and Shabelle River basins the Horn of Africa. *International Journal of Agricultural Policy and Research*, *2*(June), 238–255. http://www.journalissues.org/journals-home.php?id=1

Sebhat, M. Y. (2015). Assessments of water demands for the Juba and Shabelle Rivers in Somalia. *Journal of Agriculture and Environment for International Development (JAEID)*, *109*(2 SE-Research Papers). https://doi.org/10.12895/jaeid.20152.318

Sivakumar, S. S. (2015). Flood mitigation strategies adopted in Sri Lanka a review. *International Journal of Scientific and Engineering Research*, *3*(6).

Street, B., & Niksic, M. (2020). FLOODS ON THE RIVER BELICA AT JAGODINA, SERBIA IN 2014. *Journal of Environmental Protection and Ecology*, *21*(1), 308–316.

Sumi, T., Kantoush, S. A., & Saber, M. (2022). *Wadi Flash Floods: Challenges and Advanced Approaches for Disaster Risk Reduction*. Springer Nature.

U.N ESCAP. (2015). *Overview of natural disasters and their impacts in Asia and the Pacific 1970-2014*. United Nations. https://hdl.handle.net/20.500.12870/3096

UNDP. (2004). *Reducing disaster risk: A challenge for development. United Nations Development Programme*.

UNDP. (2012). *Disaster Risk Reduction and Integrated Programme 2012-2016: Building a Safer, More Resilient Kenya.*

USACE. (2022a). *HEC-HMS Technical Reference Manual*. U.S. Army Corps of Engineers.

https://www.hec.usace.army.mil/confluence/hmsdocs/hmstrm/introduction

USACE. (2022b). *HEC-RAS Mapper User's Manual* (Version 6.). U.S. Army Corps of Engineers. https://www.hec.usace.army.mil/confluence/rasdocs/rmum/latest

USACE. (2022c). *HEC-RAS Technical Reference Manual*. U.S. Army Corps of Engineers. https://www.hec.usace.army.mil/confluence/rasdocs/rasum/latest/introduction-to-hec-ras

Vivekanandan, N. (2015). Flood frequency analysis using method of moments and L-moments of probability distributions. *Cogent Engineering*, *2*(1), 1018704.

WHO. (n.d.). *Floods*. https://www.who.int/health-topics/floods#tab=tab_1

World Population Review. (2020). *World Population Review*. https://worldpopulationreview.com/

Wu, H., Adler, R. F., Hong, Y., Tian, Y., & Policelli, F. (2012). Evaluation of Global Flood Detection Using Satellite-Based Rainfall and a Hydrologic Model. *Journal of Hydrometeorology*, *13*(4), 1268–1284. https://doi.org/10.1175/jhm-d-11-087.1

Zaifoglu, H., Yanmaz, A. M., & Akintug, B. (2019). Developing flood mitigation measures for the northern part of Nicosia. *Natural Hazards*, *98*(2), 535–557. https://doi.org/10.1007/s11069-019-03713-1

APPENDICES

APPENDIX A

Annual Maximum Discharge data from the Baledwayne Station (2002- 2020)

Month / Year	Jan	Feb	Mar	Apr	May	Jun	Jul	Aug	Sep	Oct	Nov	Dec	Maximum
2002	0.0	0.0	0.0	197.3	188.3	36.4	21.7	79.7	97.0	126.7	72.1	30.6	**197.3**
2003	84.1	19.7	8.7	197.0	301.2	115.8	104.6	176.8	181.1	79.7	39.6	37.4	**301.2**
2004	23.7	19.5	9.8	238.7	238.7	36.4	78.2	109.9	102.8	144.8	144.8	140.7	**238.7**
2005	18.3	17.5	41.9	254.0	465.7	477.2	130.0	155.7	182.5	132.6	101.1	81.3	**477.2**
2006	28.2	24.5	64.9	179.7	274.3	154.4	117.2	223.6	210.2	282.9	472.7	253.9	**472.7**
2007	143.4	49.1	39.6	219.7	201.2	164.1	124.8	172.5	309.2	315.7	150.2	99.3	**315.7**
2008	45.4	40.8	37.4	89.3	122.9	94.2	54.8	172.5	158.5	186.8	383.6	113.5	**383.6**
2009	45.4	45.4	33.2	101.1	122.9	51.6	34.2	75.1	82.9	333.6	269.6	54.8	**333.6**
2010	31.7	79.7	259.4	261.8	448.1	452.5	131.3	277.4	346.0	332.0	122.9	51.6	**452.5**
2011	44.2	25.9	34.2	45.4	271.1	269.6	75.9	225.9	231.1	234.9	250.2	151.6	**271.1**
2012	18.3	7.1	14.9	143.4	234.9	95.9	68.5	118.2	470.1	333.6	205.0	78.2	**470.1**
2013	21.1	17.5	104.6	362.6	358.4	183.2	113.5	244.8	261.8	332.0	323.8	257.9	**362.6**
2014	51.6	39.6	64.9	122.9	212.4	171.1	39.6	153.7	247.9	443.7	435.0	121.0	**443.7**
2015	45.4	41.3	61.4	346.0	323.8	197.7	61.4	70.7	83.6	277.4	305.2	176.1	**346.0**
2016	25.4	31.7	65.0	268.0	470.1	346.0	131.3	210.2	144.8	138.0	122.9	104.6	**470.1**
2017	23.7	35.0	64.9	165.5	319.0	216.1	66.3	144.8	225.9	286.9	207.2	94.2	**319.0**
2018	16.7	2.0	59.4	469.9	469.9	335.1	190.3	122.7	223.5	110.6	201.2	174.5	**469.9**
2019	3.4	2.0	2.0	7.1	210.2	214.6	131.3	293.2	297.2	470.1	470.1	435.0	**470.1**
2020	116.3	1.5	2.0	323.8	470.1	265.7	325.5	430.7	470.1	413.4	201.4	192.6	**470.1**

Result of the goodness of fit Test for the EasyFit Software Estimated Parameters of distribution

Fitting Results

#	Distribution	Parameters
1	Gen. Extreme Value	k=-0.68701 σ=103.86 μ=368.2
2	Gumbel Max	σ=71.332 μ=341.2
3	Log-Pearson 3	α=4.9523 β=-0.11959 γ=6.5075
4	Lognormal	σ=0.25903 μ=5.9153
5	Normal	σ=91.487 μ=382.37

Goodness of Fit - Details [hide]

Gen. Extreme Value [#1]

Kolmogorov-Smirnov

Sample Size	19				
Statistic	0.18982				
P-Value	0.44568				
Rank	1				

α	0.2	0.1	0.05	0.02	0.01
Critical Value	0.23735	0.27136	0.30143	0.33685	0.36117
Reject?	No	No	No	No	No

Anderson-Darling

Sample Size	19				
Statistic	0.8949				
Rank	2				

α	0.2	0.1	0.05	0.02	0.01
Critical Value	1.3749	1.9286	2.5018	3.2892	3.9074
Reject?	No	No	No	No	No

Chi-Squared

Deg. of freedom	1				
Statistic	0.84358				
P-Value	0.35837				
Rank	5				

α	0.2	0.1	0.05	0.02	0.01
Critical Value	1.6424	2.7055	3.8415	5.4119	6.6349
Reject?	No	No	No	No	No

Goodness of Fit - Details [hide]

Gumbel Max [#2]

Kolmogorov-Smirnov

Sample Size Statistic P-Value Rank	19 0.26221 0.12161 5				
α	0.2	0.1	0.05	0.02	0.01
Critical Value	0.23735	0.27136	0.30143	0.33685	0.36117
Reject?	Yes	No	No	No	No

Anderson-Darling

Sample Size Statistic Rank	19 1.5234 5				
α	0.2	0.1	0.05	0.02	0.01
Critical Value	1.3749	1.9286	2.5018	3.2892	3.9074
Reject?	Yes	No	No	No	No

Chi-Squared

Deg. of freedom Statistic P-Value Rank	1 0.04585 0.83045 2				
α	0.2	0.1	0.05	0.02	0.01
Critical Value	1.6424	2.7055	3.8415	5.4119	6.6349
Reject?	No	No	No	No	No

Goodness of Fit - Details [hide]

Log-Pearson 3 [#3]

Kolmogorov-Smirnov

Sample Size Statistic P-Value Rank	19 0.20127 0.37433 2				
α	0.2	0.1	0.05	0.02	0.01
Critical Value	0.23735	0.27136	0.30143	0.33685	0.36117
Reject?	No	No	No	No	No

Anderson-Darling

Sample Size Statistic Rank	19 0.85764 1				
α	0.2	0.1	0.05	0.02	0.01
Critical Value	1.3749	1.9286	2.5018	3.2892	3.9074
Reject?	No	No	No	No	No

Chi-Squared

Deg. of freedom Statistic P-Value Rank	1 0.43793 0.50812 4				
α	0.2	0.1	0.05	0.02	0.01
Critical Value	1.6424	2.7055	3.8415	5.4119	6.6349
Reject?	No	No	No	No	No

Goodness of Fit - Details [hide]

Lognormal [#4]

Kolmogorov-Smirnov

Sample Size Statistic P-Value Rank	19 0.23004 0.22901 4				
α	0.2	0.1	0.05	0.02	0.01
Critical Value	0.23735	0.27136	0.30143	0.33685	0.36117
Reject?	No	No	No	No	No

Anderson-Darling

Sample Size Statistic Rank	19 1.0107 4				
α	0.2	0.1	0.05	0.02	0.01
Critical Value	1.3749	1.9286	2.5018	3.2892	3.9074
Reject?	No	No	No	No	No

Chi-Squared

Deg. of freedom Statistic P-Value Rank	1 0.0441 0.83368 1				
α	0.2	0.1	0.05	0.02	0.01
Critical Value	1.6424	2.7055	3.8415	5.4119	6.6349
Reject?	No	No	No	No	No

Goodness of Fit - Details [hide]

Normal [#5]

Kolmogorov-Smirnov

Sample Size Statistic P-Value Rank	19 0.22243 0.26263 3				
α	0.2	0.1	0.05	0.02	0.01
Critical Value	0.23735	0.27136	0.30143	0.33685	0.36117
Reject?	No	No	No	No	No

Anderson-Darling

Sample Size Statistic Rank	19 0.96367 3				
α	0.2	0.1	0.05	0.02	0.01
Critical Value	1.3749	1.9286	2.5018	3.2892	3.9074
Reject?	No	No	No	No	No

Chi-Squared

Deg. of freedom Statistic P-Value Rank	1 0.38642 0.53419 3				
α	0.2	0.1	0.05	0.02	0.01
Critical Value	1.6424	2.7055	3.8415	5.4119	6.6349
Reject?	No	No	No	No	No

APPENDIX C

Detailed results of upstream and downstream corrections in the study area.
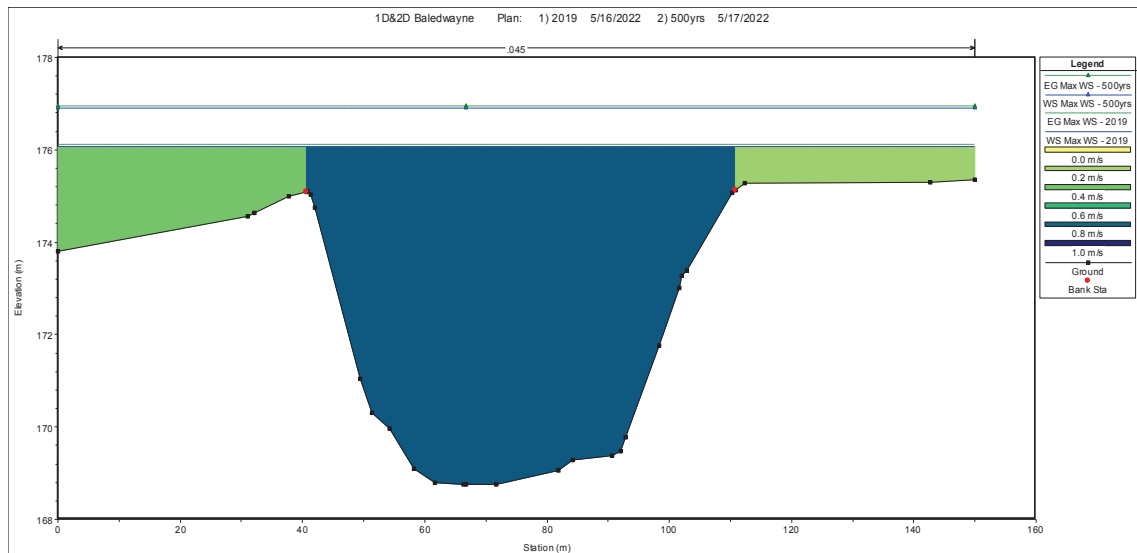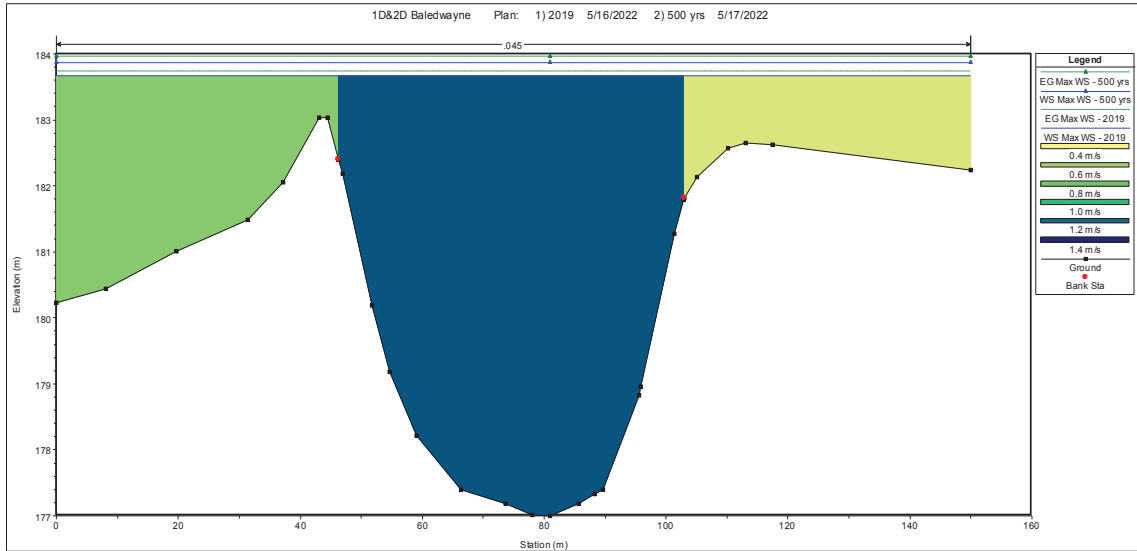
Cross Section Output

River: Shabelle Profile: Max WS

Reach: Shabelle RS: 39000 Plan: 2019

Plan: 2019 Shabelle Shabelle RS: 39000 Profile: Max WS

		Element	Left OB	Channel	Right OB
E.G. Elev (m)	183.73	Wt. n-Val.	0.045	0.045	0.045
Vel Head (m)	0.07	Reach Len. (m)	313.50	300.00	284.20
W.S. Elev (m)	183.67	Flow Area (m2)	109.62	297.32	58.11
Crit W.S. (m)		Area (m2)	109.62	297.32	58.11
E.G. Slope (m/m)	0.000350	Flow (m3/s)	76.92	366.50	27.26
Q Total (m3/s)	470.68	Top Width (m)	46.30	56.70	47.00
Top Width (m)	150.00	Avg. Vel. (m/s)	0.70	1.23	0.47
Vel Total (m/s)	1.01	Hydr. Depth (m)	2.37	5.24	1.24
Max Chl Dpth (m)	6.67	Conv. (m3/s)	4112.4	19593.3	1457.2
Conv. Total (m3/s)	25163.0	Wetted Per. (m)	49.98	58.22	48.47
Length Wtd. (m)	301.72	Shear (N/m2)	7.53	17.52	4.11
Min Ch El (m)	177.00	Stream Power (N/m s)	5.28	21.60	1.93
Alpha	1.25	Cum Volume (1000 m3)	2435.39	13558.98	1582.27
Frctn Loss (m)	0.09	Cum SA (1000 m2)	1568.63	2384.64	1561.50
C & E Loss (m)					

Errors, Warnings and Notes

Cross Section Output

River: Shabelle Profile: Max WS

Reach: Shabelle RS: 300 Plan: 2019

Plan: 2019 Shabelle Shabelle RS: 300 Profile: Max WS

		Element	Left OB	Channel	Right OB
E.G. Elev (m)	176.11	Wt. n-Val.	0.045	0.045	0.045
Vel Head (m)	0.03	Reach Len. (m)			
W.S. Elev (m)	176.07	Flow Area (m2)	70.31	382.32	30.63
Crit W.S. (m)	171.07	Area (m2)	70.31	382.32	30.63
E.G. Slope (m/m)	0.000150	Flow (m3/s)	26.61	315.92	6.99
Q Total (m3/s)	349.52	Top Width (m)	40.60	70.20	39.20
Top Width (m)	150.00	Avg. Vel. (m/s)	0.38	0.83	0.23
Vel Total (m/s)	0.72	Hydr. Depth (m)	1.73	5.45	0.78
Max Chl Dpth (m)	7.32	Conv. (m3/s)	2172.2	25784.9	570.3
Conv. Total (m3/s)	28527.3	Wetted Per. (m)	42.89	72.31	39.93
Length Wtd. (m)		Shear (N/m2)	2.41	7.78	1.13
Min Ch El (m)	168.75	Stream Power (N/m s)	0.91	6.43	0.26
Alpha	1.20	Cum Volume (1000 m3)			
Frctn Loss (m)		Cum SA (1000 m2)			
C & E Loss (m)					

Errors, Warnings and Notes

Cross Section Output

River: Shabelle   Profile: Max WS
Reach: Shabelle   RS: 39000   Plan: 500yrs

Plan: 500yrs   Shabelle   Shabelle RS: 39000   Profile: Max WS

		Element	Left OB	Channel	Right OB
E.G. Elev (m)	183.99	Wt. n-Val.	0.045	0.045	0.045
Vel Head (m)	0.05	Reach Len. (m)	313.50	300.00	284.20
W.S. Elev (m)	183.94	Flow Area (m2)	122.21	312.73	70.89
Crit W.S. (m)		Area (m2)	122.21	312.73	70.89
E.G. Slope (m/m)	0.000278	Flow (m3/s)	81.84	355.17	33.69
Q Total (m3/s)	470.70	Top Width (m)	46.30	56.70	47.00
Top Width (m)	150.00	Avg. Vel. (m/s)	0.67	1.14	0.48
Vel Total (m/s)	0.93	Hydr. Depth (m)	2.64	5.52	1.51
Max Chl Dpth (m)	6.94	Conv. (m3/s)	4911.5	21315.6	2022.0
Conv. Total (m3/s)	28249.1	Wetted Per. (m)	50.25	58.22	48.75
Length Wtd. (m)	301.64	Shear (N/m2)	6.62	14.62	3.96
Min Ch El (m)	177.00	Stream Power (N/m s)	4.43	16.61	1.88
Alpha	1.23	Cum Volume (1000 m3)	3738.14	15444.81	2921.46
Frctn Loss (m)	0.07	Cum SA (1000 m2)	1667.63	2387.18	1729.11
C & E Loss (m)					

Errors, Warnings and Notes

Cross Section Output

River: Shabelle   Profile: Max WS
Reach: Shabelle   RS: 300   Plan: 500yrs

Plan: 500yrs   Shabelle   Shabelle RS: 300   Profile: Max WS

		Element	Left OB	Channel	Right OB
E.G. Elev (m)	176.93	Wt. n-Val.	0.045	0.045	0.045
Vel Head (m)	0.04	Reach Len. (m)			
W.S. Elev (m)	176.90	Flow Area (m2)	103.67	440.00	62.84
Crit W.S. (m)	171.47	Area (m2)	103.67	440.00	62.84
E.G. Slope (m/m)	0.000146	Flow (m3/s)	49.54	394.05	22.53
Q Total (m3/s)	466.13	Top Width (m)	40.60	70.20	39.20
Top Width (m)	150.00	Avg. Vel. (m/s)	0.48	0.90	0.36
Vel Total (m/s)	0.77	Hydr. Depth (m)	2.55	6.27	1.60
Max Chl Dpth (m)	8.15	Conv. (m3/s)	4097.2	32590.0	1863.7
Conv. Total (m3/s)	38551.0	Wetted Per. (m)	43.71	72.31	40.75
Length Wtd. (m)		Shear (N/m2)	3.40	8.72	2.21
Min Ch El (m)	168.75	Stream Power (N/m s)	1.62	7.81	0.79
Alpha	1.20	Cum Volume (1000 m3)			
Frctn Loss (m)		Cum SA (1000 m2)			
C & E Loss (m)					

Errors, Warnings and Notes